1-1-1983

Jet condenser design for a power system in space.

Marco F. Bucchi

JET CONDENSER DESIGN
FOR A POWER SYSTEM
IN SPACE

by

Marco F. Bucchi

A Thesis

Presented to the Graduate Committee

of Lehigh University

in Candidacy for the Degree of

Master of Science

in

Mechanical Engineering

Lehigh University

1983

CERTIFICATE OF APPROVAL

This thesis is accepted and approved in partial fulfillment of the requirements for the degree of Master of Science.

May 5, 1983
(date)

Professor in Charge

Chairman of Department

ACKNOWLEDGEMENTS

I would like to express my sincerest thanks to my advisor, Dr. Charles R. Smith for his guidance throughout this effort. His technical communication and advice have brought uniformity and cohesiveness to this paper, and will allow the reader to ascertain the principles of the presented material.

Particular acknowledgement is expressed to both the Department of Energy and Sundstrand Corporation, who gave me the opportunity to perform the research and development, and permitted me to include many figures, diagrams, plots, and other data.

Special thanks are due to Diane Stahley, Brenda Roxberry, Nanette Anderson, and Sue Colarusso who helped type the numerous revisions of the manuscript.

Finally to my wife, Karin, who has given me support and understanding throughout this effort, and has assisted me in ways too numerous to mention, I express my deepest gratitude.

TABLE OF CONTENTS

	PAGE
LIST OF TABLES.	vi
LIST OF FIGURES	vii
ABSTRACT.	1
CHAPTER 1 INTRODUCTION.	3
1.1 Background Information.	5
1.2 Design Parameters	12
CHAPTER 2 JET CONDENSER ANALYTICAL MODEL.	15
2.1 Introduction.	15
2.2 Steam/Water Model Analysis Pure Vapor Condensation Rate.	16
2.3 Thermal Performance Analysis.	48
2.4 Stanton Number Multiplier caused by Noncondensable Gas Accumulation	76
CHAPTER 3 JET CONDENSER MECHANICAL COMPONENTS	83
3.1 General	83
3.2 Vapor Nozzle.	86
3.3 Injector Head and Liquid Nozzles.	88
3.4 Mixing Chamber.	91
3.5 Throat.	94
3.6 Diffuser	96

TABLE OF CONTENTS

	PAGE
CHAPTER 4 TEST LOOP APPARATUS AND PROCEDURES	99
4.1 Steam/Water Test Apparatus (Single Nozzle)	99
4.2 Liquid Dowtherm Test Rig (Single Nozzle)	102
4.3 Jet Condenser Focusing Test Rig (Multiple Nozzle)	109
4.4 Liquid Dowtherm Test Rig (Multiple Nozzle)	117
4.5 Instrumentation	121
4.6 Augmented Pressure	123
CHAPTER 5 RESULTS ON CONDUCTED TESTS	126
5.1 Stability of Flow	126
5.2 Condensation Length	128
5.3 Single Nozzle Design	130
5.4 Multiple Nozzle Design	135
5.5 Scavenging	141
CHAPTER 6 SUMMARY AND DISCUSSION	146
CHAPTER 7 CONCLUSIONS	149
REFERENCES	151
APPENDIX A - NONCONDENSABLE GASES	154
APPENDIX B - CONDENSER GAS BOUNDARY LAYER ANALYSIS	159
APPENDIX C - MISALIGNMENT	162
APPENDIX D - PROPERTY VALUES USED IN ANALYSIS	168
VITA	169

LIST OF TABLES

TABLE		PAGE
1	SUMMARY OF DESIGN PARAMETERS	14
2	SINGLE NOZZLE TEST DATA SHEET	110
3	TYPICAL FOCUS TEST DATA SHEET	115
4	TYPICAL RECOVERY TEST DATA SHEET	116
5	RESULTS ON INDIVIDUAL NOZZLE COMPARISONS TESTED ON LIQUID DOWTHERM	132
6	DOWTHERM MULTIPLE NOZZLE THERMAL PERFORMANCE RESULTS	138
C-7	MISALIGNMENT RESULTS	166

LIST OF FIGURES

FIGURE		PAGE
1	JET CONDENSER FLOW PATH.	7
2	45 NOZZLE JET CONDENSER.	10
3	NOZZLE WITH SHORT SHARP-EDGED ORIFICE.	11
4	EQUATIONS RELATING VAPOR AND LIQUID AT ANY AXIAL LOCATION OF THE LIQUID JET	20
5	SHEAR VELOCITY FOR STEAM/WATER ANALYSIS.	24
6	GRAPH USED TO FIND STANTON NUMBER THAT MATCHES DATA	26
7	NOZZLES THAT PROMPTED TURBULENCE	27
8	STANTON NUMBER MEAN VALUE AND RANGE.	29
9	JET STANTON NUMBERS VS. DISTANCE FROM EJECTOR. . .	30
10	JET STANTON NUMBER FOR .254 AND .3683 MM DIAMETER NOZZLES	33
11	HEAT TRANSFER COEFFICIENT VS. HEAT FLUX.	34
12	AVERAGE HEAT TRANSFER COEFFICIENT VS. HEAT FLUX. .	38
13	STANTON NUMBER AT ZERO HEAT FLUX	39
14	JET TEMPERATURE PROFILES - .3683 MM NOZZLE	40
15	JET TEMPERATURE PROFILES - .2540 MM NOZZLE	41
16	.254 MM DIAMETER NOZZLE FOR 50.8 MM JET LENGTH . .	42
17	.254 MM DIAMETER NOZZLE FOR 127 MM JET LENGTH. . .	43

LIST OF FIGURES

FIGURE		PAGE
18	.254 MM DIAMETER NOZZLE FOR 254 MM JET LENGTH.	44
19	.3683 MM DIAMETER NOZZLE FOR 50.8 MM JET LENGTH.	45
20	.3683 MM DIAMETER NOZZLE FOR 127 MM JET LENGTH	46
21	.3683 MM DIAMETER NOZZLE FOR 254 MM JET LENGTH	47
22	VELOCITY DISTRIBUTION REGIONS.	50
23	STANTON NUMBER FOR .254 AND .3683 MM DIAMETER NOZZLES (DOWTHERM)	56
24	STANTON NUMBER AT ZERO INTERFACIAL VELOCITY.	57
25	NONCONDENSABLE GAS INTERACTION WITH VAPOR AND LIQUID	59
26	SCHMIDT NUMBERS VS. SUCTION PARAMETER.	62
27	DETAILED RESULTS - 45 NOZZLE SYSTEM.	71
28	COMPARISON OF MEASURED AND PREDICTED VALUES 45-.3683 MM DIAMETER NOZZLES	73
29	DETAILED RESULTS - 90 NOZZLE SYSTEM.	74
30	COMPARISON OF MEASURED AND PREDICTED VALUES 90-.254 MM DIAMETER NOZZLES.	75
31	50.8 MM JET LENGTH DATA FOR .254 AND .3683 MM DIAMETER NOZZLES	77

LIST OF FIGURES

FIGURE		PAGE
32	RATIO OF MASS TRANSFER COEFFICIENT NORMAL TO THE WALL VS. SUCTION PARAMETER	81
33	JET CONDENSER DESIGN SPECIFICATIONS AND COMPONENTS	84
34	JET CONDENSER DETAILED MECHANICAL COMPONENTS	87
35	STAINLESS STEEL JET CONDENSER NOZZLE	92
36	JEWEL SAPPHIRE JET CONDENSER NOZZLE	93
37	STEAM AND WATER TEST STAND	100
38	INJECTOR JET END TEMPERATURE MEASUREMENT	101
39	JET CONDENSER SINGLE NOZZLE DOWTHERM TEST RIG	107
40	JET CONDENSER FOCUSING TEST RIG.	114
41	JET CONDENSER MULTIPLE NOZZLE DOWTHERM TEST STAND.	119
42	SCAVENGE FLOW AREAS.	142
43	SYSTEM BEARING SCAVENGE FLOW AT THE THROAT	145
A-44	INSOLUBILITY OF NONCONDENSABLES IN LIQUID.	155
A-45	NONCONDENSABLE CONCENTRATION RESULTS	158
C-46	JET CONDENSER FLOW DEFLECTIONS	163
C-47	DEFLECTION EFFECTS	167

ABSTRACT

The design of a jet condenser for space applications on an Organic Rankine Cycle Power System is demonstrated on the basis of results from an analytical model, and actual testing of designed hardware.

Saturated dowtherm vapor condenses on the subcooled liquid to form the condensation process of the condenser. The vapor operates at a low pressure (.69 kPa) to eliminate high backpressures on the upstream system turbine. To optimize condensation rates and achieve hydraulic stability jet lengths of 50.8, 127, and 254mm, and nozzle orifice configurations of .216, .254 and .3683mm in diameter were tested on Steam/Water and Liquid Dowtherm. Stanton Numbers related the velocity differences to jet heat transfer coefficients, and helped establish the 254 mm optimum jet length.

Noncondensable gas affected the jet condenser by raising the saturated vapor pressure beyond design (.69 kPa), and reduced the vapor velocity, such that the condenser initially underperformed. Developmental testing on liquid dowtherm showed a Synthetic Sapphire Jewel Nozzle to be superior in thermal performance, (370°K vs. 373.3°K) and produced the smallest amount of noncondensable gas while maintaining hydraulic stability limits within $\pm$ .762 mm.

90 individual nozzles at 348.9°K provided adequate performance by allowing the vapor at 392.2°K to condense to 370°K, and pass through a throat and recover 57% of the 552 kPa injection pressure.

With all operating performance parameters satisfied, the analytical model accurately predicts the performance of the jet condenser when the effects of noncondensable gas are included. With good agreement between the actual operating data and the analytical predictions of the model, the feasibility of the Jet Condenser Design for a Power System in Space has been demonstrated.

CHAPTER 1. INTRODUCTION

Electrical power systems which are based on the Organic Rankine Cycle have been in various stages of development for the past 20 years. This thermodynamic cycle requires that the working fluid be condensed from a saturated vapor to a liquid, after it leaves the heat engine or working turbine, and that the heat of condensation be rejected. One of the key components of the system is the jet condenser. It allows expansion of the working fluid through the turbine at low backpressures.

This thesis will describe the design and evaluation of performance characteristics of a jet condenser which is suitable for use in Orbiting Space Vehicles as part of an Organic Rankine Cycle Power Conversion System.

Unlike conventional condensers in industrial power plants which depend on gravity to combine the liquid and vapor and direct the combined fluid (condensate) to a pump,[1] the condenser must be able to operate under zero gravity conditions, in a space power system.

Most of the Rankine Cycle Power Systems that have been investigated have two basic operations: condensation and heat rejection. These two operations are performed directly in a combined condenser-radiator (see Hays[2]).

There are several types of condensers which are commonly employed for space operation. The first is a direct condenser that consists of finned tubes through which both the vapor and condensate flow, and which radiates the heat of condensation directly into space. A second type of condenser that has been used for space operation consists of a compact shell and tube heat exchanger in which the vapor is condensed separately from the liquid radiator. The third type eliminates the separating walls and allows the vapor to mix with a cooler liquid of the same component. The resultant warmer liquid is then cooled in a finned radiator, after which a portion is returned to the heat source, and the remainder is returned to the condenser inlet to continue the condensation process.

This thesis will concentrate on the last type of condenser, which is a derivative of an industrial jet condenser modified to permit operation at zero gravity conditions. This type of condenser provides for contact of the superheated vapor and the coolant, which yields both a good heat transfer rate and an increase in static pressure from the vapor inlet to the condensate outlet.

The objective of this study is to demonstrate that this particular type of jet condenser is capable of use as a component in an Organic Rankine Power System for space applications. In support of this objective, the following approach is taken:

1. An analytical model is developed which allows prediction of the condenser operating parameters and geometrical design.
2. Based on the analytical model, the hardware associated with the condenser components is designed for use in developmental tests using both steam/water and the actual working fluid, Dowtherm "A".
3. The developmental tests and results are discussed and a comparison is made between the actual operating data and the analytical predictions.
4. Based on items 1-3 above, conclusions are drawn as to the feasibility of the condenser for space applications.

1.1 Background Information

An Organic Rankine Power System for space utilizes a jet condenser to allow satisfactory liquid and vapor contact in all attitudes and under zero "g" conditions. The jet condenser is a device in which low pressure vapor is ducted into a funnel

coaxially with liquid jets of subcooled working fluid (Figure 1). The liquid jets are injected into the vapor at a high velocity and aimed at the throat of the vapor funnel. The vapor condenses on the subcooled liquid jet and the combined liquid jet passes through a throat into a diffuser, as shown in Figure 1. The liquid jet undergoes a sudden expansion within the diffuser, filling the entire cross section. During the sudden expansion there is a loss of total pressure, but a gain in static pressure of the liquid stream. Further recovery of static pressure occurs as the liquid continues through the diffuser. The behavior of the liquid jet within the diffuser is identical to that which occurs in the diffuser of a cavitating venturi. The outlet pressure from the diffuser can vary from essentially zero up to about 60% of the inlet pressure depending on where the jet stream expands to fill the diffuser.

The condensation process within the jet condenser is limited by the probability of collision of vapor molecules with the liquid jets, i.e., it is vapor density limited. By locating the liquid jets such that each jet has approximately the same vapor volume surrounding it, the jet condenser is capable of operating with the liquid outlet subcooled by only 2.78°K with respect to the mixing chamber saturation temperature, or 8.34°K with respect to the jet condenser inlet saturation temperature.

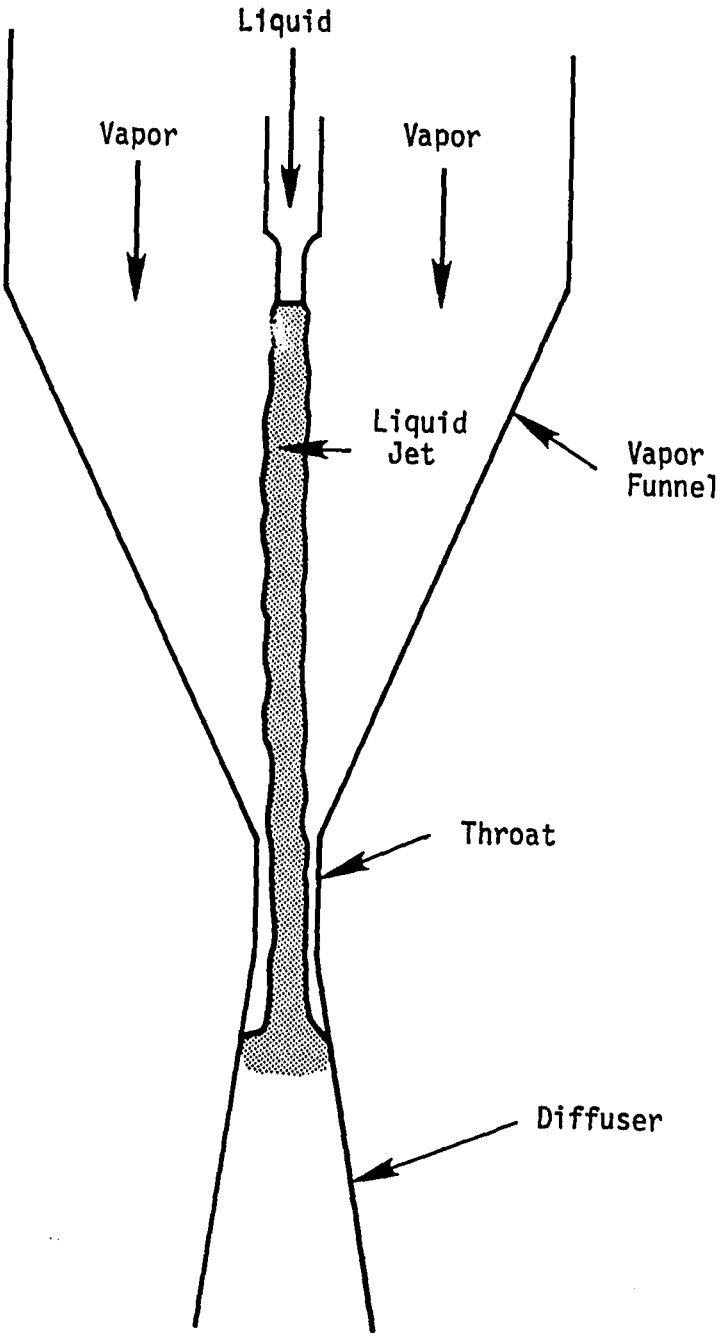

JET CONDENSER FLOW PATH

FIGURE 1.

The jet condenser design is extrapolated on the premise that the rate of condensation per unit surface area of jet is directly proportional to the vapor pressure in the jet condenser mixing chamber, such that the liquid outlet temperature will be subcooled by ~2.8°K with respect to the mixing chamber pressure.

Previous studies conducted by Platt[3] and Garcia[4] have shown that a jet condenser can replace a standard surface condenser, and condense vapor from a turbine with a given liquid. Platt's[3] exploratory investigation ejected steam through a single central nozzle, and allowed water to enter through an annular nozzle or funnel. Although certain principles that Platt demonstrated were similar to the thesis herein (condensation process for a power system), the associated hardware and his complete design technique were radically different. Garcia did emit liquid via a nozzle, and vapor in a funnel, but again the basis for the employed design was altered. A single liquid stream emitted by a nozzle was used in an attempt to verify the condensation process for a power conversion system.

The remainder of the sources that were investigated dealt with the condensation process and its rate, and were not concerned with a jet condenser for a power system. Zero

gravity conditions for condensers were also not available, as most systems dealt strictly with Heat Transfer Rates for Condensation (Isachenko et al.[5], Miyazaki et al.[6], and Kaplan et al.[7]), Expansion Ratios (Irodov[8]), Liquid/Vapor Condensation Rates (Mochalova et al.[9], and Maa[10]), and Controlled Vacuum Condensation (Blume[1]).

An initial design of the jet condenser, utilizing 45 liquid injector nozzles, is shown in Figure 2. Each injector nozzle has a .3683 mm diameter with a liquid jet length of 254 mm to the diffuser. The use of sharp-edged orifices, as shown in Figure 3, resulted in a well-columnated focused stream which passes through the throat of the vapor funnel and is resistant to brooming. Brooming is defined as the atomization or breakup of the columnated stream. The jets must pass through the throat without any significant impingement on the walls of the vapor funnel. If the liquid does impinge on the walls, it will slow down and collect near the throat section. This collection of fluid impedes the other jets to the point where there is insufficient pressure recovery in the diffuser to keep the liquid flowing in the forward direction, (i.e., diffuser outlet pressure is less than accumulator reservoir pressure). This condition will be referred to as "floodout" since the liquid will no longer pass through the funnel and results in a shutdown of the liquid injection system.

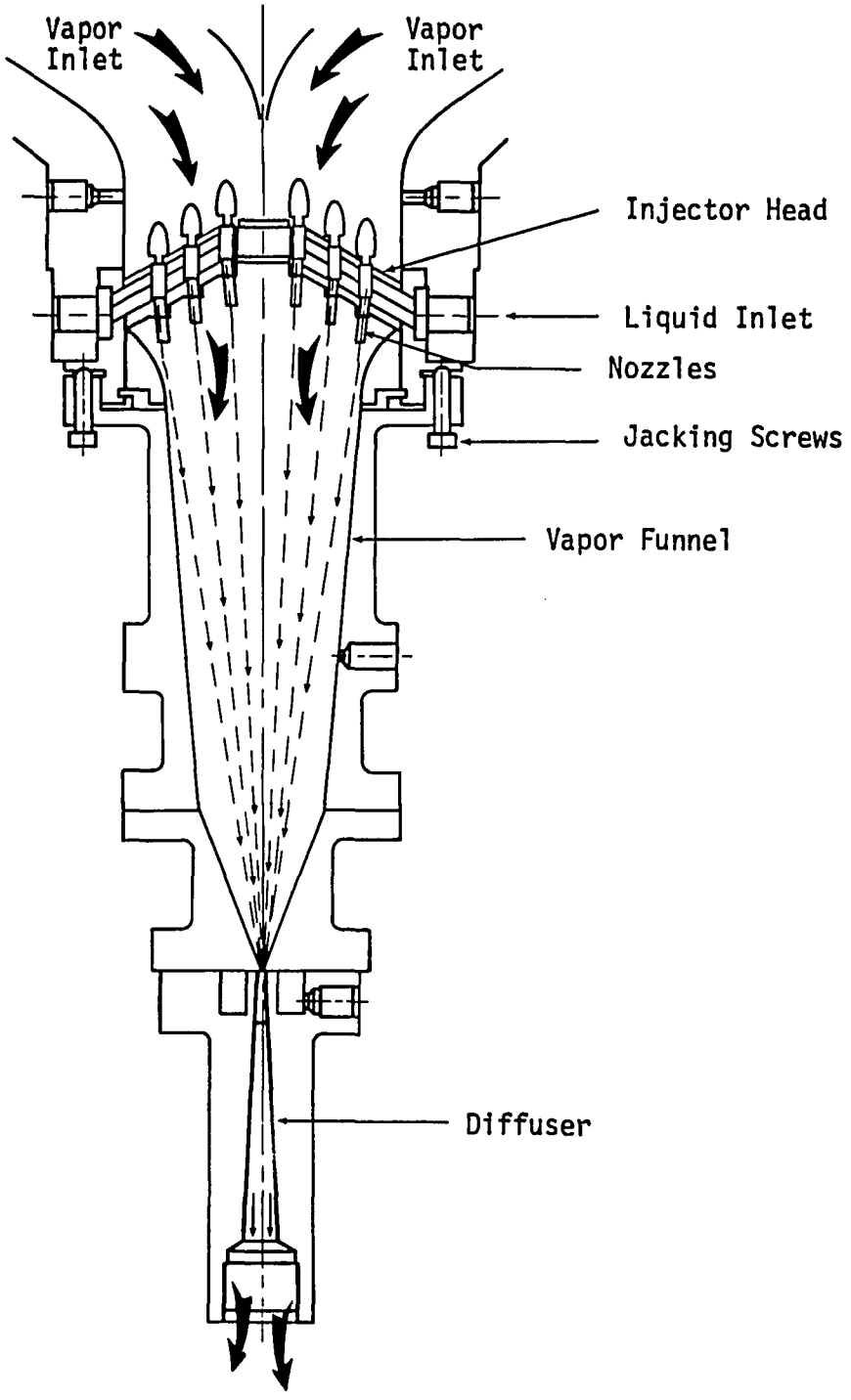

45 NOZZLE JET CONDENSER

FIGURE 2.

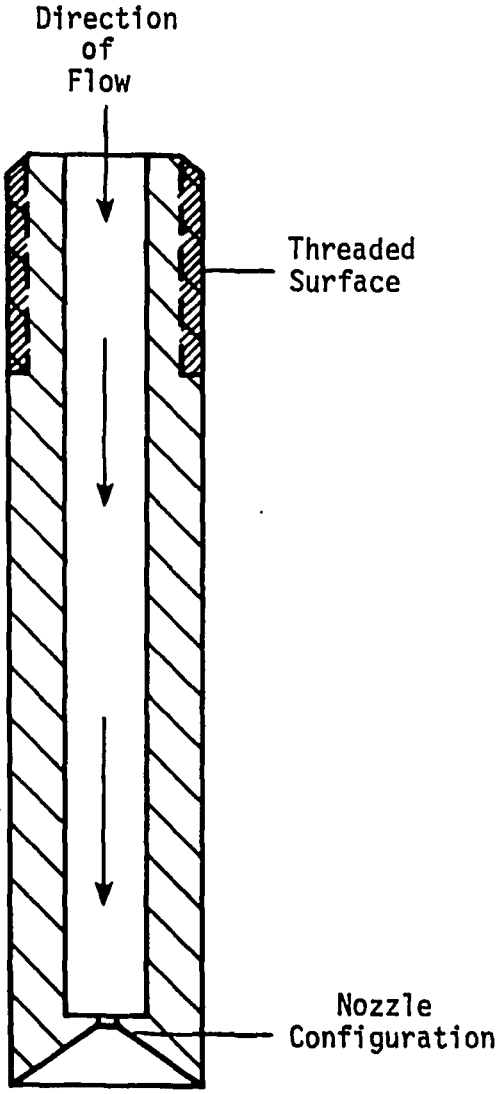

NOZZLE WITH SHORT SHARP-EDGED ORIFICE

FIGURE 3.

1.2 Summary of Jet Condenser Design Parameters

Certain design parameters are presented at this point to give the reader an idea of the operating range of temperatures and pressures for the jet condenser. Some of the ranges are dictated by other major components within the Power Conversion System of the Organic Rankine Cycle Power System. (An example of this case would be the inlet vapor temperature which is a function of the turbine exhaust.) Table 1. is a summary of the pertinent parameters that are used in the overall system design.

Thermal performance of the condenser is achieved with a liquid outlet temperature as low as possible in relation to the combined liquid and vapor inlet, and recovery pressure (rise) as high as possible. The pressure of the vapor is extremely low (.69 kPa) when it combines with the liquid at 552 kPa. Since there is a loss of total pressure but a gain in static pressure after the liquid passes the throat (See Figure 2), the diffuser enables the pressure recovery (rise) to take place. The recovery pressure is measured in relation to the liquid inlet, so it is 100% (percent) at 552 kPa. Testing and results in Chapters 4 and 5 will show that a 50% (percent) recovery measured at the diffuser outlet is achievable.

Jet lengths of 50.8, 127, and 254 mm were used in testing, to help determine the condensation performance of the jet condenser. Primarily the rates of condensation were investigated at the various lengths, for comparison to the predicted values that are analytically established in Chapter 2.

The number of rings, n, in Table 1. corresponds to the three circular rings of the liquid injector head that holds the injector nozzles, as shown in Figure 2. The initial injector head design contained 45 nozzles. The final design that yielded the best performance contained 90 nozzles, with 18 on the inside, 30 in the middle, and 42 nozzles on the outside ring. The components are further explained in detail in Chapter 3. Various tests employed to simulate the different conditions and establish the actual performance of the jet condenser are described in Chapter 4. Chapter 5 presents the results of the conducted tests. Chapter 6 discusses the main findings, limitations, and tradeoffs of the jet condenser. Finally, conclusions are drawn in Chapter 7.

TABLE 1.

SUMMARY OF DESIGN PARAMETERS

		Location		
		Liquid In	Vapor In	Liquid Out
MASS FLOW	(kg/sec)	.1247	.0136	.1424
TEMPERATURE	(°K)	348.9	392.2	< 372.8
PRESSURE	(kPa)	552	.704	≥ 220.8

Liquid Jet Length	L = 254 mm
Mixture Chamber Pressure	P_{mix} = .5865 kPa
Number of Nozzles	N = 90
Orifice Diameter	D_o = .254 mm
Effective Vapor Diameter at the Liquid Injector	D_{mix} = 79.756 mm
Diameter at the Liquid Injector	D_i = 101.6 mm
Number of Injector Rings	n = 3
Vapor Velocity at the Liquid Injector	V_V = 305.4 km/hr
Liquid Velocity	V_L = 113.02 km/hr at Re_D = 8140
Throat Diameter	D_t = 3.38 mm

CHAPTER 2. JET CONDENSER ANALYTICAL MODEL

2.1 Introduction

The performance/sizing of the analytical model is based on one-dimensional gas dynamics in the vapor funnel, a kinetic theory representation of the vapor/liquid interface condensing process, and empirical correlation of the jet heat transfer coefficient from the vapor/liquid interface to the bulk liquid.

The analytical model is used to predict the condenser vapor inlet pressure that is required to condense a given vapor flow rate with a specified liquid flow rate, liquid inlet injector temperature, and funnel geometry. The model is essentially a set of differential equations that describes the vapor momentum and continuity of the liquid. These are integrated from inlet to outlet of the jet condenser for a range of vapor inlet pressures to determine a value of pressure which results in the required amount of vapor condensation.

The energy equation for the vapor is not considered because all other forms of heat transfer are negligible relative to condensation on the liquid jets. The momentum

equation for the vapor is not considered, because the vapor molecules near the interface of the liquid jets have a bulk axial velocity similar to the bulk liquid jet velocity.

2.2 Steam/Water Model Analysis

Pure Vapor Condensation Rate[11]

The accepted physical model of evaporation and condensation is based on proposals of Hertz[12] in 1882 and of Knudsen[13] in 1915. The kinetic theory of gases yields the rate at which molecules strike the condensed phase from equilibrium vapor as $n_g c_g/4$;

where:

n_g = Concentration of molecules.

c_g = Average molecular speed.

$$C(T) = \sqrt{\frac{8\,RTgo}{\pi}} \qquad \text{EQN 2.1}$$

R = Gas constant of vapor.

T = Absolute temperature of vapor.

g_o = Gravitation constant.

A "condensation/evaporation coefficient" is used to account for the fraction of the incident molecules which enter the condensed phase, the remainder being reflected. The flux

of molecules leaving the condensed phase is given by $fn_s C_s/4$ where n_s and c_s are the molecular density and speed based on saturated liquid surface conditions and f is the "evaporation coefficient" in order for the equilibrium situation to be attainable. During net phase change, the bulk vapor velocity normal to the interface affects the molecular velocity distribution; Schrage[14] took this into account and derived the following expression for the net condensation rate:

$$w = f\left(\Gamma \frac{n_g c_g}{4} \quad \frac{n_s c_s}{4}\right) \quad \frac{\text{mole}}{m^2 - \text{sec.}} \qquad \text{EQN 2.2}$$

where:

w = Net Condensation Rate.

$$\Gamma = e^{-s^2} + \sqrt{\pi}\, s\,(1 + \text{erf}\,(s)) \qquad \text{EQN 2.3}$$

$$s = \frac{u}{\sqrt{2RTg_o}} \qquad \text{EQN 2.4}$$

u = Bulk Velocity of Vapor normal to jet.

The net condensation rate can be written in terms of the mass flux condensed as:

$$\frac{\dot{m}}{A}\ \text{cond.} = f\left(\frac{\Gamma \rho_g C_g}{4} - \frac{\rho_s C_s}{4}\right) \quad \frac{kg}{m^2\ \text{sec}} \qquad \text{EQN 2.5}$$

where:

ρ_g is the vapor density, $\frac{kg}{m^3}$

ρ_s is the saturated vapor density based on liquid surface temperature, $\frac{kg}{m^3}$

Based on the arguments of Mills and Seban[11], the evaporation coefficient is taken as unity in this work. For the net condensation of saturated vapor it is clear the ρ_s must be less than ρ_g, because the temperature of the condensate surface must be less than the saturation temperature of the vapor. The factors that affect ρ_s (or T_s, The liquid surface temperature) are the bulk liquid jet temperature T_B, the condensation rate, w, and the ability of the liquid jet to transport heat from its surface to its bulk liquid. The factors that affect the vapor pressure near the liquid jet surface are the vapor flow area schedule in the vapor funnel, the condensation rate, w, and the amount of noncondensable gas present in the vapor. Initially, to establish the basic relationships it will be assumed that there is no noncondensable gas present.

Figure 4 illustrates the situation between the vapor and liquid at any axial location of the liquid jet. At any axial

location the liquid jet is characterized by its bulk temperature, T_{BL}, its mass flow rate, $\dot{m}_L$, its bulk absolute velocity, V_L, its density, ρ_L, and its bulk enthalpy, h_L. The surface of the liquid jet is assumed to be at a temperature, T_{SL}, which is higher than the bulk, and consequently, has a liquid enthalpy, h_{VSL}, which is higher than the bulk. Also associated with the liquid surface is a saturated vapor density, ρ_{VSL}. The vapor at any corresponding axial location has temperature, T_V, pressure, P_V, density, ρ_V, and enthalpy, h_V. These are assumed to be static properties defined by the local vapor static conditions in Isachenko et al.[5]

Due to the difference in vapor density, ρ_V, and the saturation vapor density at the liquid surface, ρ_{VSL}, a net condensation flux, W/A cond., occurs which is given by equation (2.5), when f = 1

$$\frac{W\text{cond.}}{A} = \Gamma \left[\frac{\rho_V}{4} C(T_V) - \frac{\rho_{VSL}}{4} C(T_{VSL}) \right] \qquad \text{EQN 2.6}$$

where:

$$u = \frac{W\text{cond.}}{A\rho V} \qquad \text{EQN 2.7}$$

and Γ is given by equation (2.3).

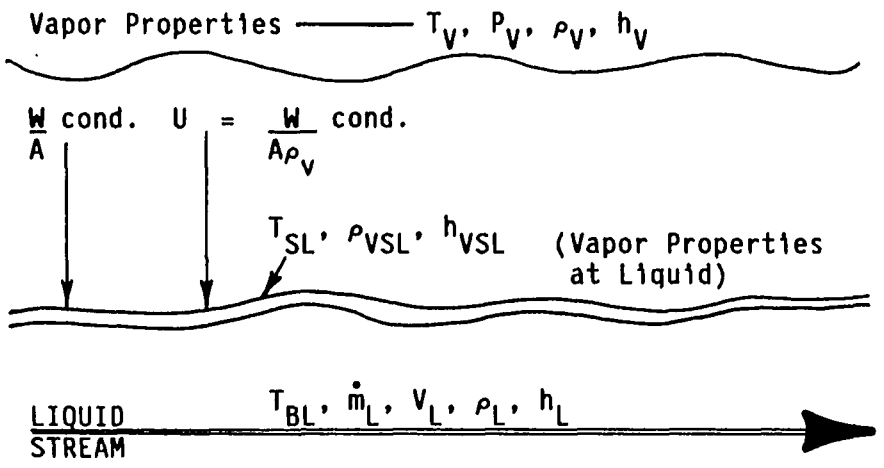

$$\cdot \left.\frac{Q}{A}\right|_{\text{VAPOR TO SURFACE}} = \left.\frac{Q}{A}\right|_{\text{SURFACE TO BULK}}$$

$$\cdot \frac{W}{A}\text{ cond. } (h_V - h_{LSL}) = H(T_{SL} - T_{BL})$$

Related by T_{SL}

$$\frac{W}{A}\text{ cond.} = \left[\frac{(\Gamma\rho_V)}{4} C(T_V) - \frac{\rho_{VSL}}{4} C(T_{VSL})\right]$$

$$U = \frac{W}{A}\frac{\text{cond.}}{\rho_V}$$

$$s = \frac{u}{\sqrt{2g\ RT_V}}$$

$$C(T) = \sqrt{\frac{8}{\pi} R_V\ g_o\ T}$$

$$\Gamma = e^{-s^2} + \sqrt{\pi}\ s(1 + \text{erf}(s))$$

EQUATIONS RELATING VAPOR AND LIQUID AT ANY AXIAL LOCATION OF THE LIQUID JET

FIGURE 4.

C(T) is the average molecular speed given by (equation 2.1). This net condensation flux has an associated net enthalpy of $h_V - h_{LSL}$. Thus the liquid surface has a heat flux of Q/A vapor-surface imposed on it, where

$$\frac{Q}{A}\Big|_{\text{vapor-surface}} = \frac{W}{A}\text{cond.}\ (h_V - h_{LSL}) \qquad \text{EQN 2.8}$$

This same heat flux must be convected from the surface of the liquid to the bulk liquid. Defining the jet convection coefficient as H, the heat flux from the liquid surface to bulk is

$$\frac{Q}{A}\Big|_{\text{surface-bulk}} = H\ (T_{SL} - T_{BL}) \qquad \text{EQN 2.8.1}$$

combining equations (2.8) and (2.8.1) we obtain,

$$\frac{W}{A}\ \text{cond.}\ (h_V - h_{VSL}) = H\ (T_{SL} - T_{BL}) \qquad \text{EQN 2.9}$$

From the above we can say the prediction of the local condensation rate, although iterative, is not difficult if a suitable value of the jet convection coefficient, H, is available.

Initially, preliminary data reduction was based on the assumption that H was proportional to the jet velocity according to Linehan.[15] Further investigation showed a more reasonable premise upon which to establish H is by assuming that it should be based on a characteristic velocity

which is the difference between the liquid bulk velocity and the interface velocity.[16] Subsequent to the completion of work reported herein, it was found that Young and Yang[17] reported good correlation of test data of a condensing steam jet with a Stanton number based on this velocity difference. This interfacial "shear velocity" is shown in Figure 5., which is drawn for the case of zero bulk vapor velocity and is the case pertinent to the steam/water model analysis. In this figure the bulk liquid jet velocity is V_L, the interface velocity is V_i and the vapor velocity is V_V, which for this case is zero far away from the jet surface.[19]

The method of estimating the interfacial velocity is presented in Gouse, Kemper, and Brown[18] which is based on equating the vapor shear stress to the liquid shear stress, including the effect of the mass transfer from the vapor to the liquid.

Defining the vapor velocity relative to the interface as V_{Vi}, and the liquid velocity relative to the interface as V_{iL}, it is seen that:

$$V_{Vi} = V_i - V_V \qquad \text{EQN 2.10}$$
$$V_{iL} = V_L - V_i$$

According to Gouse et al.[18], the shear matching condition becomes:

$$(\tau_i)_V = (\tau_i)_L \qquad \text{EQN 2.11}$$

where:

$$(\tau_i)_V = (f_i)_V \frac{\rho_V V_{Vi}^2}{2 g_o} + \frac{W}{A} \text{ cond. } (\frac{V_{Vi}}{g_o}) \qquad \text{EQN 2.12}$$

$$(\tau_i)_L = (f_i)_L \frac{\rho_L V_{iL}^2}{2 g_o} + \frac{W}{A} \text{ cond. } (\frac{V_{iL}}{g_o}) \qquad \text{EQN 2.13}$$

and the friction factor, f_i, is based on the relative Reynolds Number, Re_r, with the assumption that the jet stream is considered as a solid surface with respect to the free flowing vapor,

$$f_i = \frac{16}{Re_r} \text{ for laminar flow}[20] \qquad \text{EQN 2.15}$$

or

$$f_i = \frac{0.046}{Re_r^{.2}} \text{ for turbulent flow}[20] \qquad \text{EQN 2.16}$$

and

$$Re_{rL} = \frac{\rho_L V_{iL} D_j}{\mu_L} \qquad \text{EQN 2.17}$$

$$Re_{rV} = \frac{\rho_V V_{Vi} D_V}{\mu_V} \qquad \text{EQN 2.18}$$

where:

D_j is the liquid jet diameter (nozzle metal diameter).

D_V is the equivalent diameter for the vapor passage.

For the steam/water testing, D_V is approximately 203.2 mm.

The heat transfer coefficient is assumed to be of the form:

$$H = S_t \cdot \rho_L \cdot C_{pL} \cdot V_{iL} \qquad \text{EQN 2.19}$$

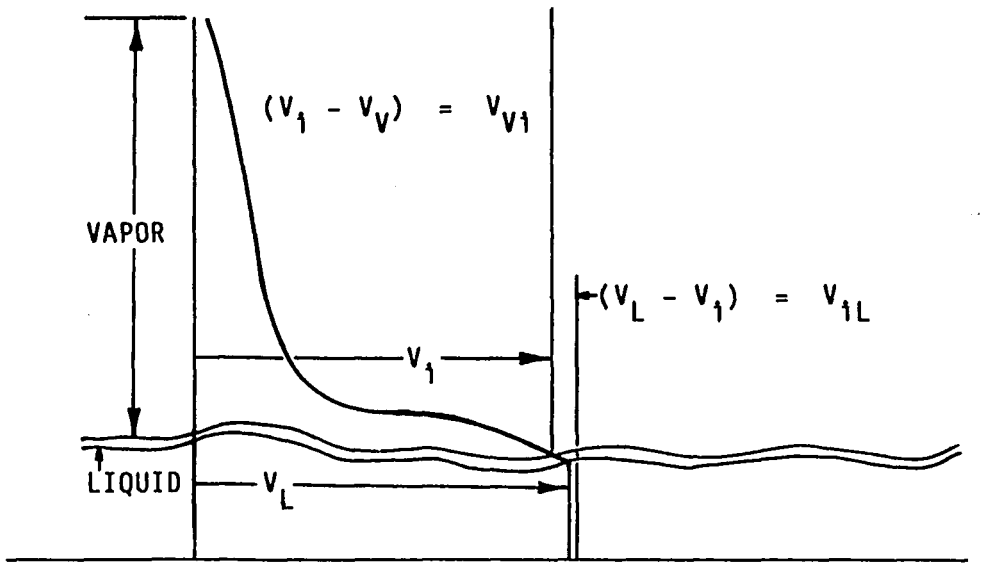

$$(\tau_i)_V = (\tau_i)_L$$

$$(\tau_i)_V = (fi)_V \frac{\rho_V V_{Vi}^2}{2 g_o} + \frac{W}{A} \text{ cond. } \left(\frac{V_{Vi}}{g_o}\right)$$

$$(\tau_i)_L = (fi)_L \frac{\rho_L V_{iL}^2}{2 g_o} + \frac{W}{A} \text{ cond. } \left(\frac{V_{iL}}{g_o}\right)$$

$$fi = \frac{16}{Re_r} \text{ or } = \frac{.046}{Re_r^{.2}}$$

$$Re_{rL} = \rho_L V_{iL} \frac{D_i}{\mu L}$$

$$Re_{rV} = \rho_V V_{Vi} \frac{D_V}{\mu V}$$

SHEAR VELOCITY FOR STEAM/WATER ANALYSIS

FIGURE 5.

$$\dot{m}_L \; Cp_L \; \frac{dT_{BL}}{d_x} = \frac{W}{A} \text{ cond.} \; (h_V - h_{LSL}) \; \pi \; D_j \qquad \text{EQN 2.20}$$

$$\frac{d\dot{m}_L}{d_x} = \frac{W}{A} \text{ cond.} \; \pi \; D_j \qquad \text{EQN 2.21}$$

where S_t is a Stanton Number which is assumed to be a constant for the jet. This is done by assuming a Stanton Number and then iterating the previous equations for a value of T_{SL} which satisfies the heat flux (equation 2.9) for a given value of T_{BL}. When equation 2.9 is satisfied, a heat and mass balance can be made on the liquid jet.

These equations are then integrated from the beginning to end of the jet, via a Runge-Kutta integration routine,[9] and the process is repeated for different values of the Stanton Number until the calculated outlet temperature matches the measured dewar temperature. This process is shown in Figure 6.

In early testing, while test and data reduction procedures were being developed, a number of nozzle configurations with different turbulence promoting devices in the feed tube prior to the nozzle throat were tested.[21] Results indicated that these upstream turbulence promoters had no substantial effect on jet performance (Figure 7).

$$\bullet \quad \frac{dm_L}{d_x} = \frac{W}{A} \text{ cond.}$$

$$\bullet \quad \frac{dT_{BL}}{d_x} = \frac{W}{A} \text{ cond.} \frac{(h_V - h_{LSL}) \pi D_j}{\dot{m}_L C_{PL}}$$

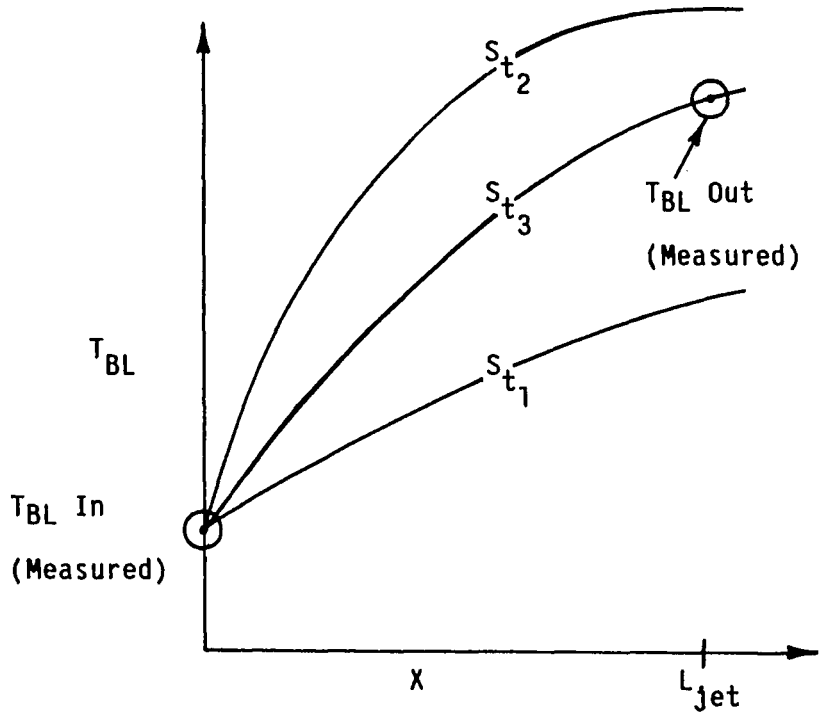

GRAPH USED TO FIND STANTON NUMBER THAT MATCHES DATA

FIGURE 6.

Nozzle A.

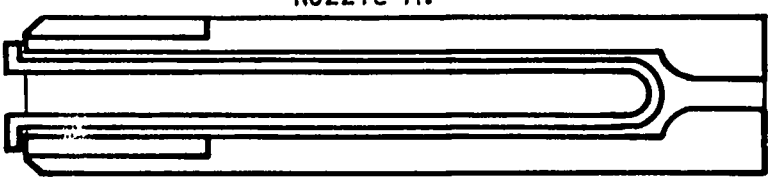

Nozzle B.

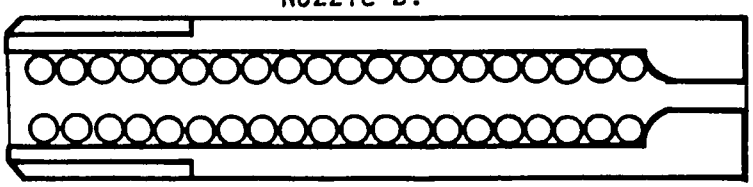

Nozzle C.

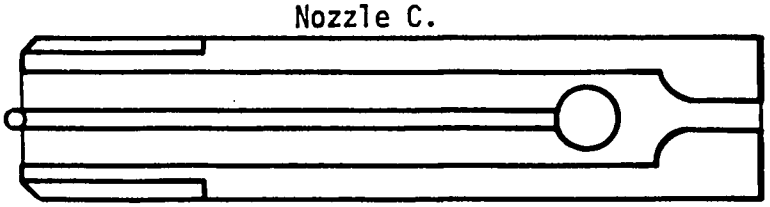

Nozzle D.

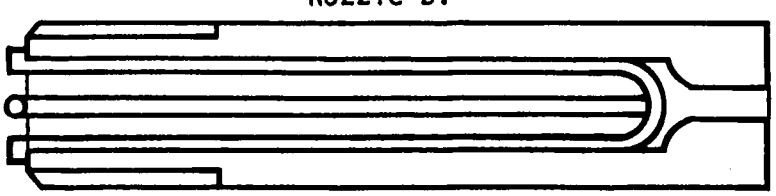

Flow is Right to Left

NOZZLES THAT PROMPTED TURBULENCE

FIGURE 7.

In order to determine the Stanton Number that correlates with the experimental data, the values of the heat transfer coefficient, H, are integrated for the jet lengths, and averaged for each test point.[22] Jet lengths of 50.8, 127, and 254 mm are tested. The mean and range of values of Stanton Numbers for each jet length (above) with .254 mm and .3683 mm diameter "turbulent" type jets are shown in Figure 8. It is recognized that there is some dependence of Stanton Numbers on jet length, although for each jet length the Stanton Number is assumed constant to reduce the test data. Because of this, a more reasonable way of presenting the mean values of the data for the different jet lengths are as constant-average-values for the entire jet lengths as shown in Figure 9.

Assuming that the average Stanton Number Value for the 127 mm jet length is comprised from 1) the average value over the first 50.8 mm (which is known from the 50.8 mm jet data), and 2) the average value of Stanton Number over the 50.8 mm to 127 mm range, the value over the 127 mm length can easily be calculated based on equal areas. That is:

$$S_{t\ 0-2} \times 2 + S_{t\ 3-5} \times 3 = S_{t\ 0-5} \times 5 \qquad \text{EQN 2.22}$$

or

$$S_{t\ 3-5} = \frac{S_{t\ 0-5} \times 5 - S_{t\ 0-2} \times 2}{3} \qquad \text{EQN 2.23}$$

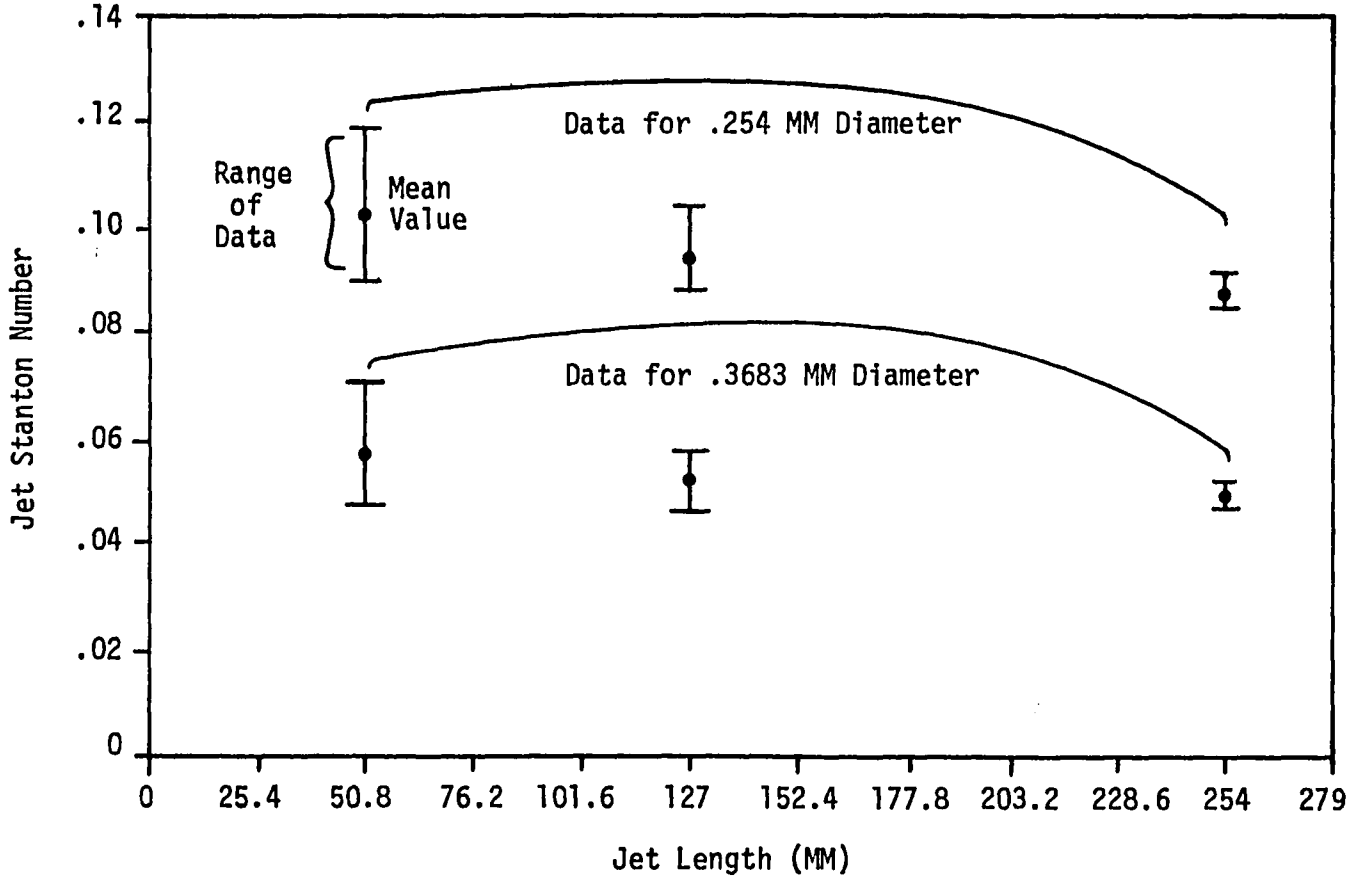

STANTON NUMBER MEAN VALUE AND RANGE

FIGURE 8.

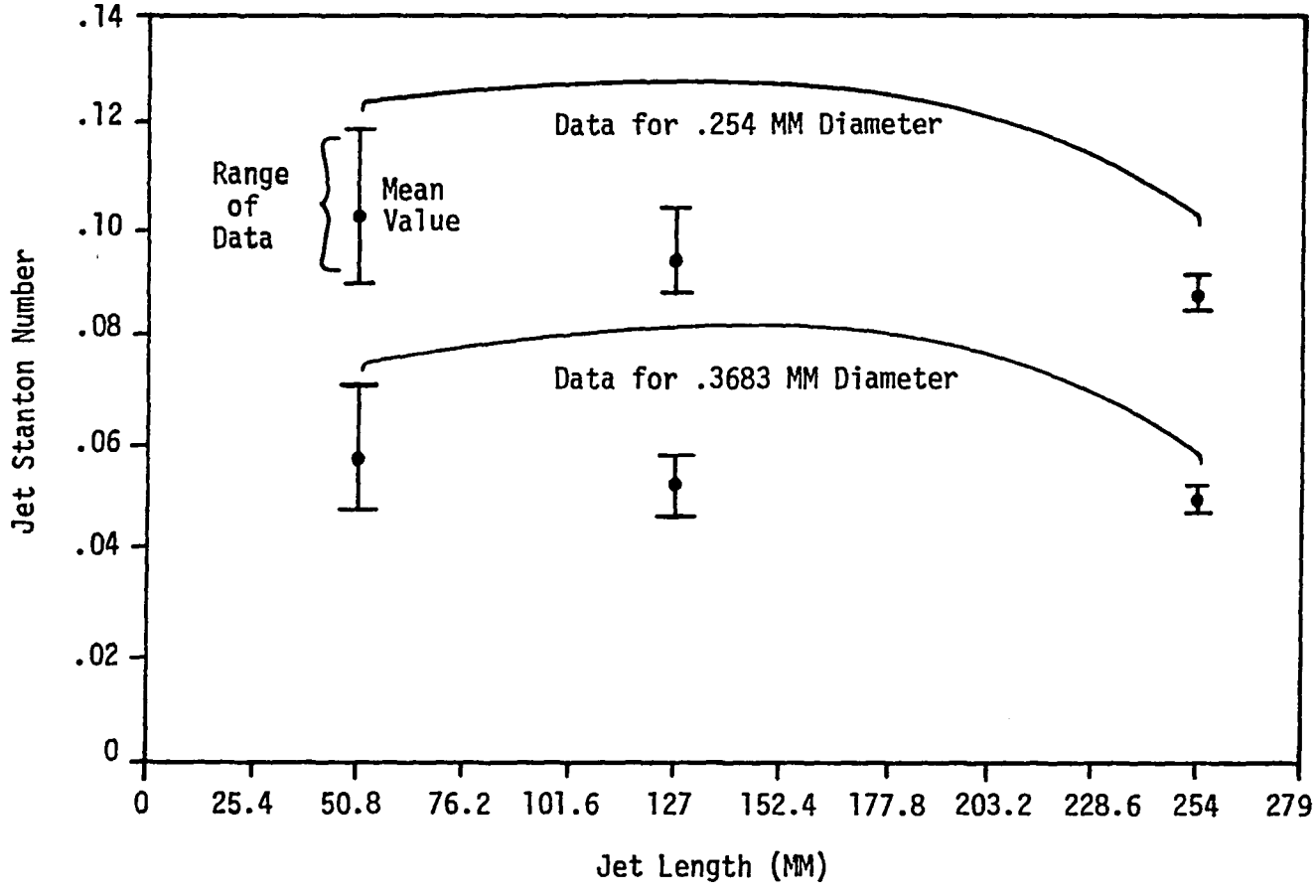

STANTON NUMBER MEAN VALUE AND RANGE

FIGURE 8.

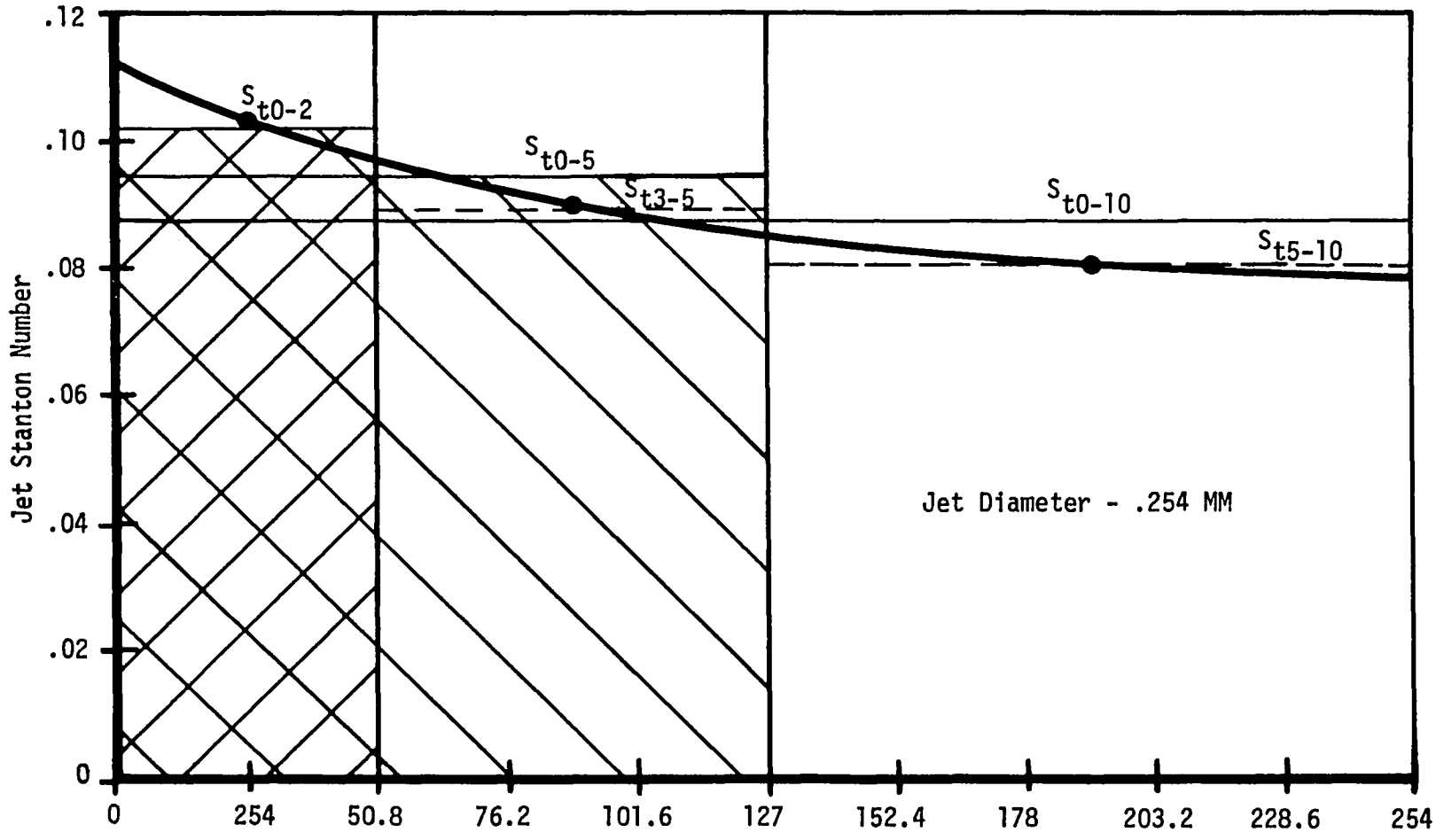

JET STANTON NUMBERS VS. DISTANCE FROM EJECTOR

FIGURE 9.

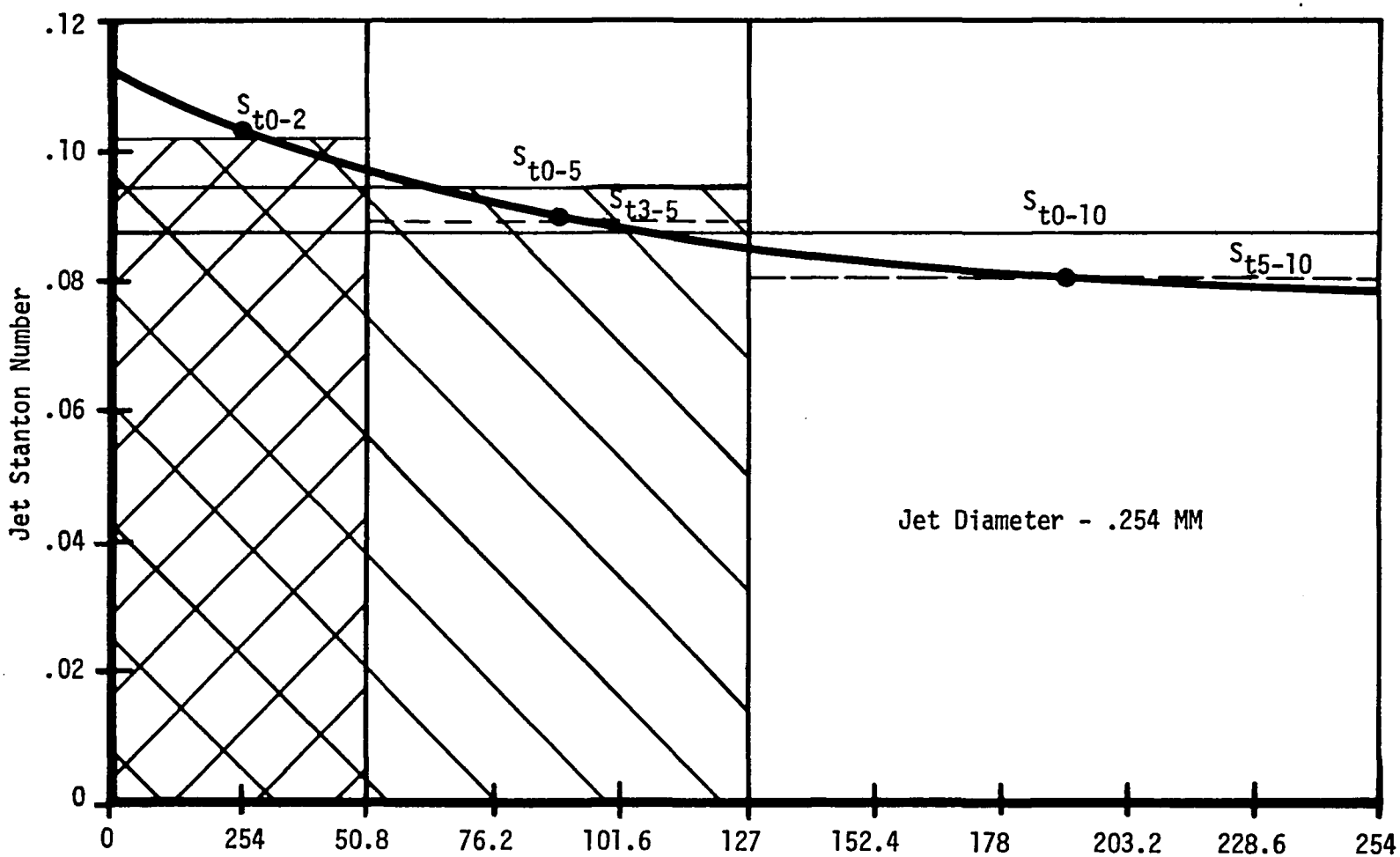

JET STANTON NUMBERS VS. DISTANCE FROM EJECTOR

FIGURE 9.

with $S_{t\ 0-2} = 0.102$, and $S_{t\ 0-5} = 0.094$,

$S_{t\ 3-5}$ is calculated to be 0.0887.

It is also found that

$$S_{t\ 5-10} = \frac{S_{t\ 0-10} \times 10 - S_{t\ 0-5} \times 5}{5} \qquad \text{EQN 2.23.1}$$

and that with $S_{t\ 0-10} = 0.087$, $S_{t\ 5-10} = 0.08$

A curve is then drawn through the three data points at their average distance from the injector, i.e., at 25.4 mm for $S_{t\ 0-2}$, at 88.9 mm for $S_{t\ 2-5}$, and at 190.5 mm for $S_{t\ 5-10}$. This curve then represents the Stanton Numbers as a function of distance from the injector. The same procedure was carried out for the .3683 mm "turbulent" jets. The resulting Stanton Numbers vs. distance for both the .3683 mm and 2.54 mm turbulent jets are shown in Figure 10.

With the Stanton Number based on liquid interfacial relative velocity, we can say that the heat transfer coefficient calculated by this technique will approach zero as the interfacial velocity approaches zero. We can also say that pure conduction through the liquid jet would result in heat transfer coefficients in the .271 - .677 cal./sec.-cm^2°K range which is a minimum value. For this reason, a minimum value of the average heat coefficient for each jet length is

deduced from the test data by plotting the average heat transfer coefficient as a function of average heat flux for each data point and extrapolating the data to the point of zero heat flux. Several data cases are shown in Figure 11 for the .254 mm jet diameter.

From Miyazaki et al.[6] it is postulated that the form of the equation showing the X dependence of this minimum value of H should be

$$H_{MIN} = H_{MIN\infty} \left(1 + \frac{K}{X}\right) \qquad \text{EQN 2.24}$$

where:

$$H_{MIN\infty} = S_{tMIN} \cdot \rho_L \cdot Cp_L \cdot V_L$$

and S_{tMIN} is a Stanton Number based on jet velocity, and K is a constant, both to be determined from the test data.

The extrapolated values of H are averaged over the different jet lengths. The value of H for the 127 mm jet is 13.55 cal./sec.-cm^2 °C, and the value of H for the 254 mm jet is 8.13 cal./sec.-cm^2 °C, so the average value of H over the 127 mm to 254 mm increment of jet length is 10.84 cal./sec.-cm^2 °C.

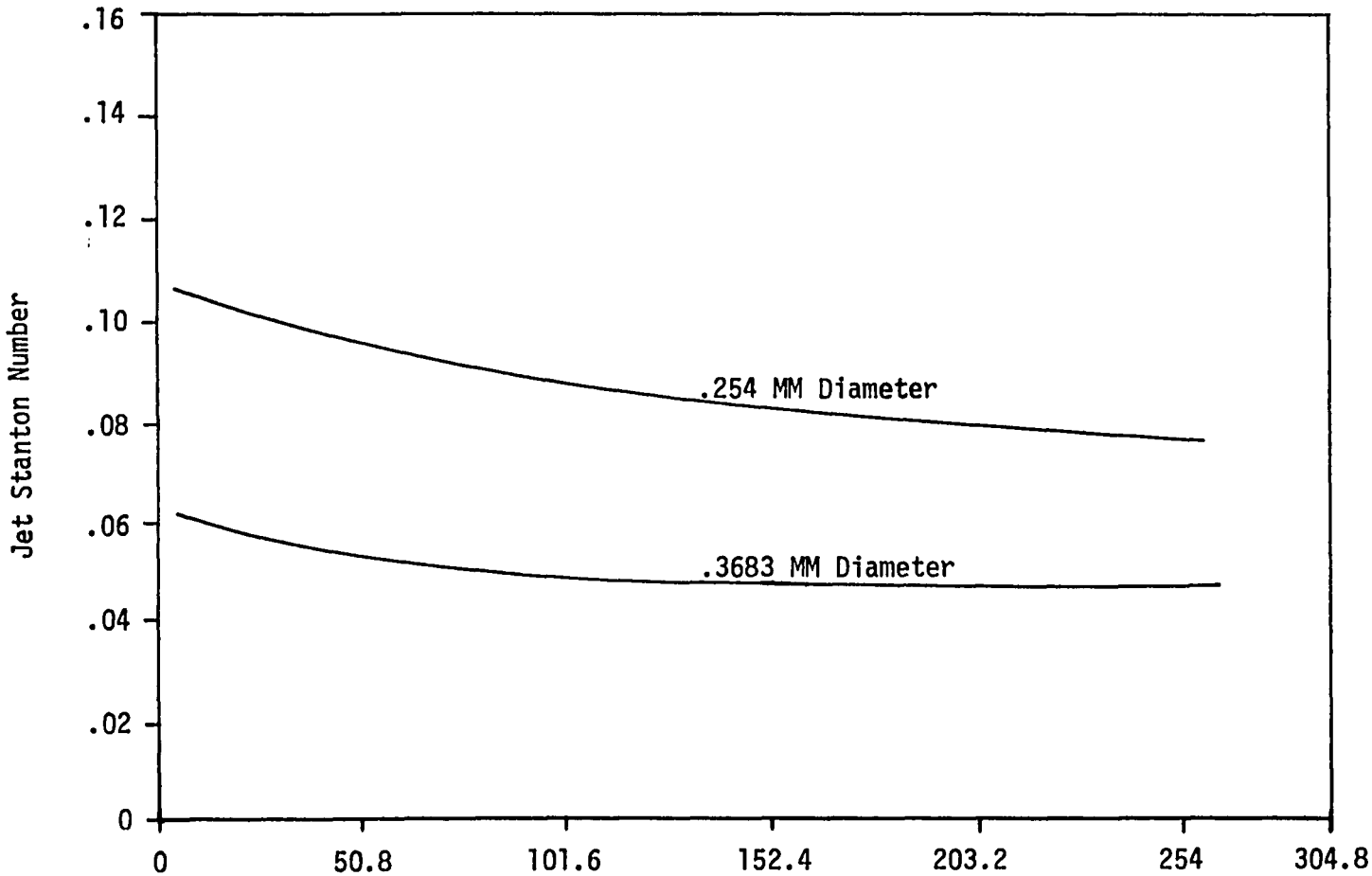

JET STANTON NUMBER FOR .254 AND .3683 MM DIAMETER NOZZLES

FIGURE 10.

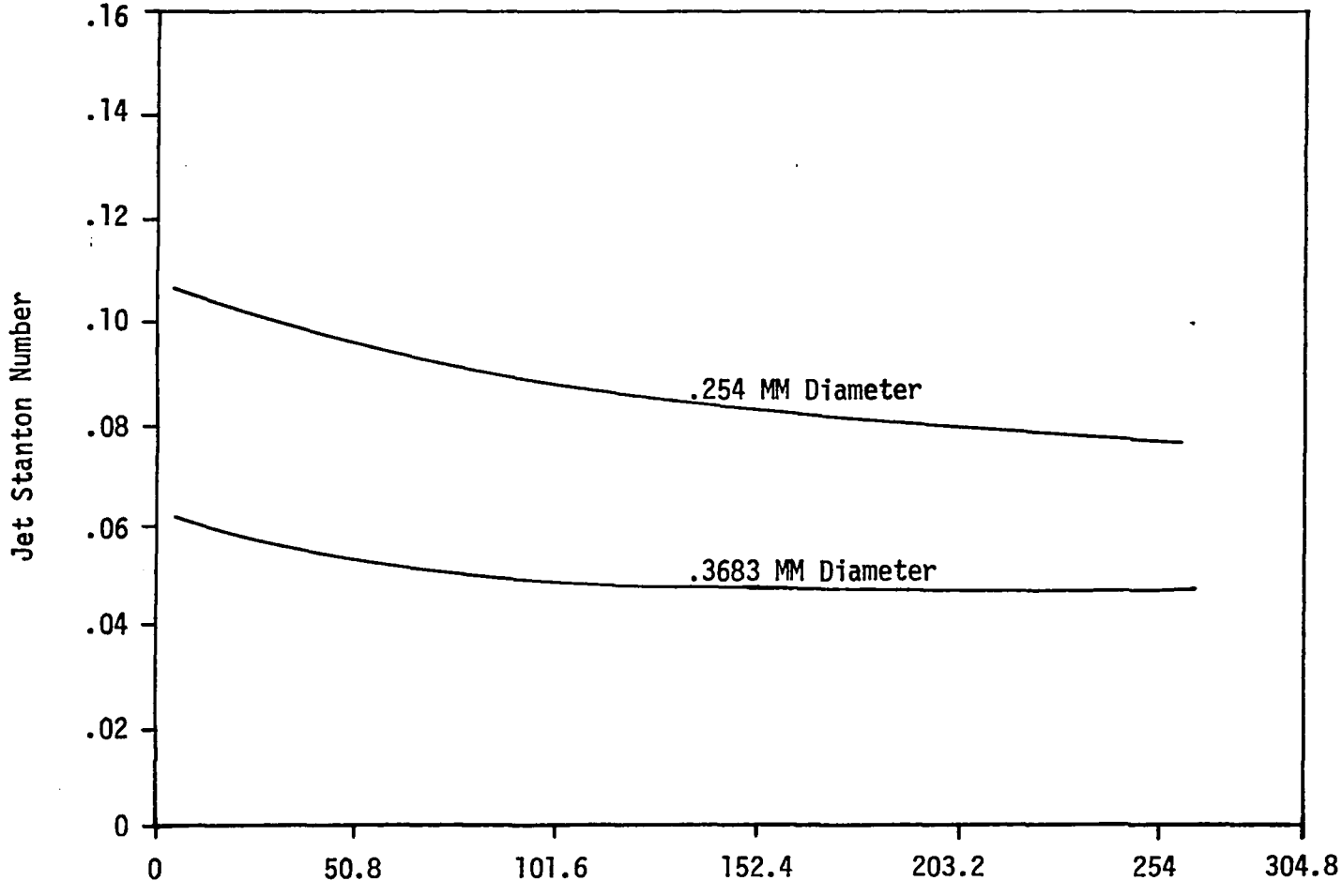

JET STANTON NUMBER FOR .254 AND .3683 MM DIAMETER NOZZLES

FIGURE 10.

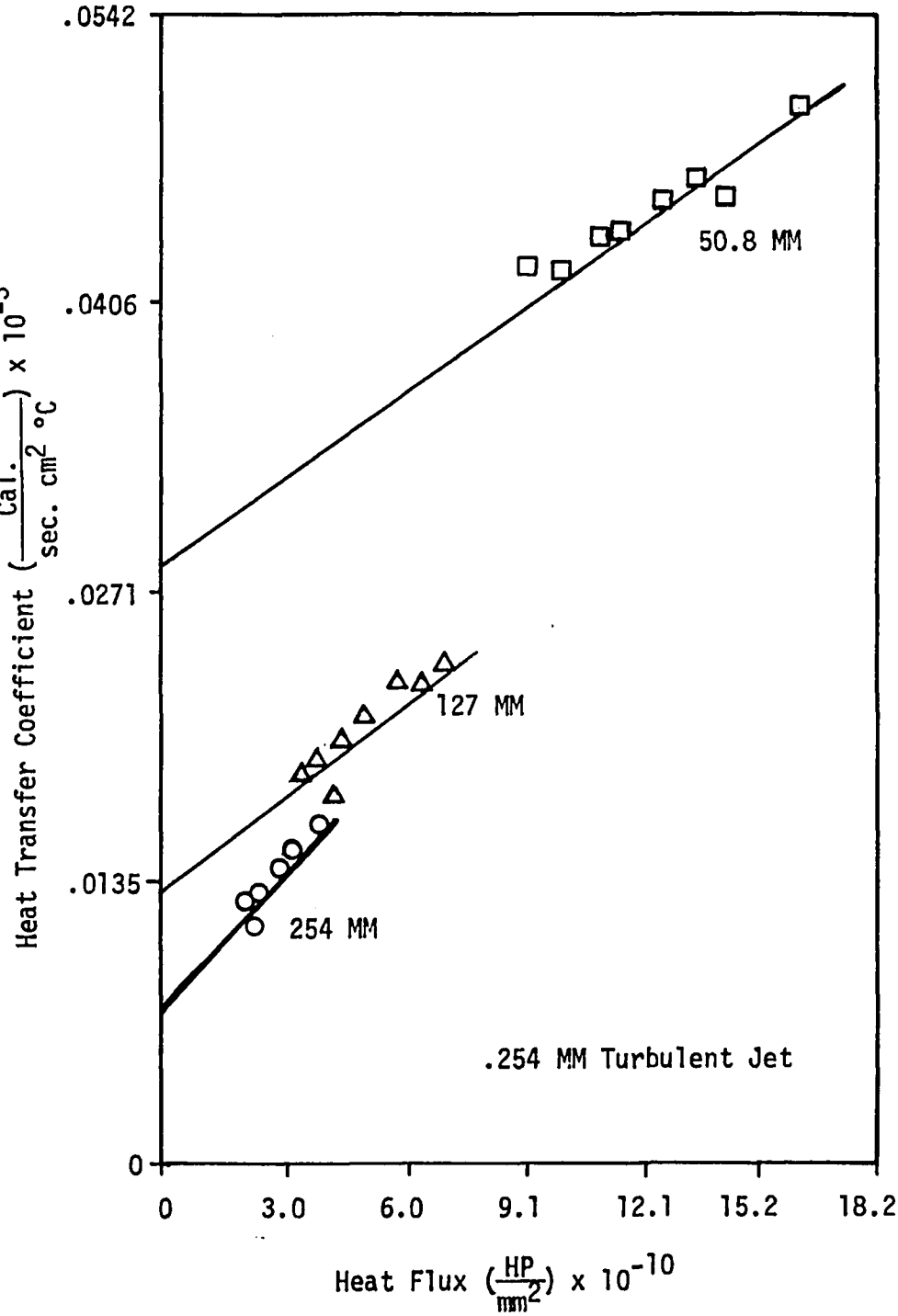

HEAT TRANSFER COEFFICIENT VS. HEAT FLUX

FIGURE 11.

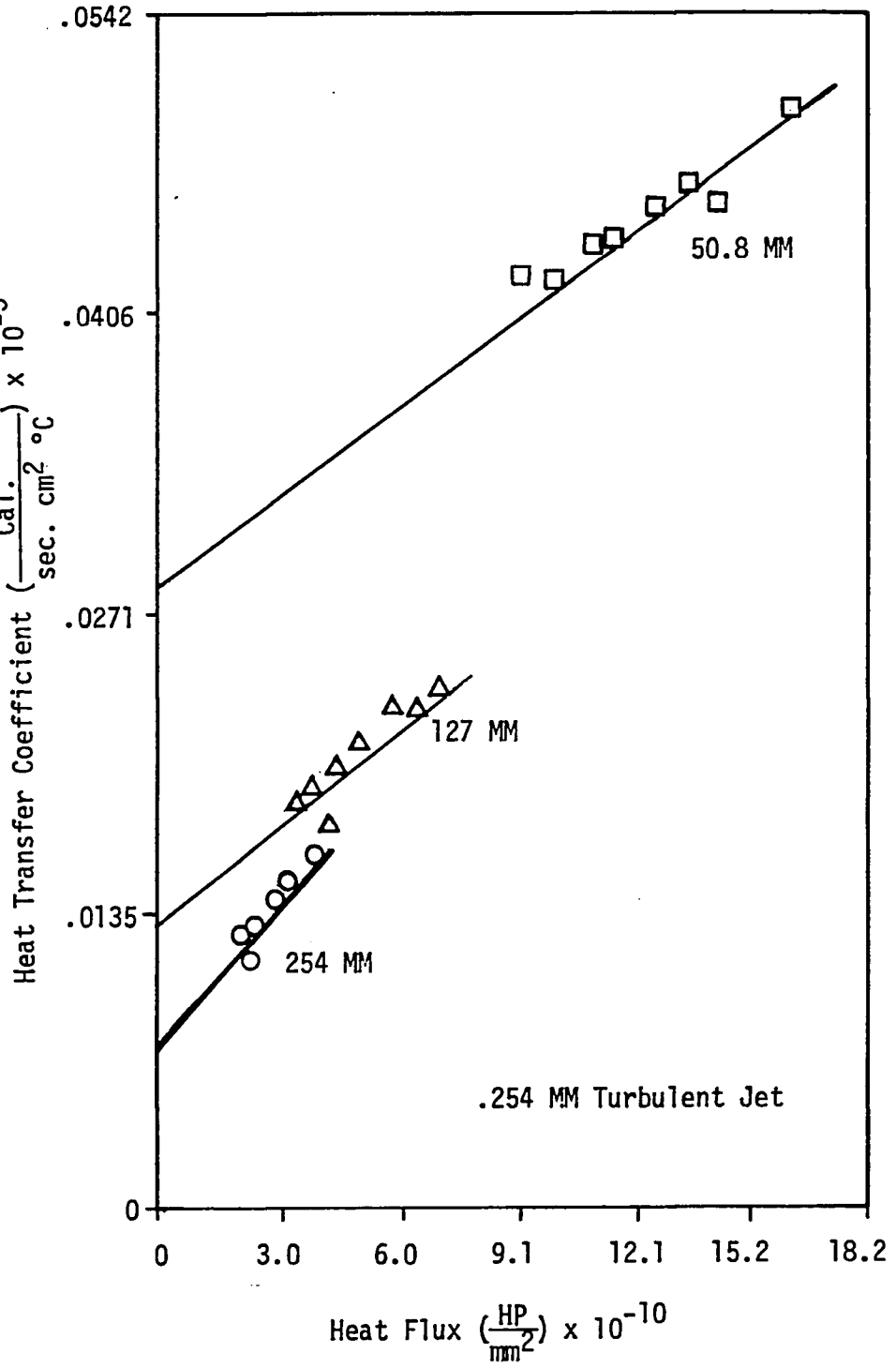

HEAT TRANSFER COEFFICIENT VS. HEAT FLUX

FIGURE 11.

The expression for H, (equation 2.24), can be integrated over a section of jet length[9] to be

$$\frac{H_{X_1} - X_2}{H_\infty} = \frac{1}{X_2 - X_1}\left(1 + \frac{K}{X_2 - X_1} \ln\frac{X2}{X_1}\right) \quad \text{EQN 2.25}$$

where

X_1 = Jet length at minimum edge of incremental jet length.

X_2 = Jet length at maximum edge of incremental jet length.

By utilizing a minimum value of X_1 = .254 mm for a.) the 254 mm jet length and its H value of 8.13, and b.) the 127 mm to 254 mm jet length and its H value of 10.84, the value of $H_{MIN\infty}$ and K are calculated to be

$$H_{MIN\infty} = 1.355 \text{ cal/sec.-cm}^2 \text{ °C} \quad \text{EQN 2.26}$$

$$K = 184.66 \text{ mm}$$

For the test conditions with water ρ_L = 63, V_L = 98, Cp = 1,

$$H_{MIN\infty} = 1.355 \text{ corresponds to } S_{tMIN} = 0.162.$$

So, the expression for S_{tMIN} for the .254 mm jet is

$$S_{tMIN} = 0.162\left(1 + \frac{184.66}{25.4X + .254}\right) \quad \text{EQN 2.26.1}$$

where X is the distance from the injector in millimeters.

The corresponding data from the steam and water testing on the .3683 mm turbulent jet is shown in Figure 12. From these data, the minimum Stanton Number is,

$$S_{tMIN} = 0.202 \left(1 + \frac{110.7}{25.4X + .254}\right) \qquad \text{EQN 2.27}$$

The graphs for the two expressions are shown in Figure 13.

The data for jet Stanton Number based on interfacial relative velocity (shown in Figure 10.) along with the values of S_{tMIN} are used in reducing the data. For this data, profiles are generated of T_{BL} and T_{SL} as a function of jet length at various liquid inlet and saturated steam temperatures. The quantities are shown on Figures 14. and 15. for the .254 and .3683 mm diameter jets for an injection pressure drop of 552 kPa, a liquid inlet temperature of 280.5°K, and a steam temperature of 305.5°K.

Plots showing the calculated jet outlet temperatures as a function of liquid inlet and steam temperature at jet lengths of 50.8, 127, and 254 mm are shown in Figures 16., 17., and 18. for the .254 mm diameter jets, and in Figures 19., 20., and 21. for the .3683 mm jet. Also shown on these plots are actual test points and the error in the predicted vs. measured liquid temperature rise. From the indicated error on the 50.8 and 127 mm jet lengths, the errors are considered to be small ($\pm$15% or less).

For Figures 16.-21., the arrow tip locates test steam and liquid temperatures, as well as predicted dewar temperature. The x locates measured dewar temperature for steam and liquid conditions that are defined by the arrow tip. Error in predicted liquid temperature is shown in parentheses. A potential cause of the error is discussed in Section 2.4.

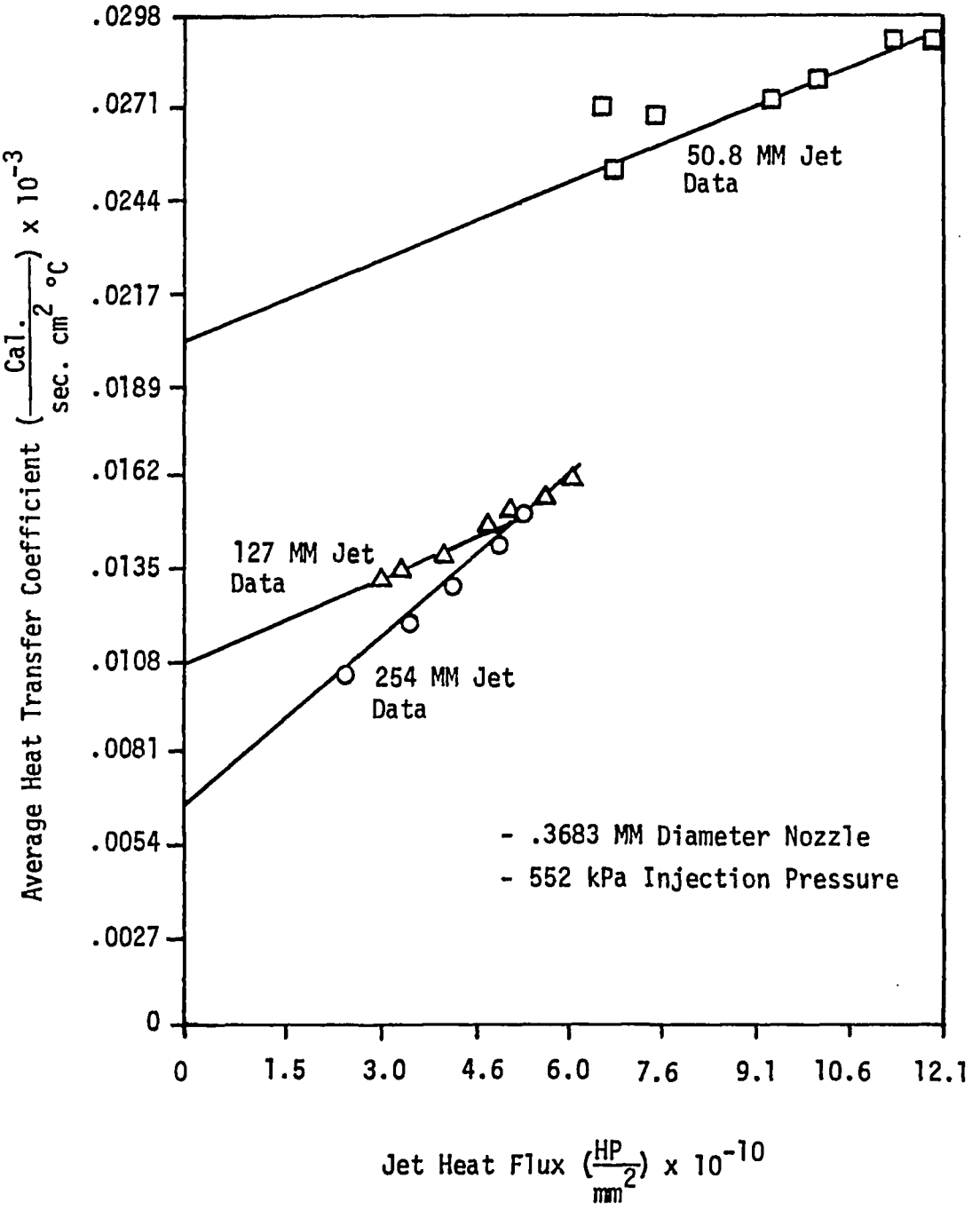

AVERAGE HEAT TRANSFER COEFFICIENT VS.
JET HEAT FLUX FOR STEAM/WATER DATA

FIGURE 12.

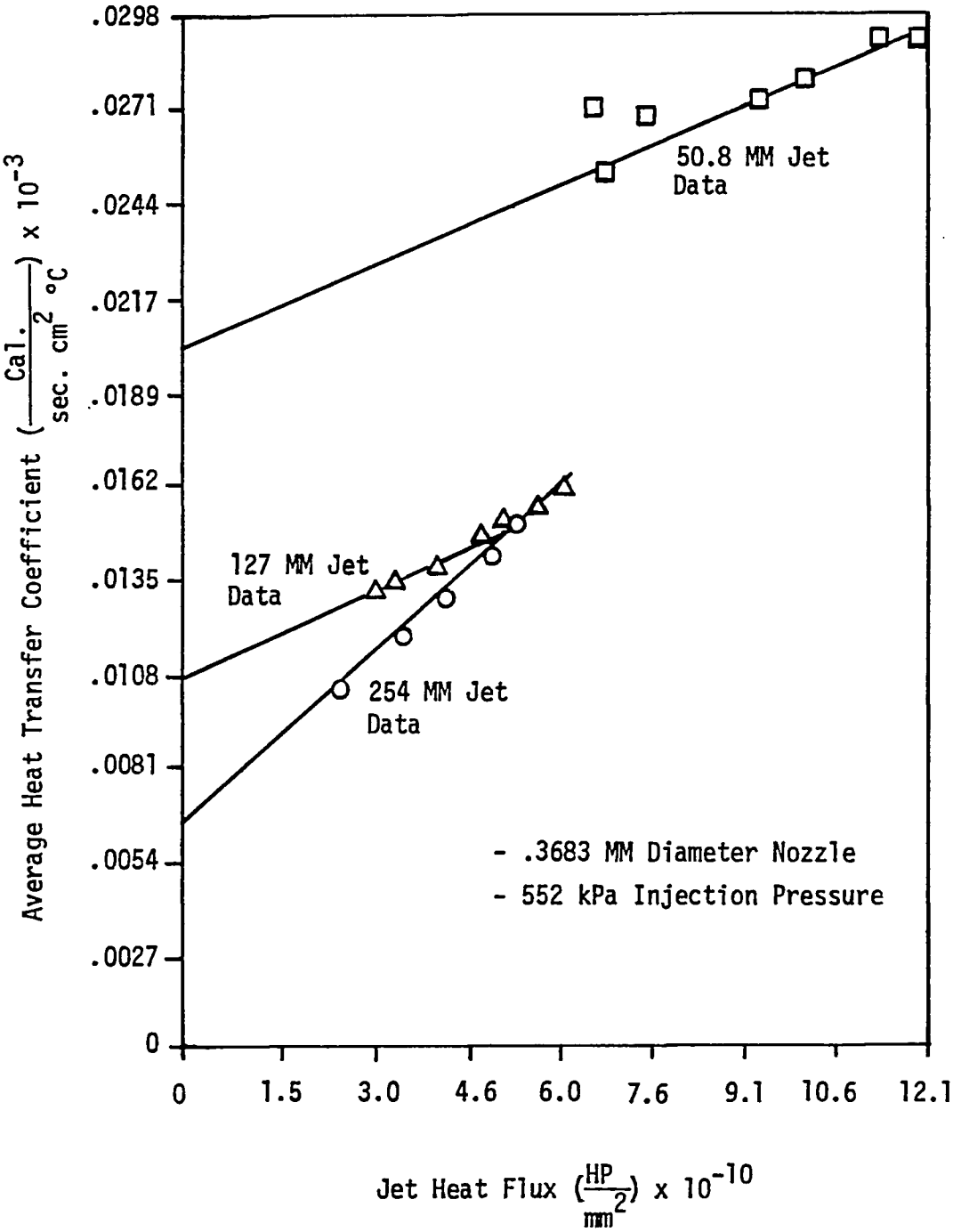

AVERAGE HEAT TRANSFER COEFFICIENT VS.
JET HEAT FLUX FOR STEAM/WATER DATA

FIGURE 12.

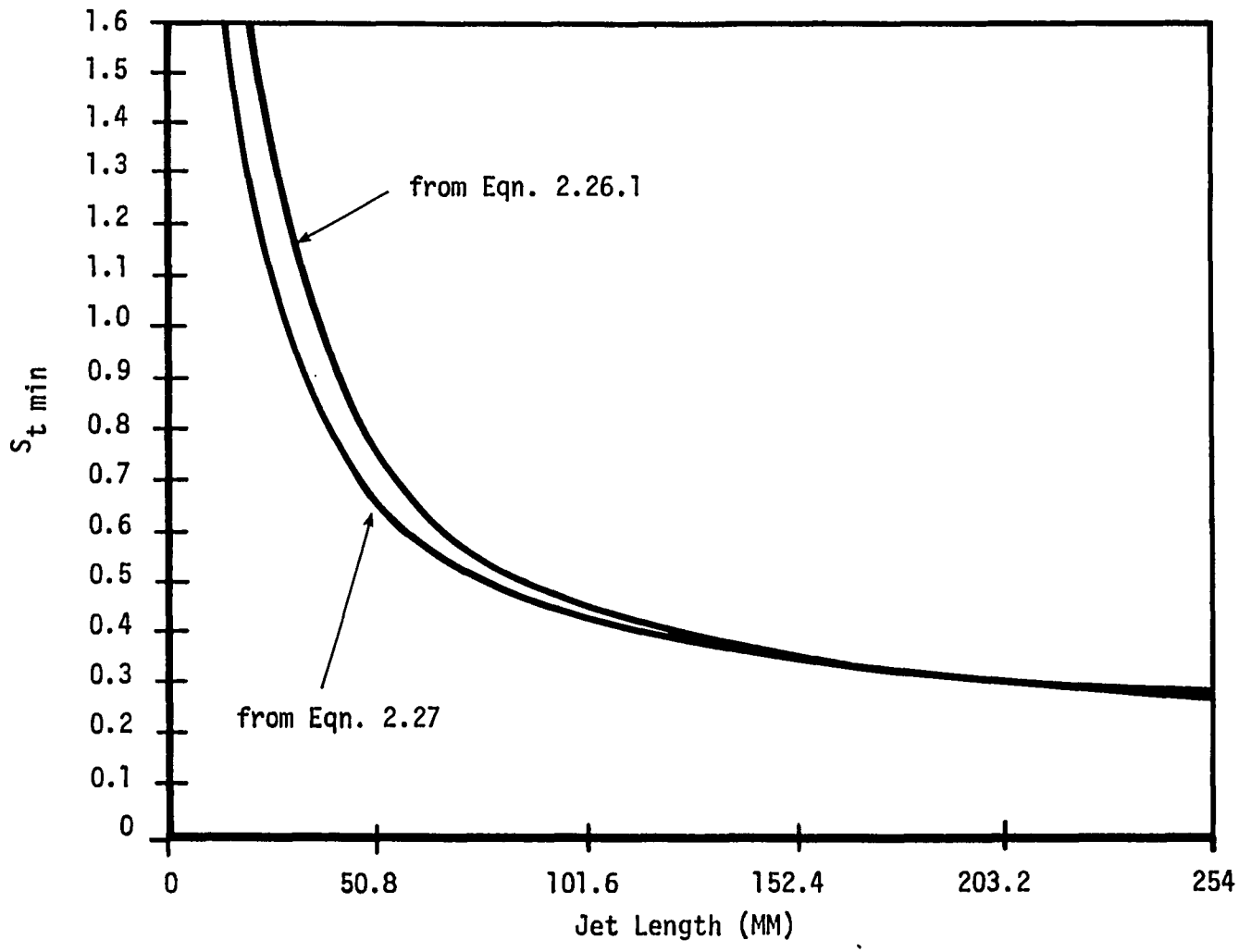

STANTON NUMBER AT ZERO HEAT FLUX FOR STEAM/WATER DATA
FIGURE 13.

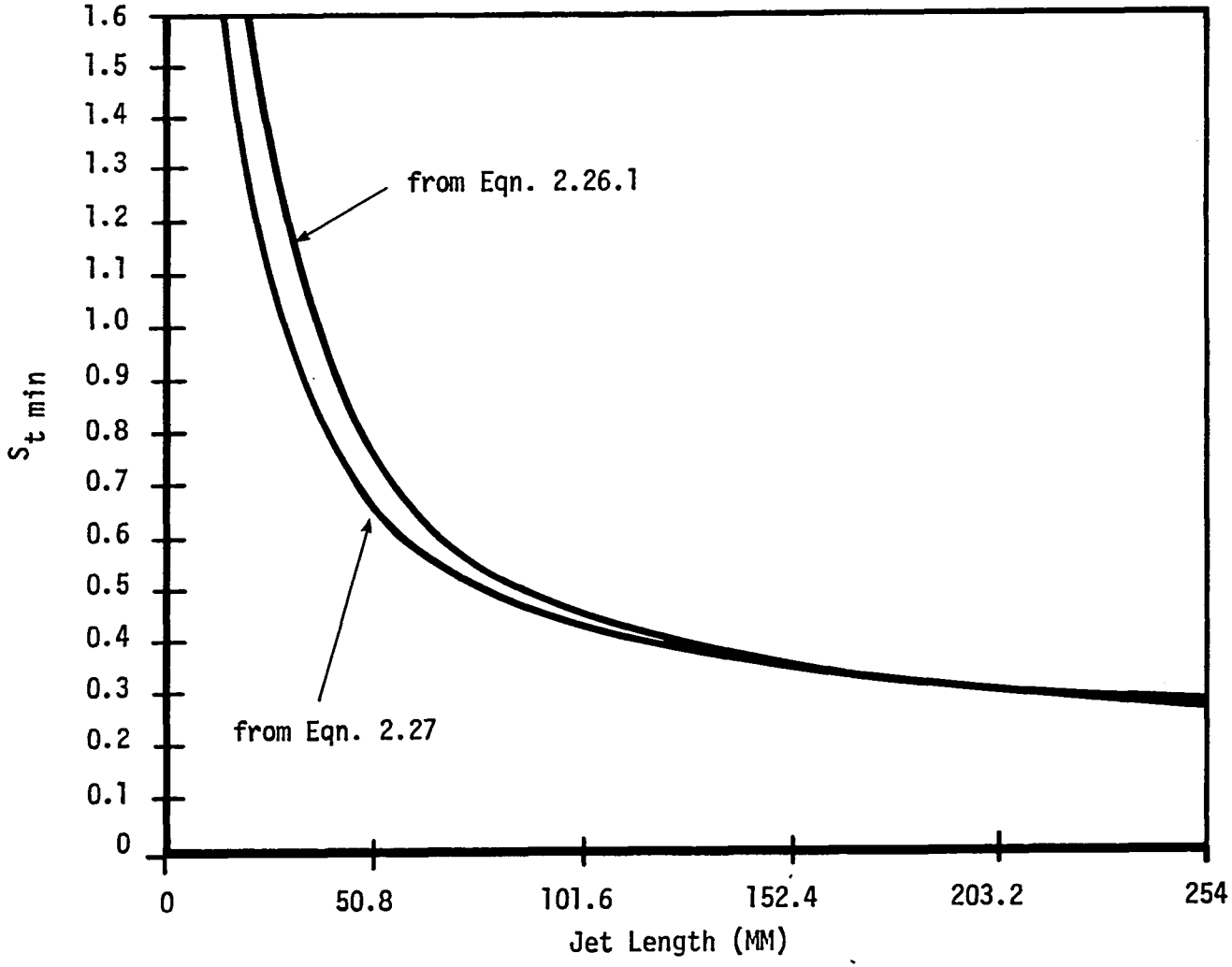

STANTON NUMBER AT ZERO HEAT FLUX FOR STEAM/WATER DATA
FIGURE 13.

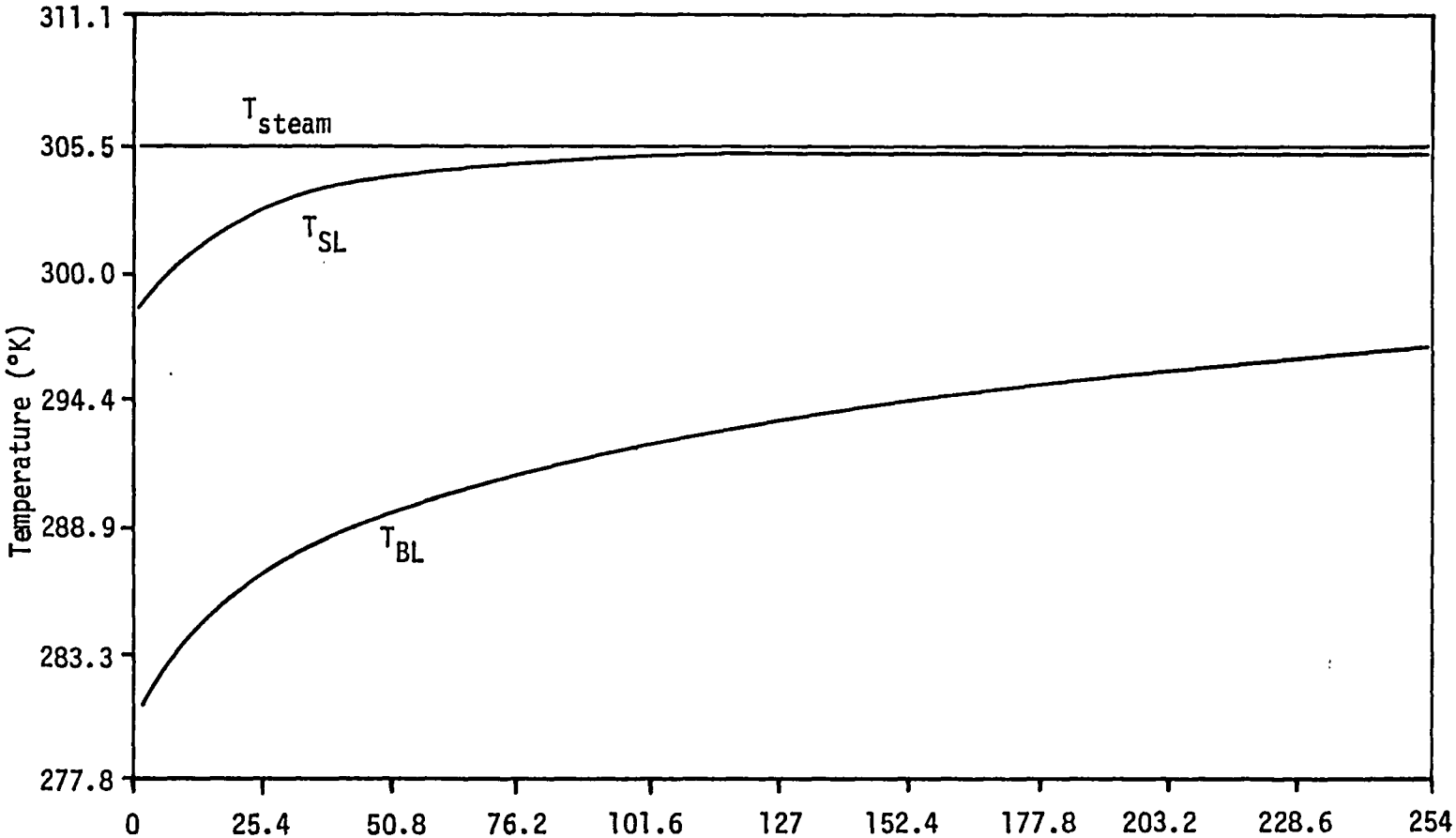

JET TEMPERATURE PROFILES - .3683 MM NOZZLE

FIGURE 14.

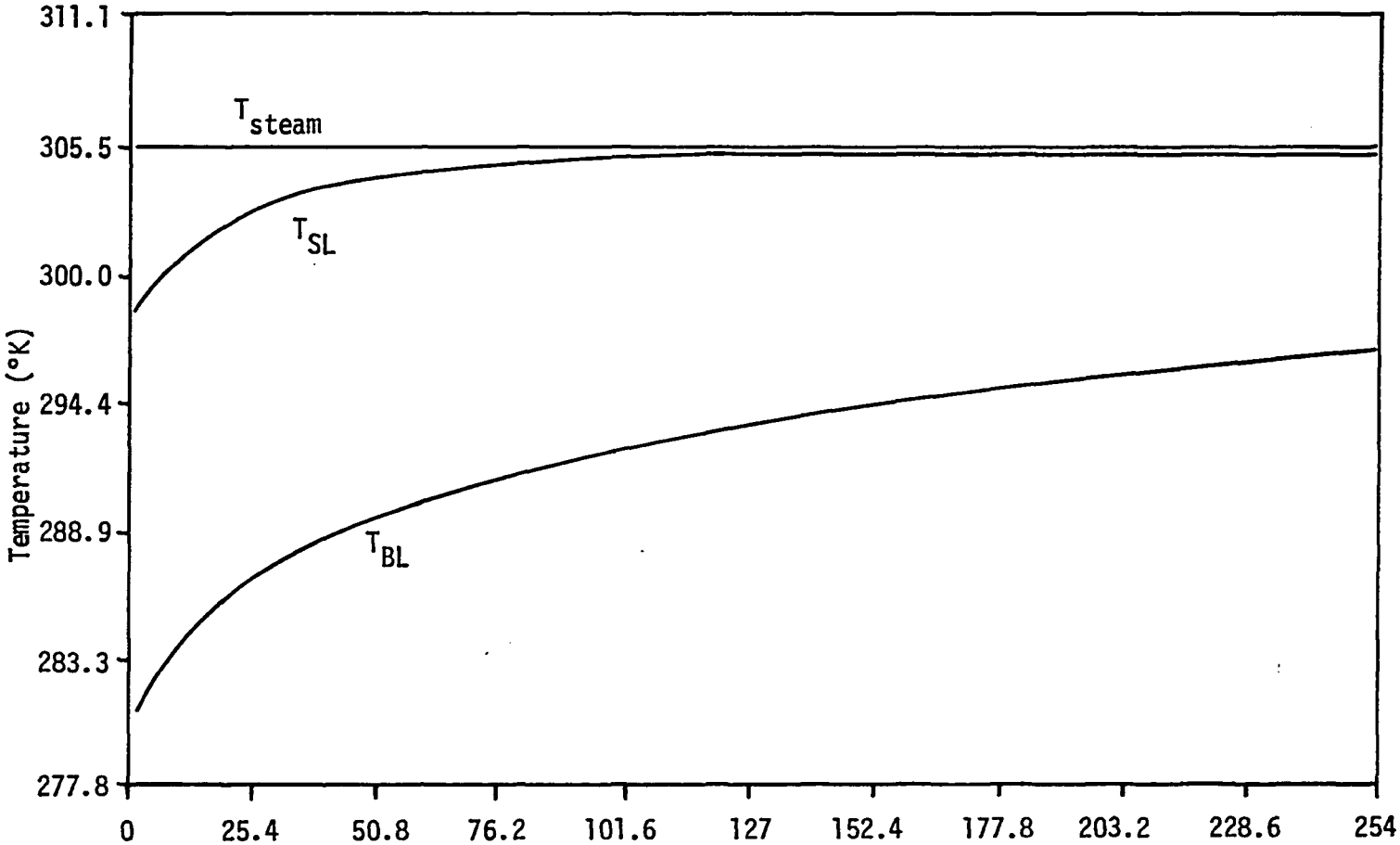

JET TEMPERATURE PROFILES - .3683 MM NOZZLE

FIGURE 14.

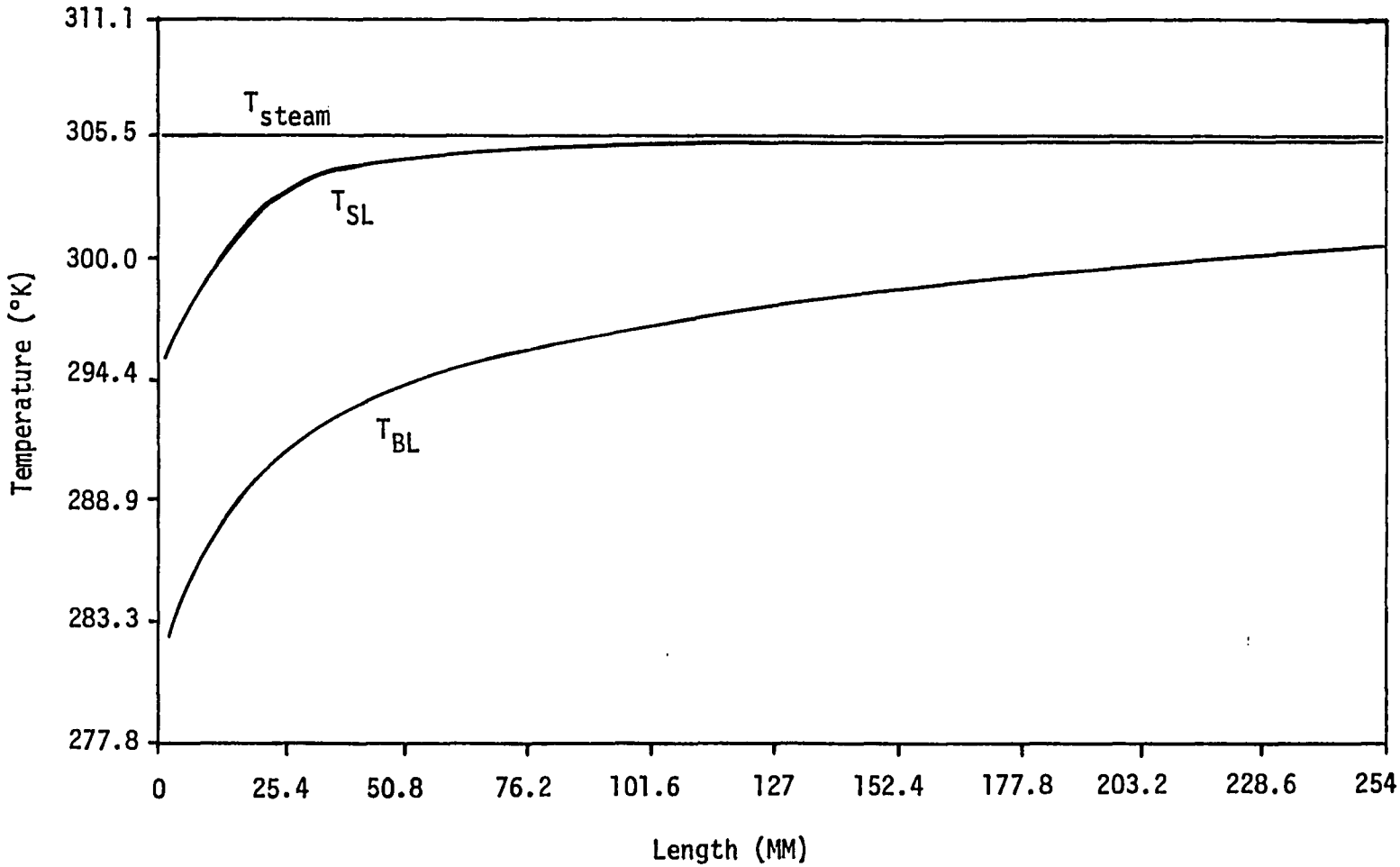

JET TEMPERATURE PROFILES - .254 MM NOZZLE

FIGURE 15.

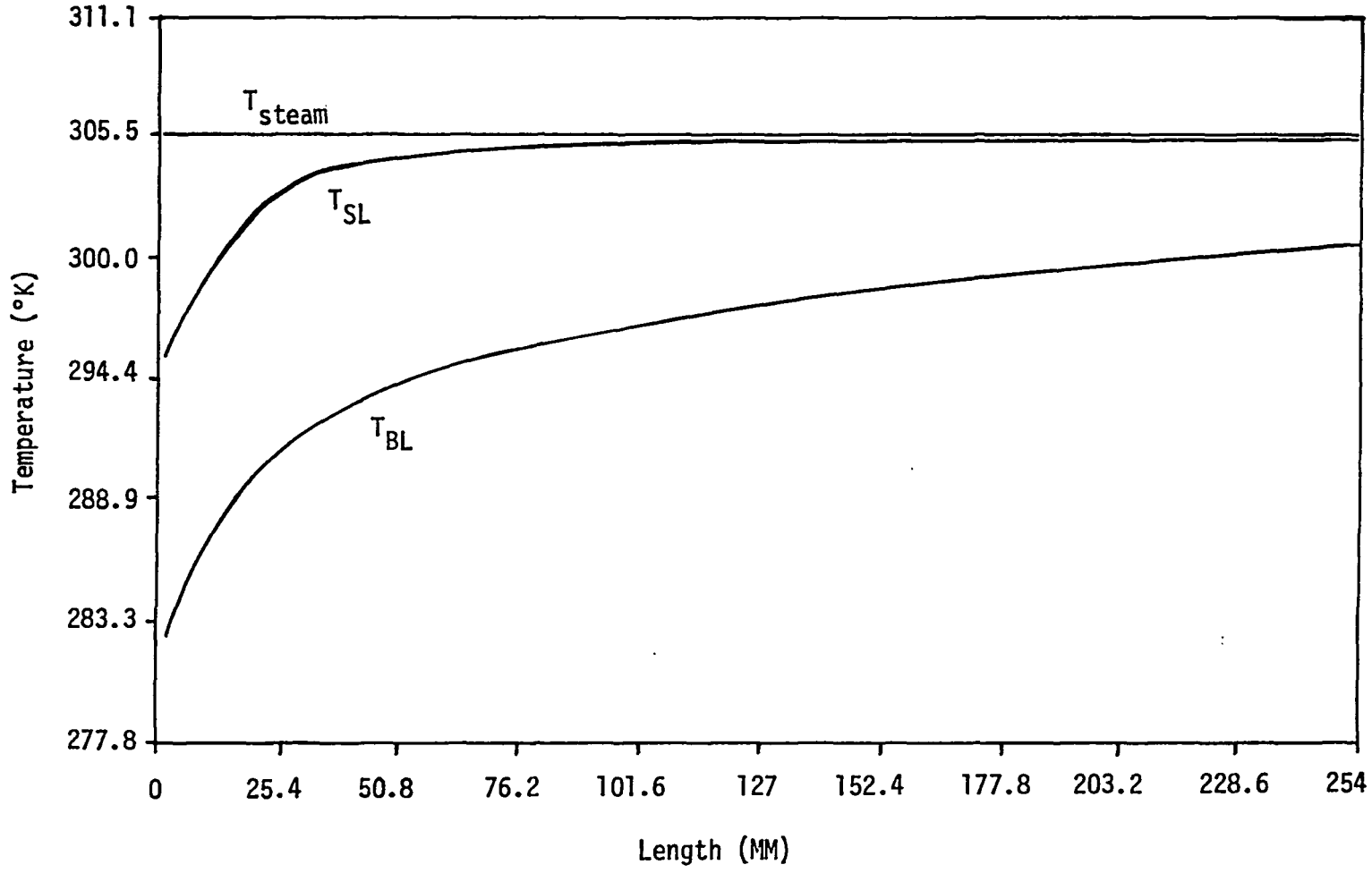

JET TEMPERATURE PROFILES - .254 MM NOZZLE

FIGURE 15.

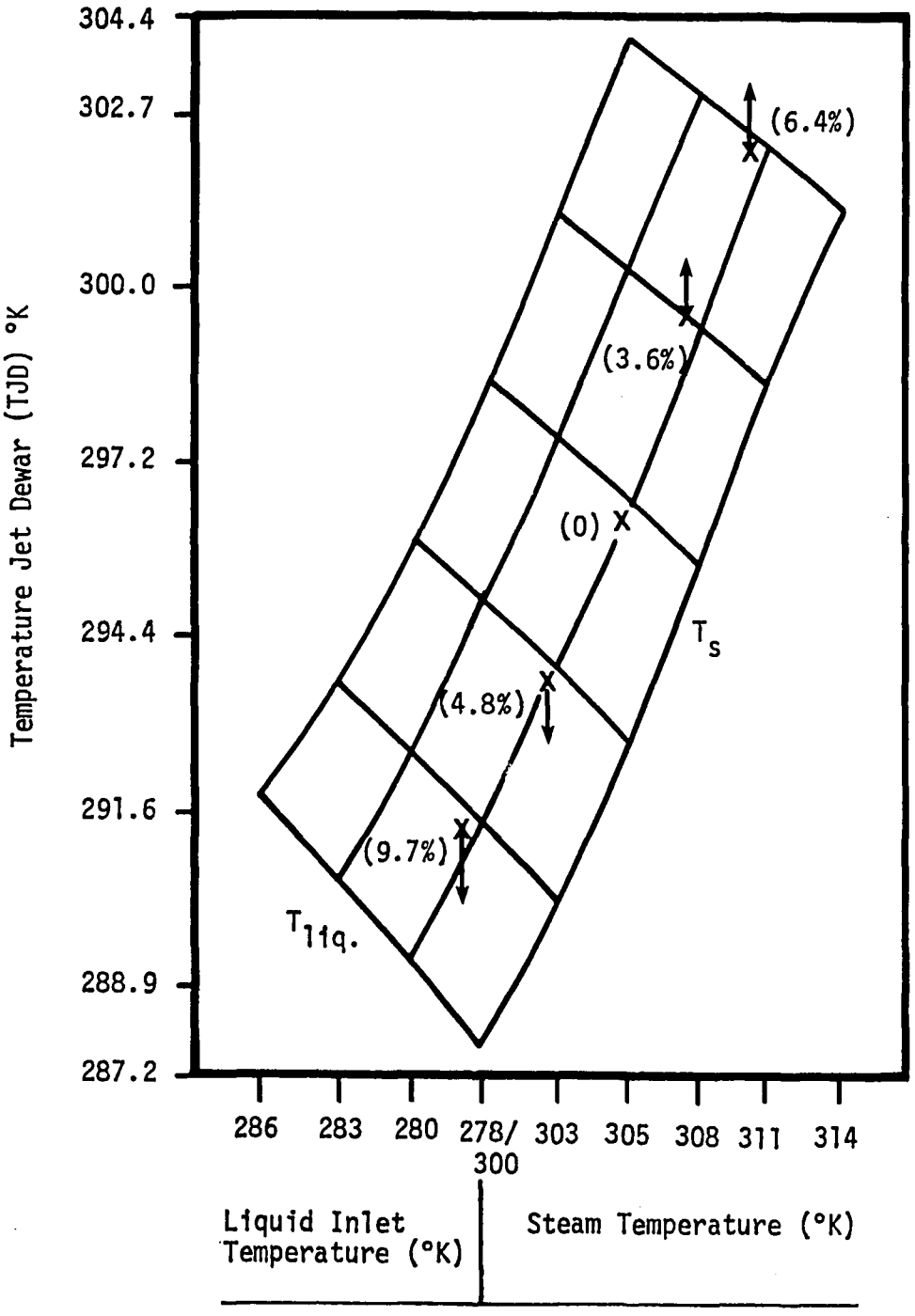

.254 MM DIAMETER NOZZLE FOR 50.8 JET LENGTH

FIGURE 16.

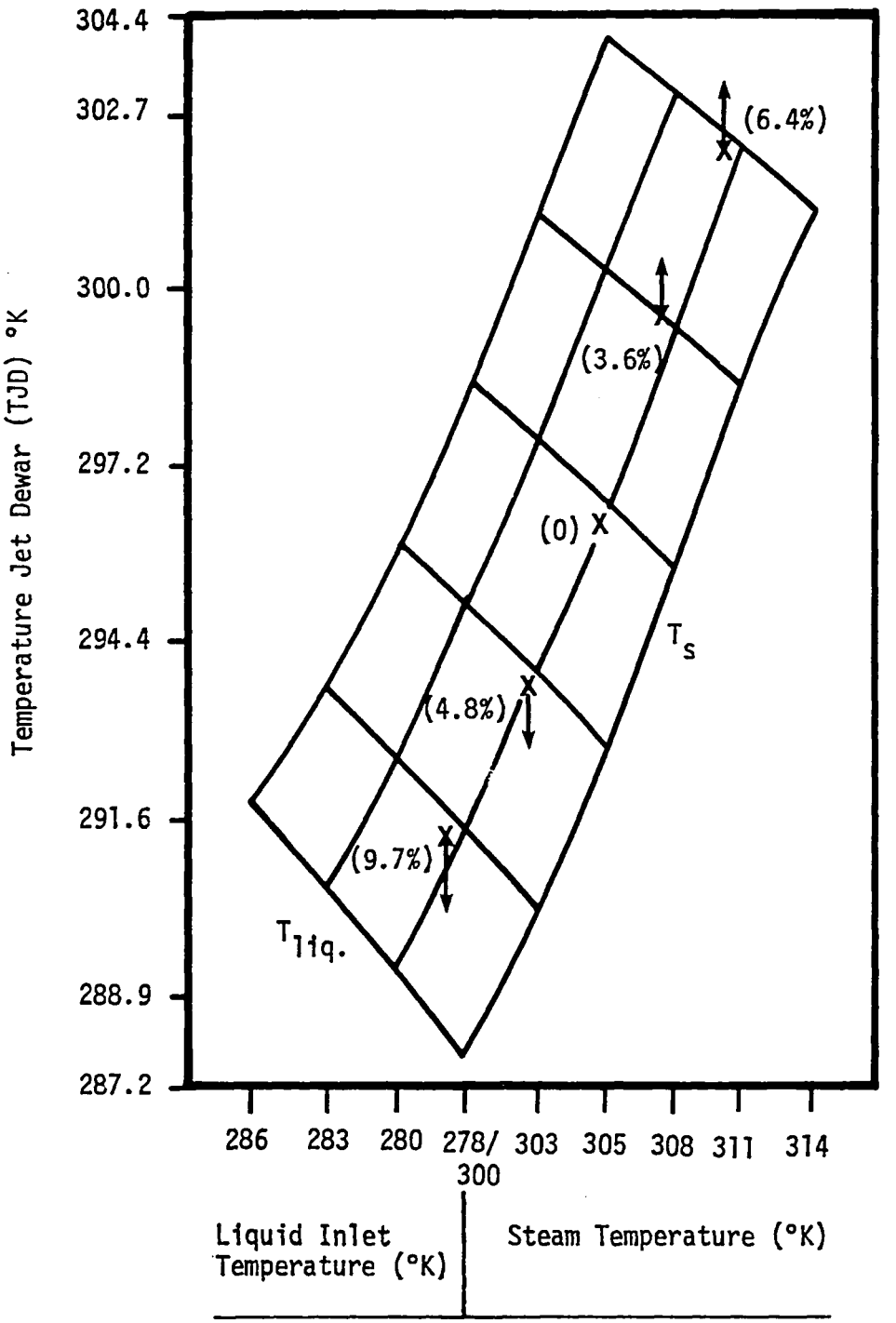

.254 MM DIAMETER NOZZLE FOR 50.8 JET LENGTH

FIGURE 16.

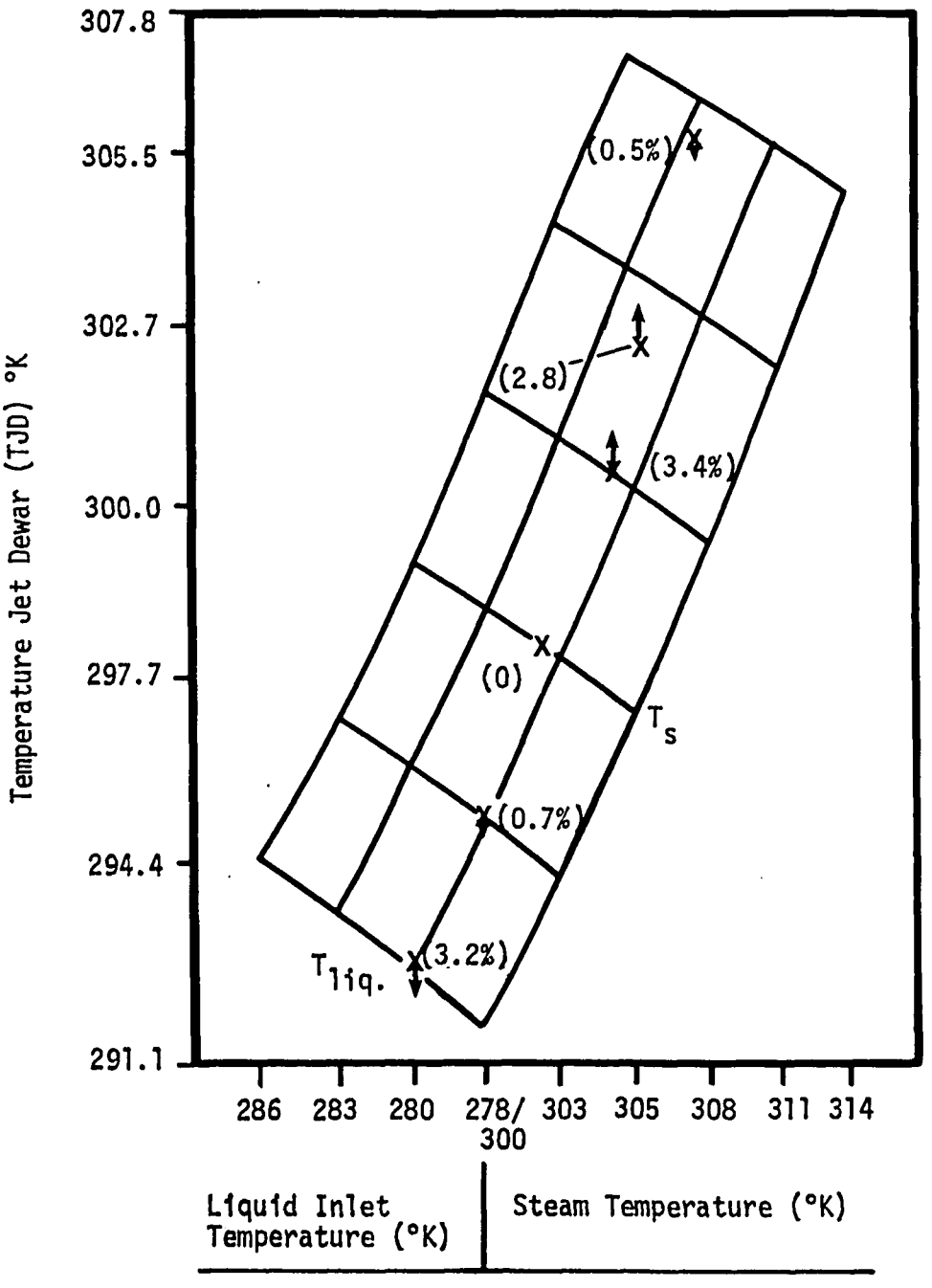

.254 MM DIAMETER NOZZLE FOR 127 MM JET LENGTH

FIGURE 17.

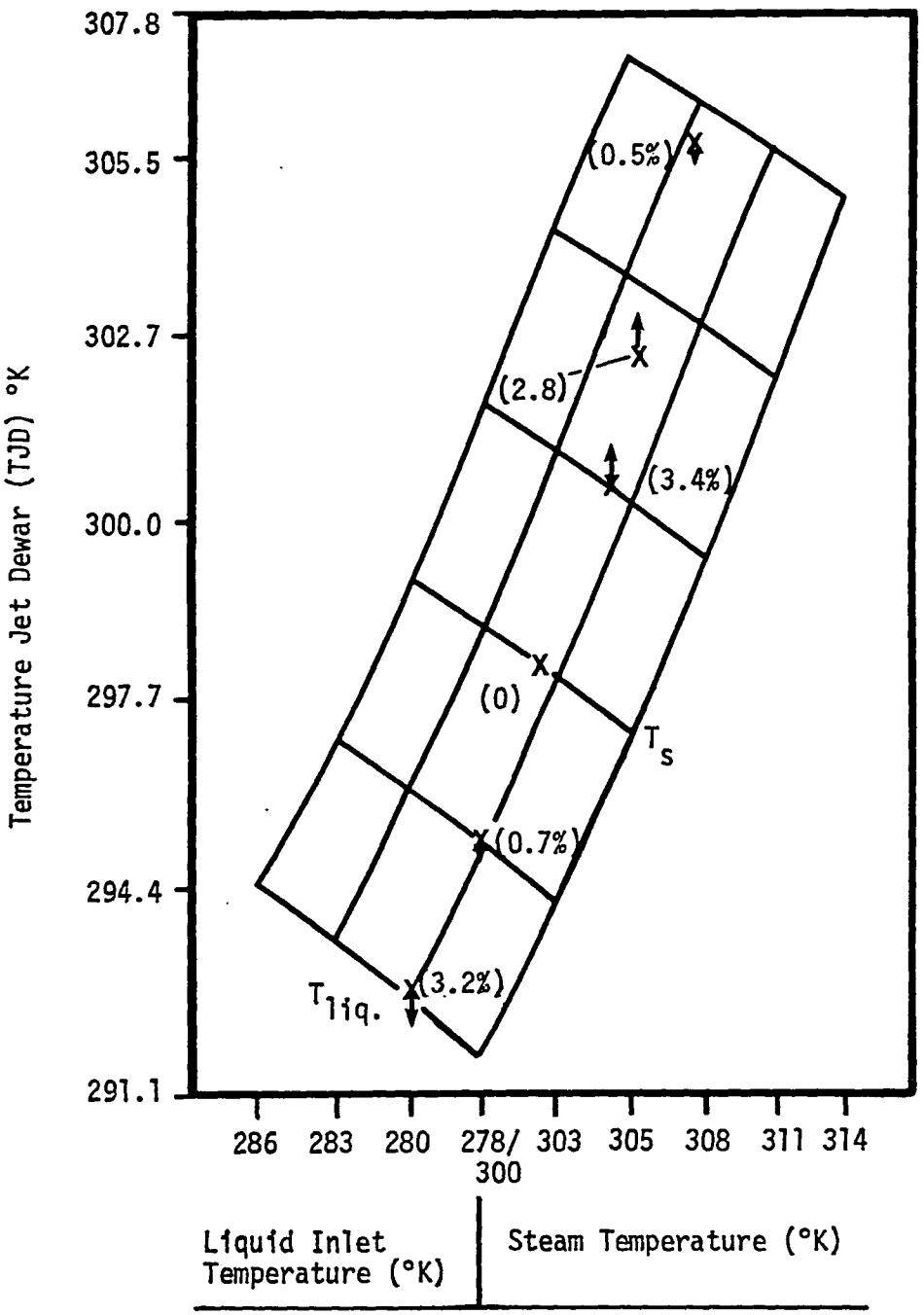

.254 MM DIAMETER NOZZLE FOR 127 MM JET LENGTH

FIGURE 17.

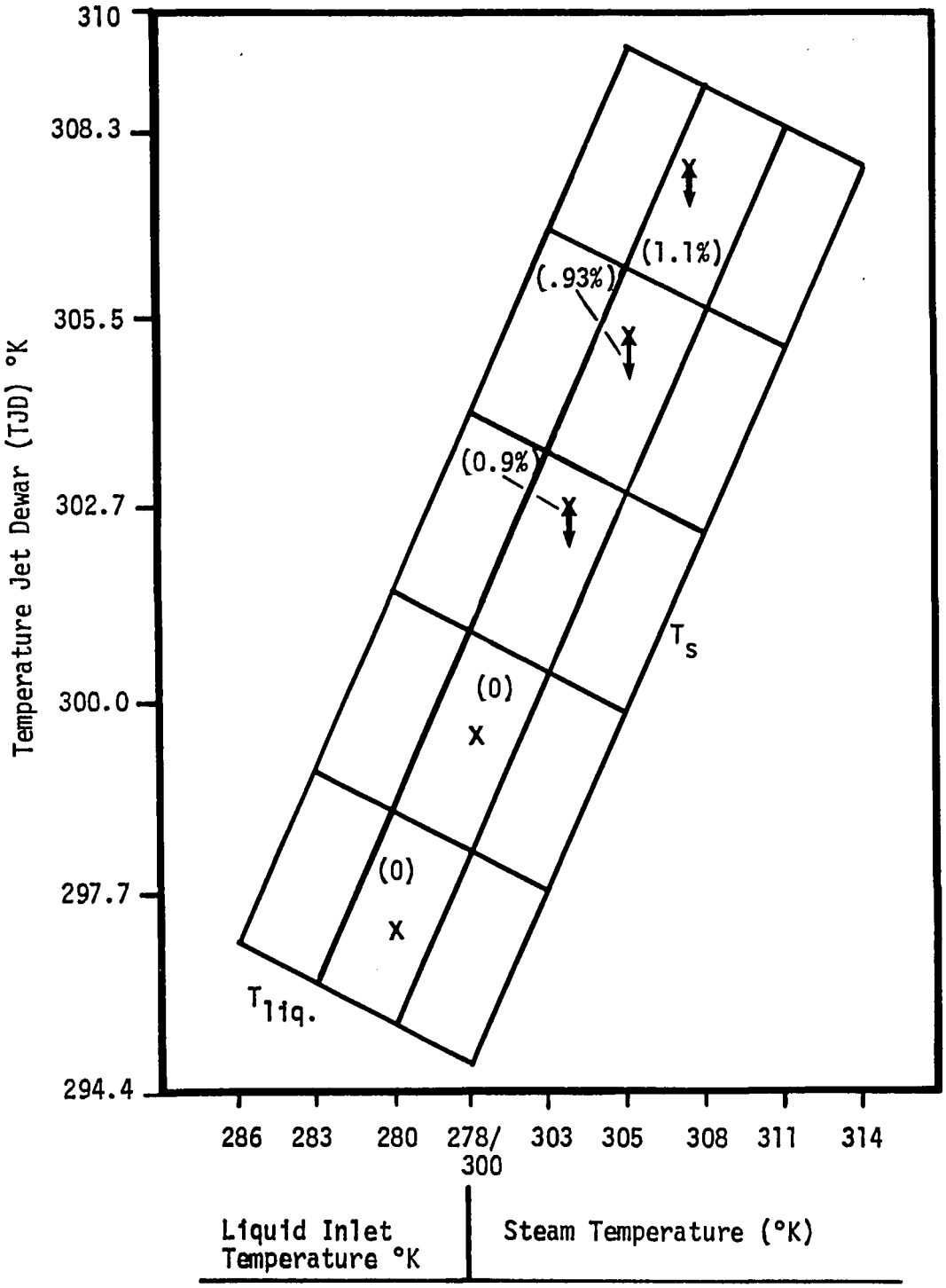

.254 MM DIAMETER NOZZLE FOR 254 MM JET LENGTH

FIGURE 18.

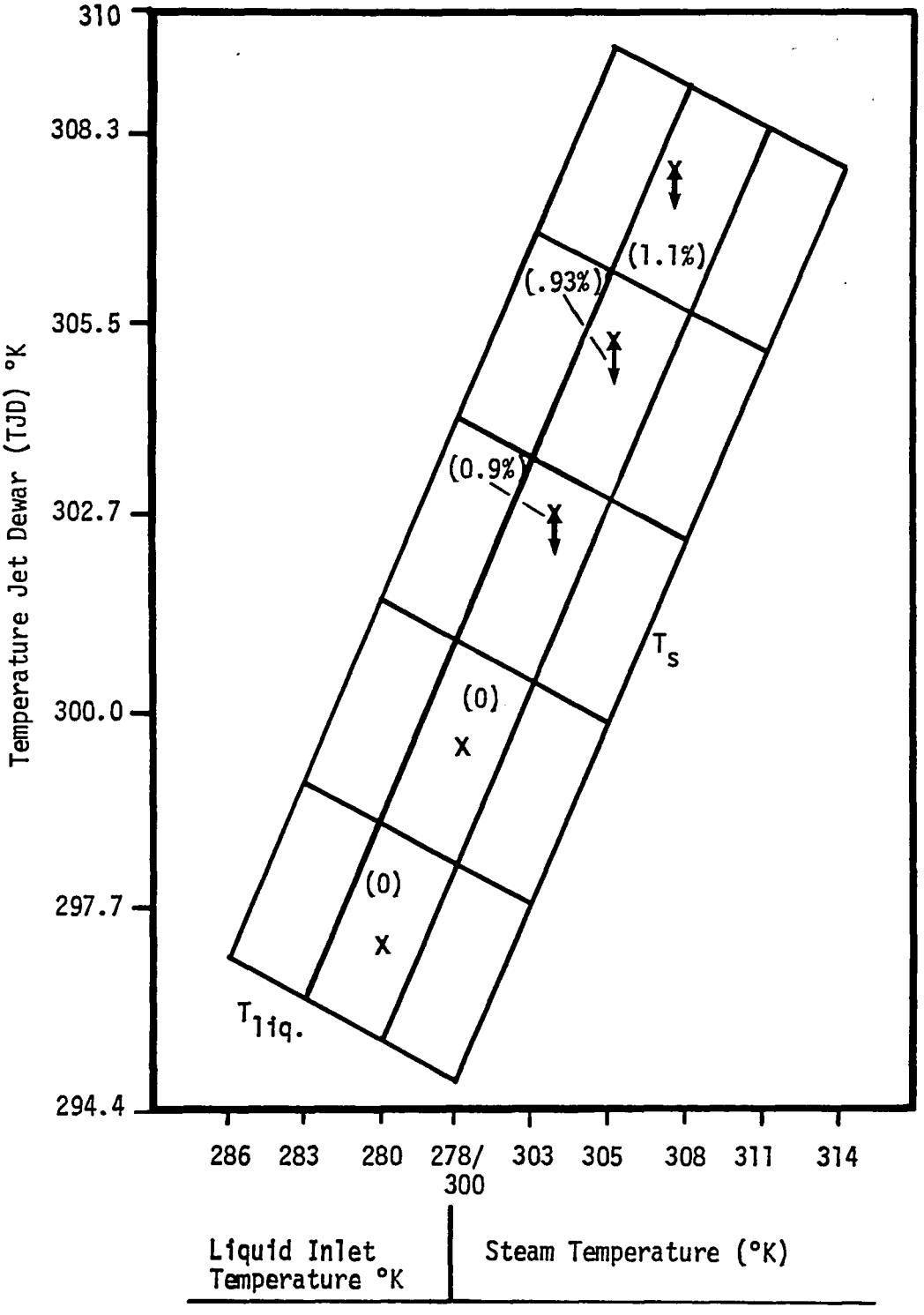

.254 MM DIAMETER NOZZLE FOR 254 MM JET LENGTH

FIGURE 18.

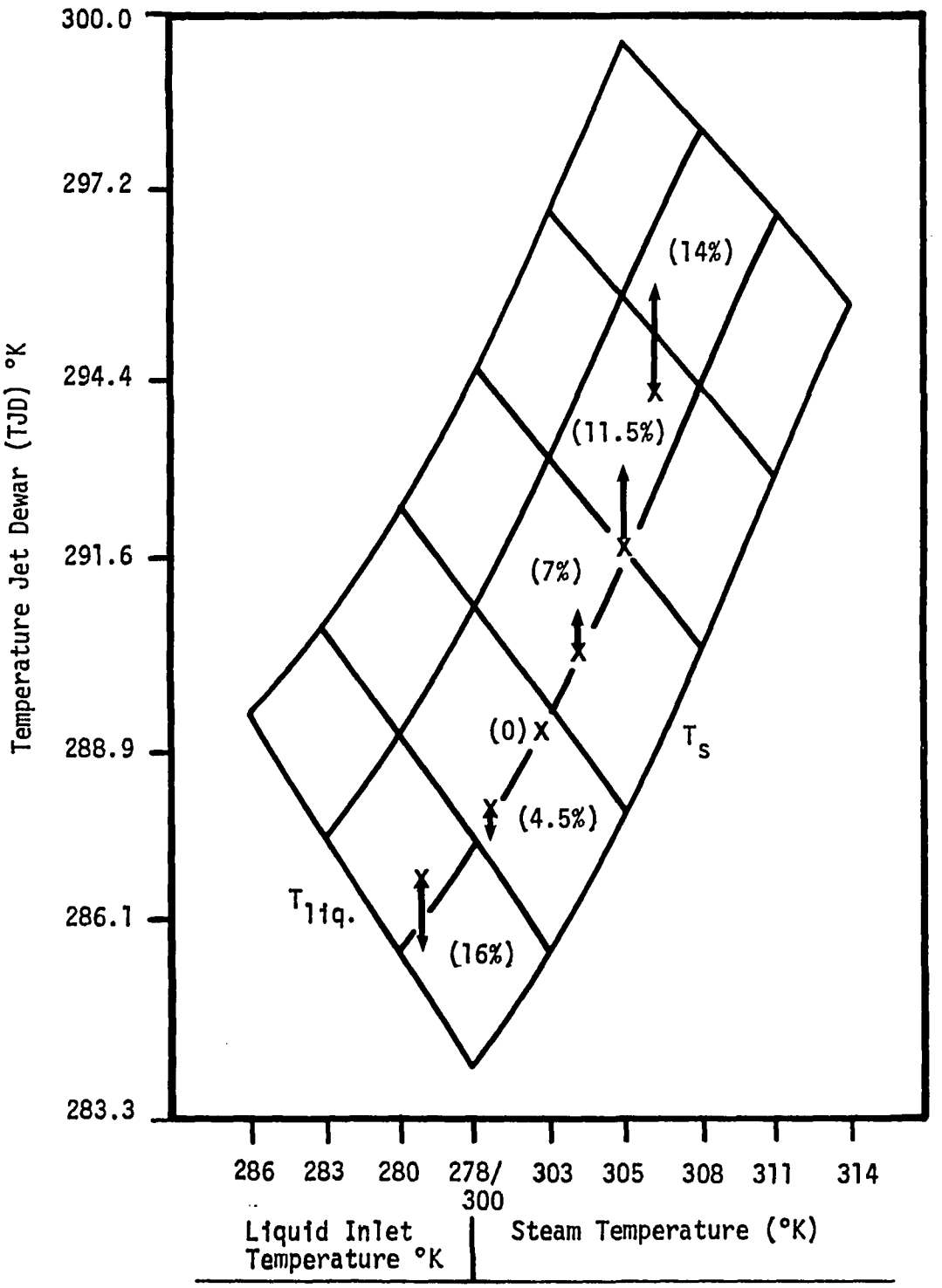

.3683 MM DIAMETER NOZZLE FOR 50.8 JET LENGTH

FIGURE 19.

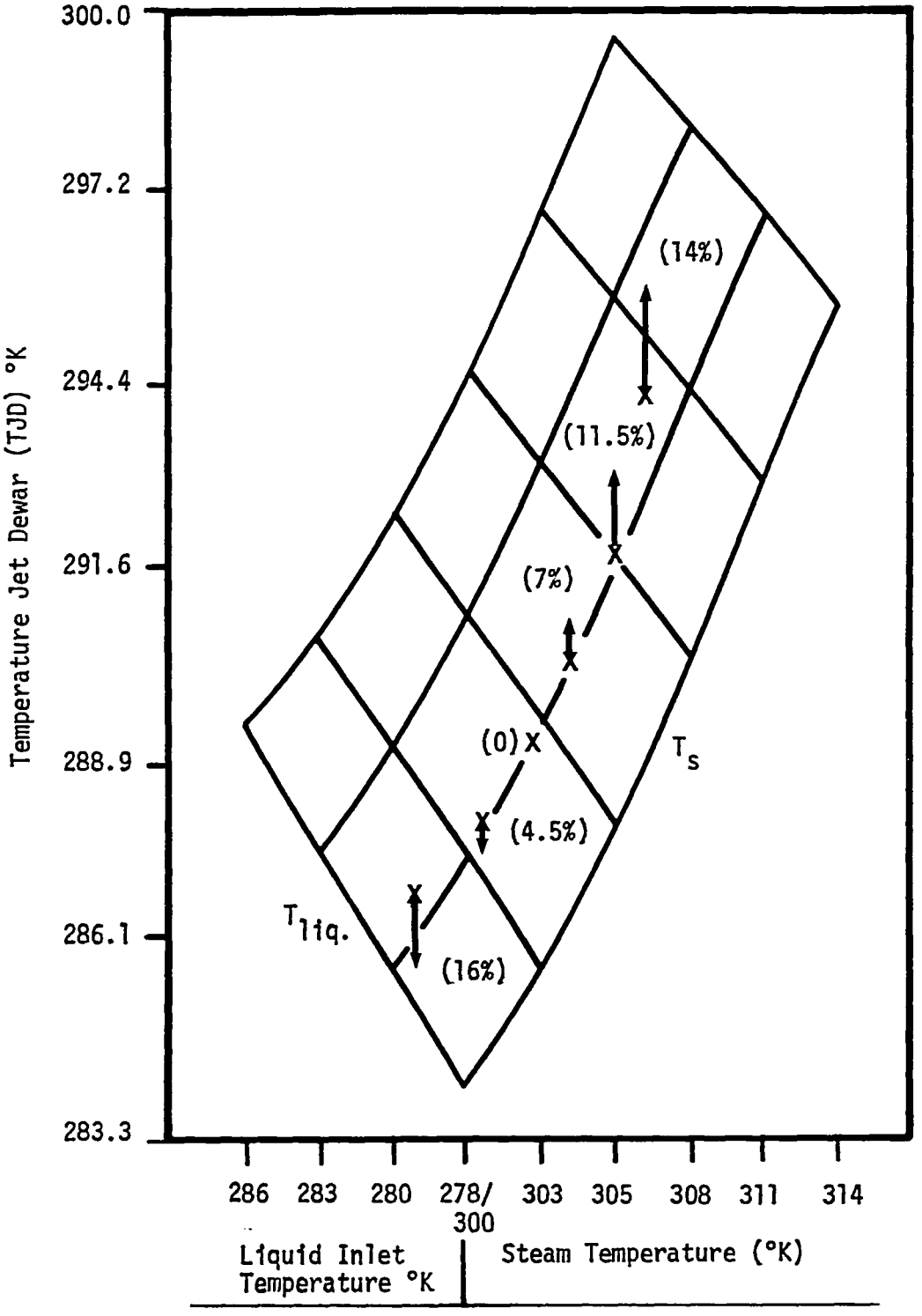

.3683 MM DIAMETER NOZZLE FOR 50.8 JET LENGTH

FIGURE 19.

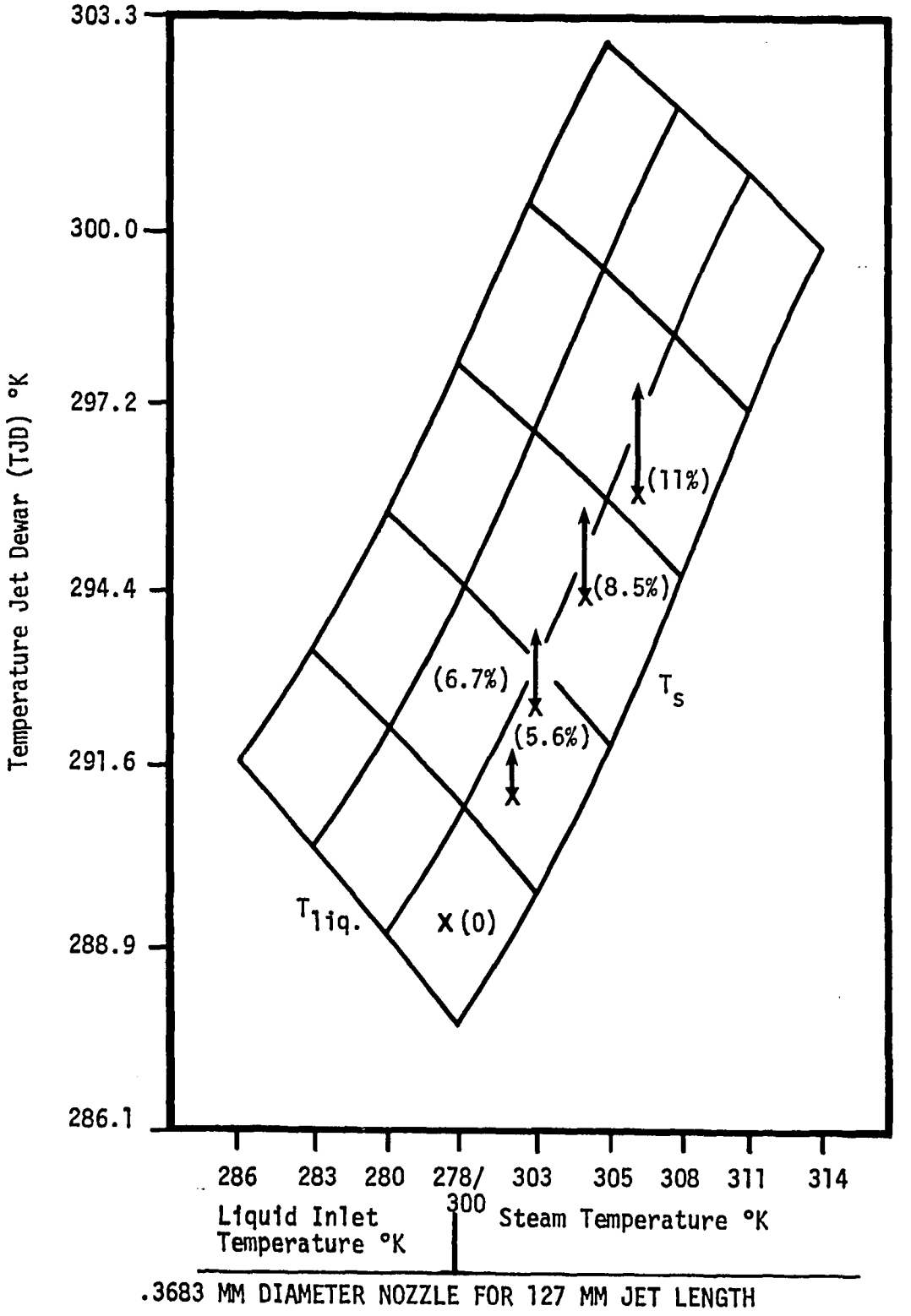
303.3
300.0
297.2
294.4
291.6
288.9
286.1
Temperature Jet Dewar (TJD) °K
(11%)
(8.5%)
(6.7%)
(5.6%)
T_s
$T_{liq.}$
X (0)
286
283
280
278/
300
303
305
308
311
314
Liquid Inlet
Temperature °K
Steam Temperature °K
.3683 MM DIAMETER NOZZLE FOR 127 MM JET LENGTH

FIGURE 20.

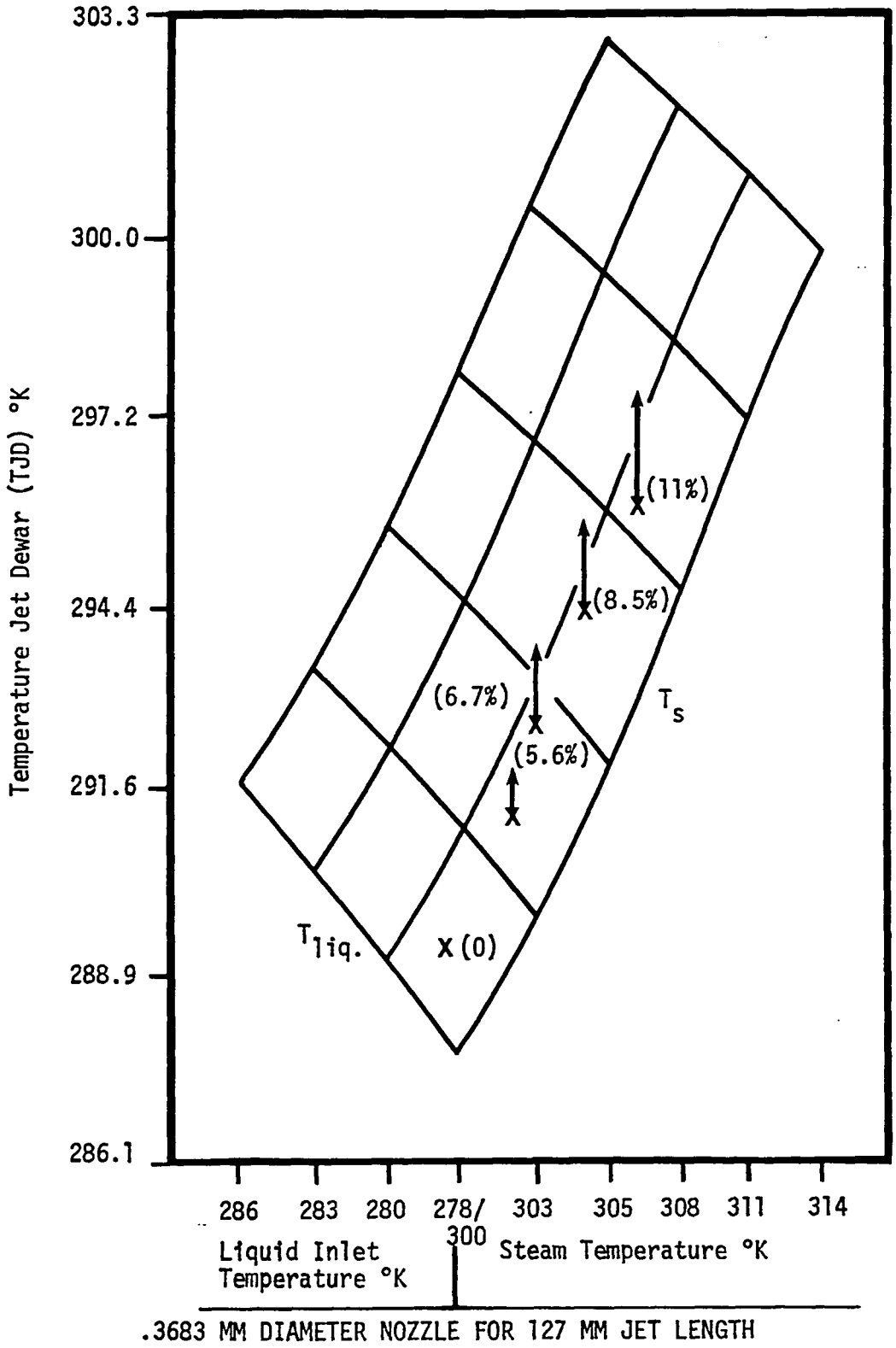
303.3
300.0
297.2
294.4
291.6
288.9
286.1
Temperature Jet Dewar (TJD) °K
(11%)
(8.5%)
(6.7%)
(5.6%)
T_s
$T_{liq.}$
X (0)
286
283
280
278/300
303
305
308
311
314
Liquid Inlet Temperature °K
Steam Temperature °K
.3683 MM DIAMETER NOZZLE FOR 127 MM JET LENGTH

FIGURE 20.

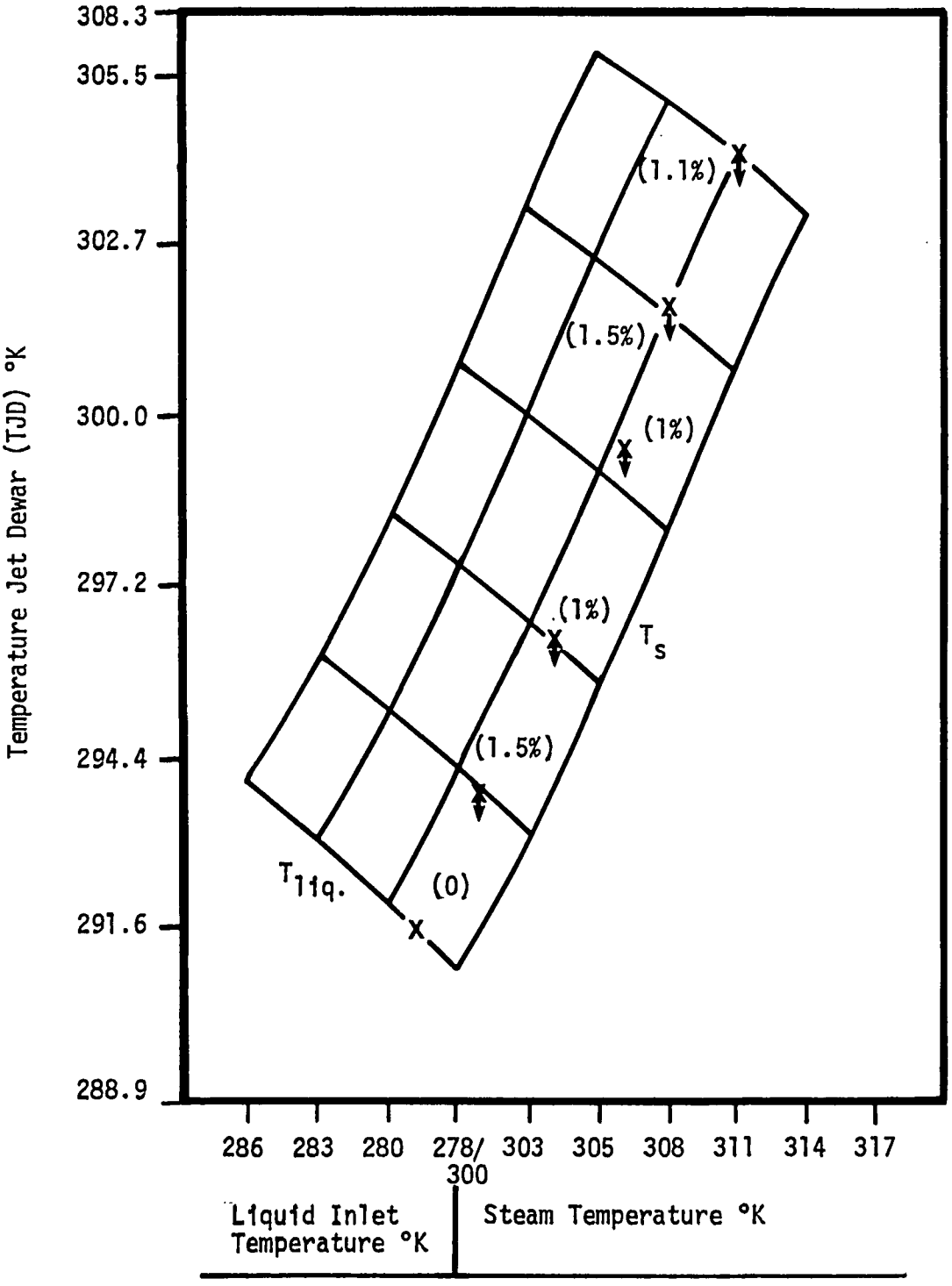

.3683 MM DIAMETER NOZZLE FOR 254 MM JET LENGTH

FIGURE 21.

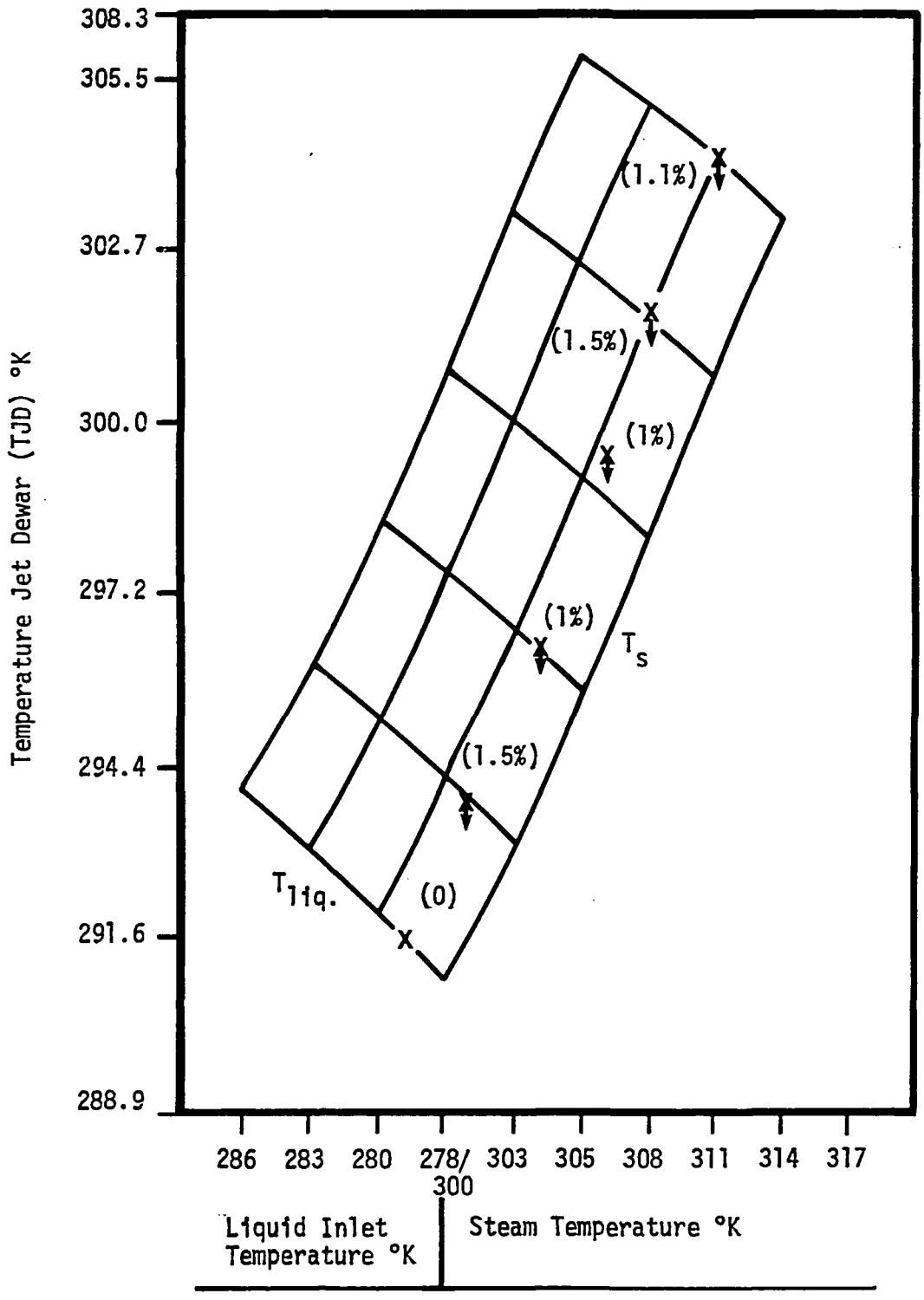

.3683 MM DIAMETER NOZZLE FOR 254 MM JET LENGTH

FIGURE 21.

2.3 Thermal Performance Analysis

The equations pertinent to the vapor phase in what follows are written for the case in which a noncondensable gas is present along with the vapor.

An assumption which facilitates this analysis is that the momentum interaction between the vapor and the liquid jets is very small in relation to the liquid jet momentum for the Rankine Power System conditions, which is in agreement with Maa.[10] From Shapiro[23], we also assume the vapor and liquid streams are at a control-surface pressure as they cross the boundary, and the angle of convergence is small.

The momentum equation for the vapor phase is taken from equation 8.21 of Shapiro[23] and is

$$\frac{dP}{P} + \frac{\rho V^2}{2gP}\frac{dV^2}{V^2} + \frac{\rho V^2}{2gP}\left(\frac{4f_w}{D_w}dx + \frac{\frac{dF}{\rho V^2}}{2g}A\right) + \frac{\rho V^2}{gP}(1-y)\frac{dW}{W} = 0 \quad \text{EQN 2.28}$$

where

P = Static pressure in the gaseous phase.

ρ = Static density of the gaseous phase.

V = Bulk axial velocity of the gaseous phase.

g = Gravitational constant.

f_w = Friction Coefficient between the gaseous phase and the funnel wall.

D_w = Funnel diameter.

F = The drag force exerted on the gaseous phase by the liquid jets.

A = The gaseous phase flow area.

W = The mass flow rate of gaseous phase.

x = Axial distance.

In Shapiro's derivation[23] dW is the total increase in mass flow of the gaseous phase and

$$y = V_i/V \qquad \text{EQN 2.29}$$

where V_i is the axial velocity of dW as it crosses the gaseous system boundary, i.e., the interfacial velocity between the liquid and gaseous phase.

A schematic of the velocity distribution in the gaseous phase, interfacial region, and in the liquid jet is shown in Figure 22 for the case where the vapor phase is moving at a higher velocity than the liquid. The subscript NG indicates the bulk velocity of the vapor (vapor + noncondensable gas) and L the bulk velocity of the liquid. In Figure 22 the gaseous phase velocity is V_{NG}, the interfacial velocity is Vi, and the liquid velocity is V_L. The gaseous phase velocity relative to the interface velocity is V_{NGi}, and the liquid velocity relative to the interface velocity is V_{iL}.

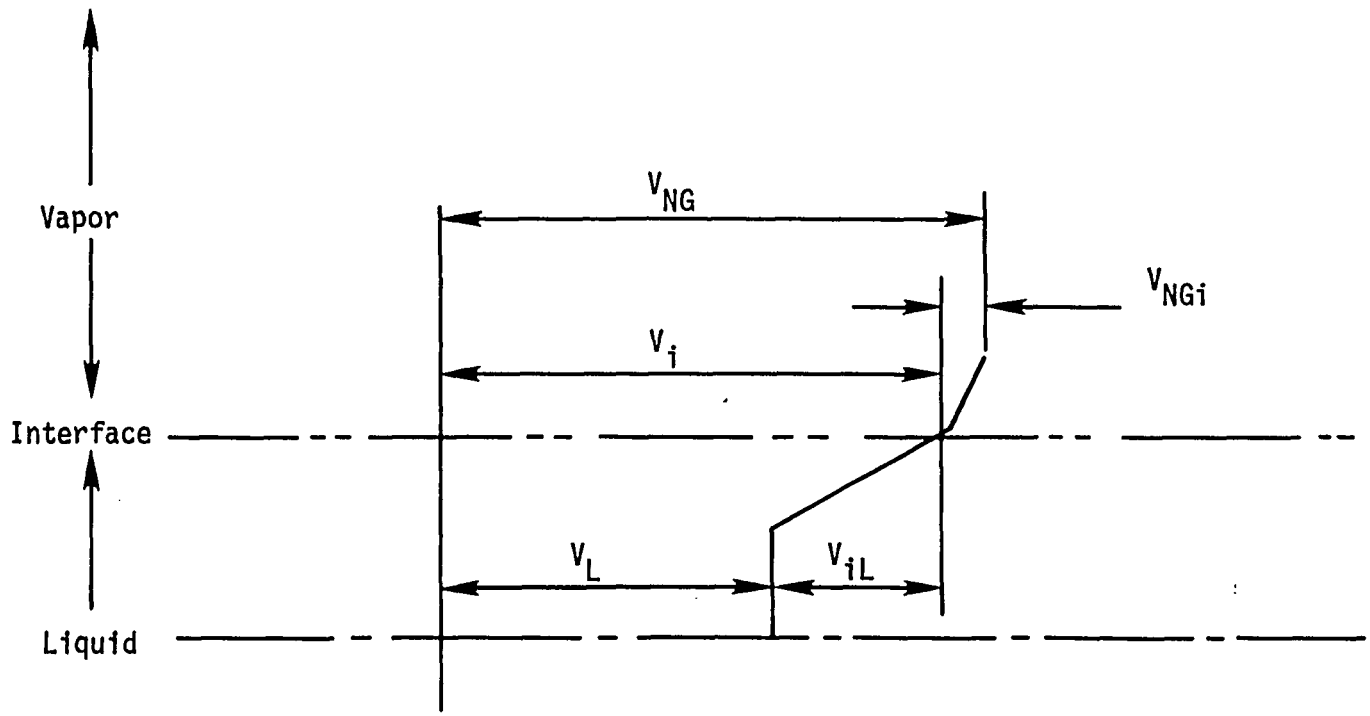

VELOCITY DISTRIBUTION REGIONS

FIGURE 22.

The drag force F is calculated for the gaseous phase of the relative interface velocity V_{NGi}, with the liquid heat transfer coefficient based on the relative liquid interfacial velocity V_{iL}. The friction coefficient f_w is based on the gaseous phase velocity V_{NG}. The method used to calculate the interface velocity is that presented by Gouse et al.[18], which involves equating the effective shear stress of the vapor and liquid at the interface.

The effective shear stress includes both the frictional component based on the velocity relative to the interface, and the momentum component that is associated with the mass transfer (condensation), occurring at the interface. Thus the effective gas phase shear stress on the interface is

$$(\tau i)_{NG} = (fi)_{NG} \frac{\rho_{NG} V_{NGi}^2}{2g} + \frac{W}{A}\text{cond.} + \frac{(V_{NGi})}{g} \qquad \text{EQN 2.30}$$

where $(fi)_{NG}$ is the gas phase drag friction factor with the Reynolds Number Re, based on the relative interfacial velocity. The liquid jet acts as a solid surface for the vapor during condensation, while V_{NGi} and the gas phase hydraulic diameter, D_v, are based on the funnel flow area, wetted perimeter of the funnel wall, and the liquid jets with

$$(fi)_{NG} = \frac{16}{Re_{NG}} \text{ or } \frac{0.046}{Re_{NG}^{.2}} \qquad \text{EQN 2.31}$$

dependency on laminar or turbulent values of the Reynolds Number, Re. The condensate mass flux from the vapor to the liquid is W/A cond.

The liquid effective interface shear stress is

$$(\tau i)_L = (fi)_L \rho_L \frac{V_{iL}^2}{2g} + \frac{W}{A}\text{ cond.} \frac{(V_{iL})}{g} \qquad \text{EQN 2.32}$$

where $(f_i)_L$ is the drag friction coefficient based on the liquid interfacial relative velocity, V_{iL}, and the liquid jet diameter, D_j. The value of V_i is that which results in

$$(T_i)_v = (T_i)_L \qquad \text{EQN 2.33}$$

The local condensing mass flux is calculated from kinetic theory[7,10,11] as

$$\frac{W}{A}\text{ cond.} = (\Gamma_V Y_{Vi} \frac{PM_v}{RT_v} \frac{C_v(T_v)}{4} - \rho_{VSL} \frac{C_v}{4}(T_{SL})) \qquad \text{EQN 2.34}$$

$$C_v(T) = \sqrt{\frac{8RT}{\pi M_v}} \qquad \text{EQN 2.35}$$

$$\Gamma_v = e^{-S^2} + \sqrt{\pi}\, s(1 + \text{erf}(s)) \qquad \text{EQN 2.36}$$

$$s = \frac{u}{\sqrt{\frac{2Rg_o T_v}{M_v}}} \qquad \text{EQN 2.37}$$

$$V_B = \frac{W}{A}\text{ cond.} \frac{RT_v}{M_v P} \qquad \text{EQN 2.38}$$

where

P = Static pressure of vapor for condenser gas mixture in funnel.

Y_{vi} = Vapor mole fraction at vapor/liquid interface.

M_v = Molecular weight of vapor.

R = Universal gas constant.

T_v = Vapor temperature in funnel.

$C_v(T)$ = Average vapor molecule molecular speed.

ρ_{VSL} = Saturated vapor density at temperature T_{SL}.

V_B = Bulk vapor velocity normal to jet surface.

s = Ratio of bulk vapor velocity normal to jet to mean molecular speed.

Γ_v = Factor which alters the molecular collision rate with the liquid jet to account for the bulk vapor flow toward the jet surface.[7,10,14]

The condensing mass flux, W/A cond., has a net enthalpy of $h_V - h_{LSL}$ associated with it, where

h_V = Vapor enthalpy.

h_{LSL} = Liquid enthalpy at the liquid/vapor interface.

The mass flux enthalpy product difference is a heat flux which is imposed on the liquid surface and must be convected to the interior of the liquid jet. Defining H as the jet convection heat transfer coefficient, from surface to bulk liquid, the equality of heat flux from the vapor to the surface and from the surface to the bulk liquid is given as

$$\frac{W}{A}_{\text{cond.}} \quad (h_V - h_{LSL}) = H\,(T_{LSL} - T_{BL}) \qquad \text{EQN 2.39}$$

where

T_{BL} = Liquid jet bulk temperature.

The local condensing rate is established when equation (2.39) is satisfied. The value of H is based on derived data generated from the steam/water analysis. A correlation of Stanton Number, S_t, is obtained for various jet configurations as a function of jet length (Section 2.2). This Stanton Number was based on the relative liquid interfacial velocity, V_{iL}. Thus H is defined as

$$H = S_t \cdot \rho_L \cdot C_{PL} \cdot V_{iL} \qquad \text{EQN 2.40}$$

where

C_{PL} = Liquid specific heat.

and

$S_t = S_t(x)$

where

x = Jet length from injector.

From the testing conducted in Sections 4.1 and 4.2, Stanton Numbers were obtained for several different nozzle types. The Stanton Numbers are given in Figure 23 for the .254 and .3683 mm diameter nozzles. The H calculated from these Stanton Numbers is compared to a minimum value H_{min}, calculated from

$$H_{min} = S_{tmin} \cdot \rho_L \cdot C_{PL} \cdot V_L \qquad \text{EQN 2.41}$$

which is based on the bulk jet velocity and a corresponding minimum Stanton Number S_{tmin}, per equations 2.26.1 and 2.27 as shown in Figure 24, and is determined from extrapolating test data (Sections 4.1 and 4.2), to the point where $V_{1L} = 0$.

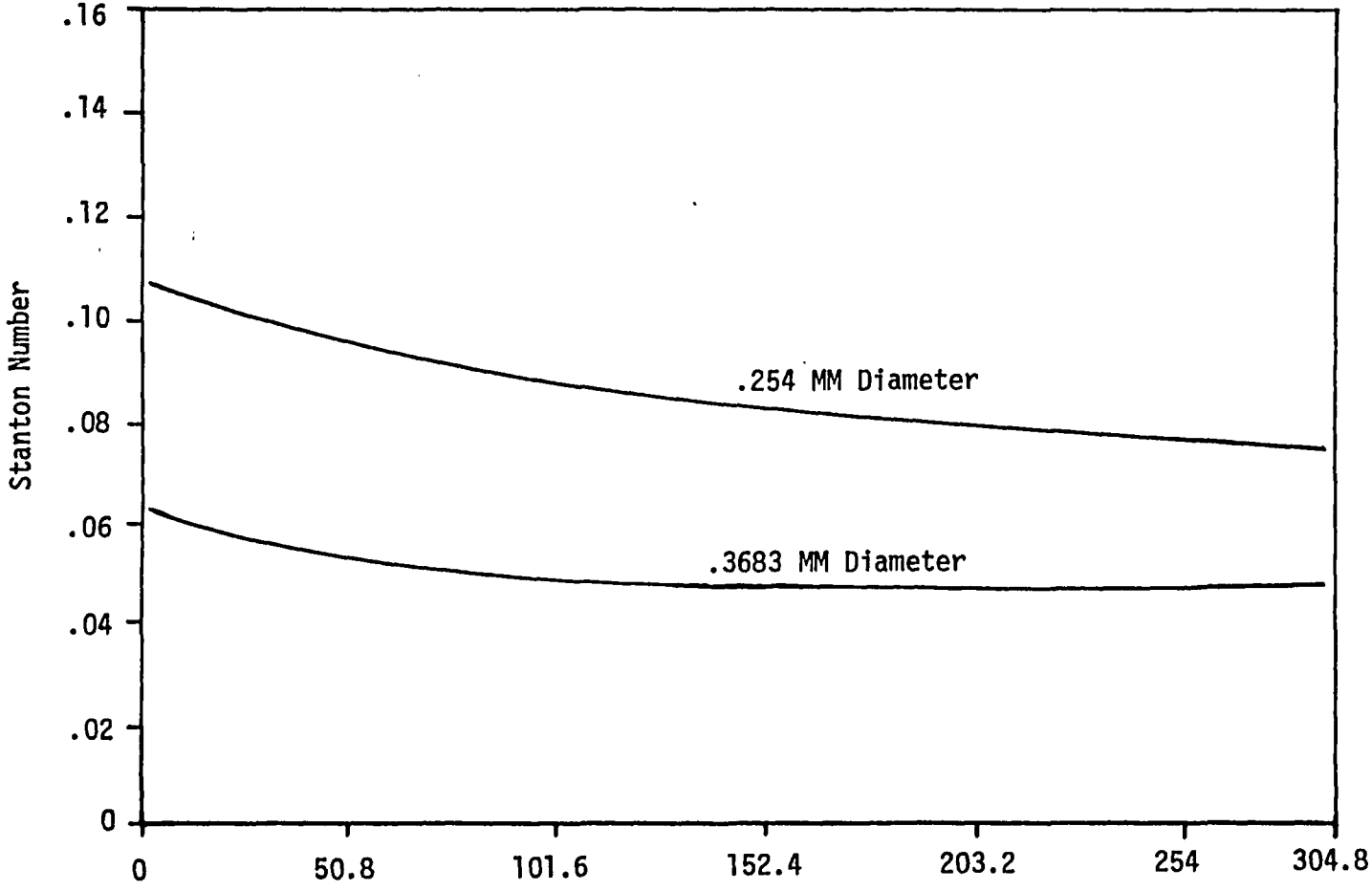

STANTON NUMBER FOR .254 AND .3683 MM DIAMETER NOZZLES
FIGURE 23.

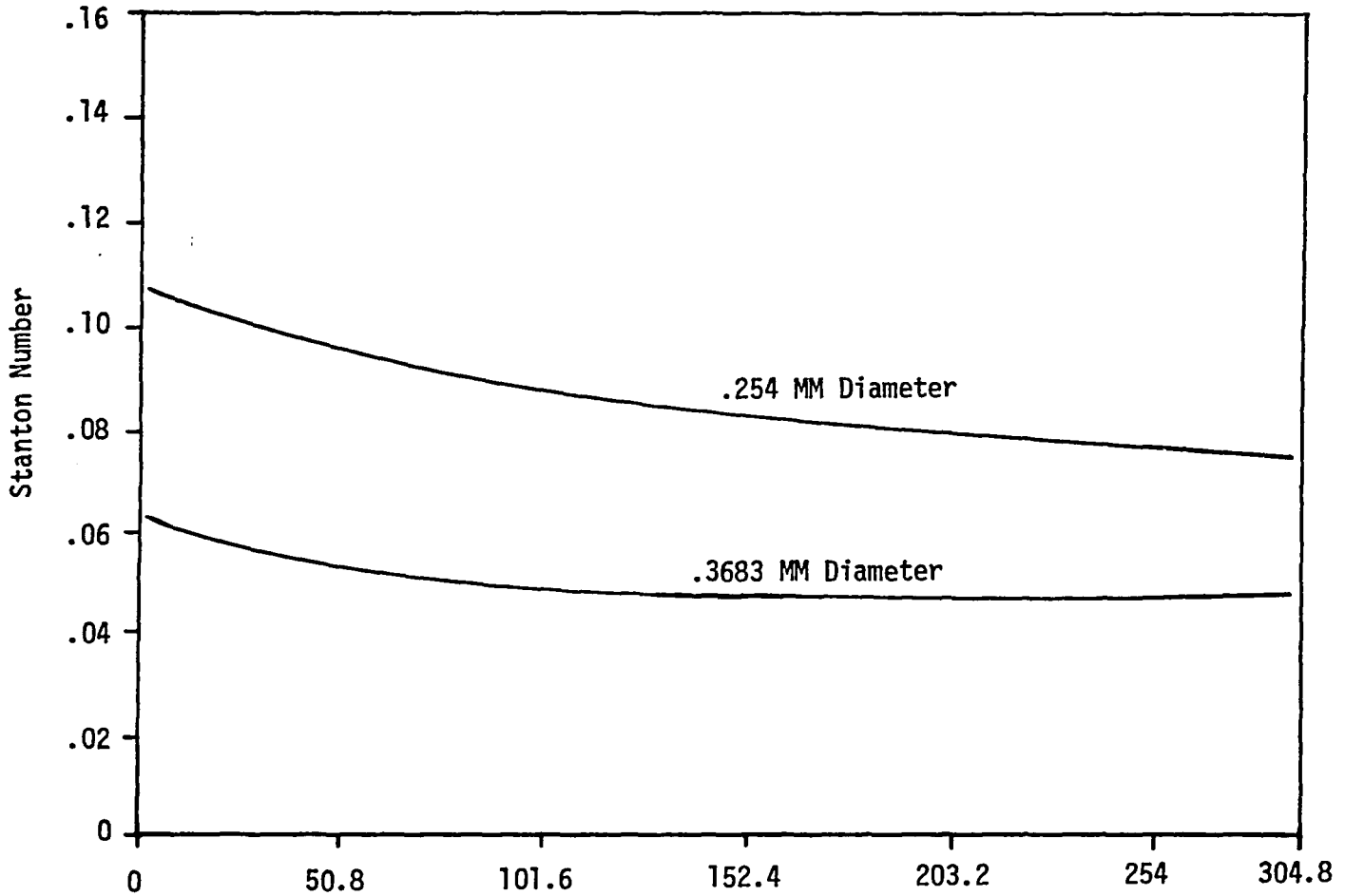

STANTON NUMBER FOR .254 AND .3683 MM DIAMETER NOZZLES
FIGURE 23.

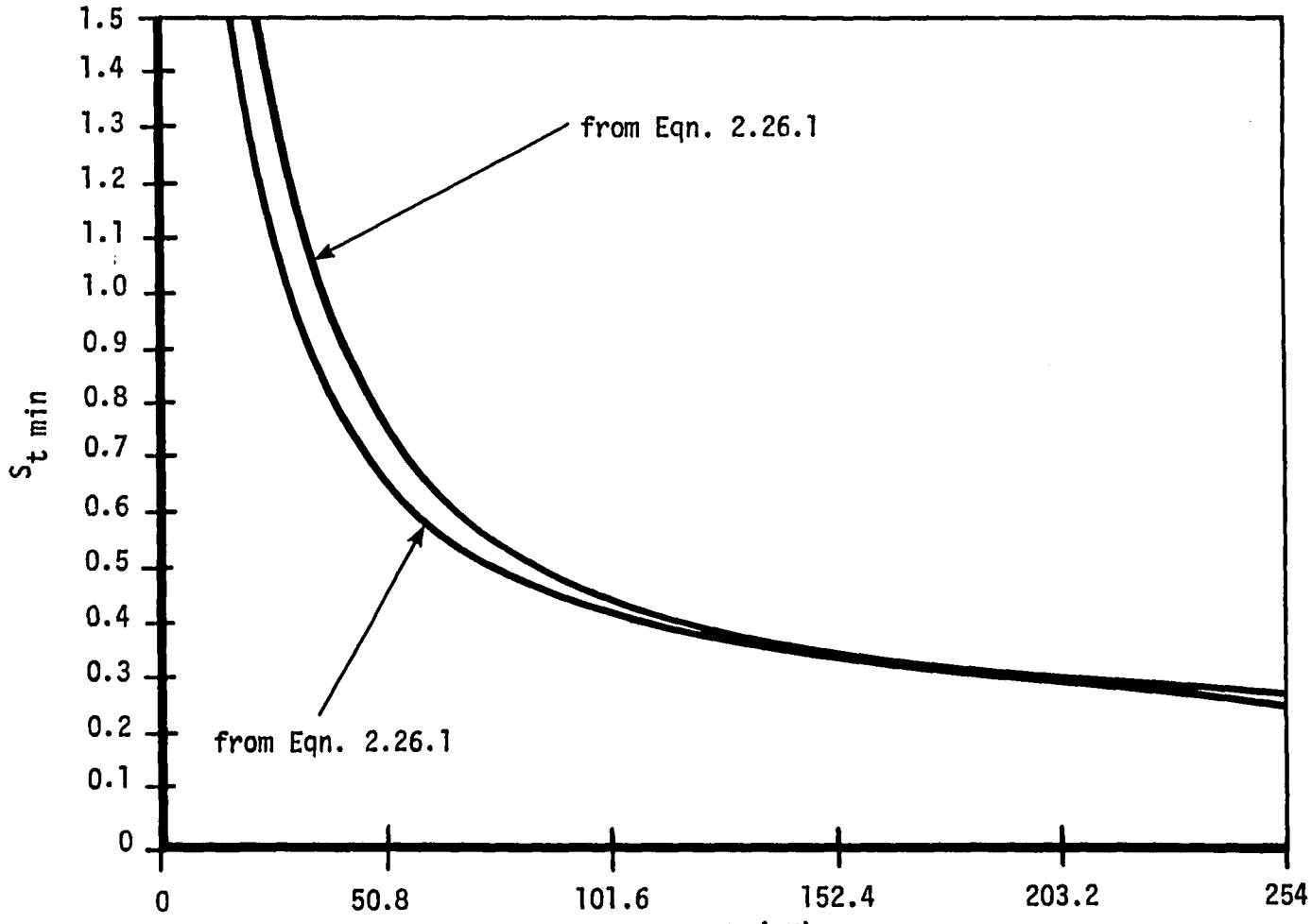

STANTON NUMBER AT ZERO INTERFACIAL VELOCITY

FIGURE 24.

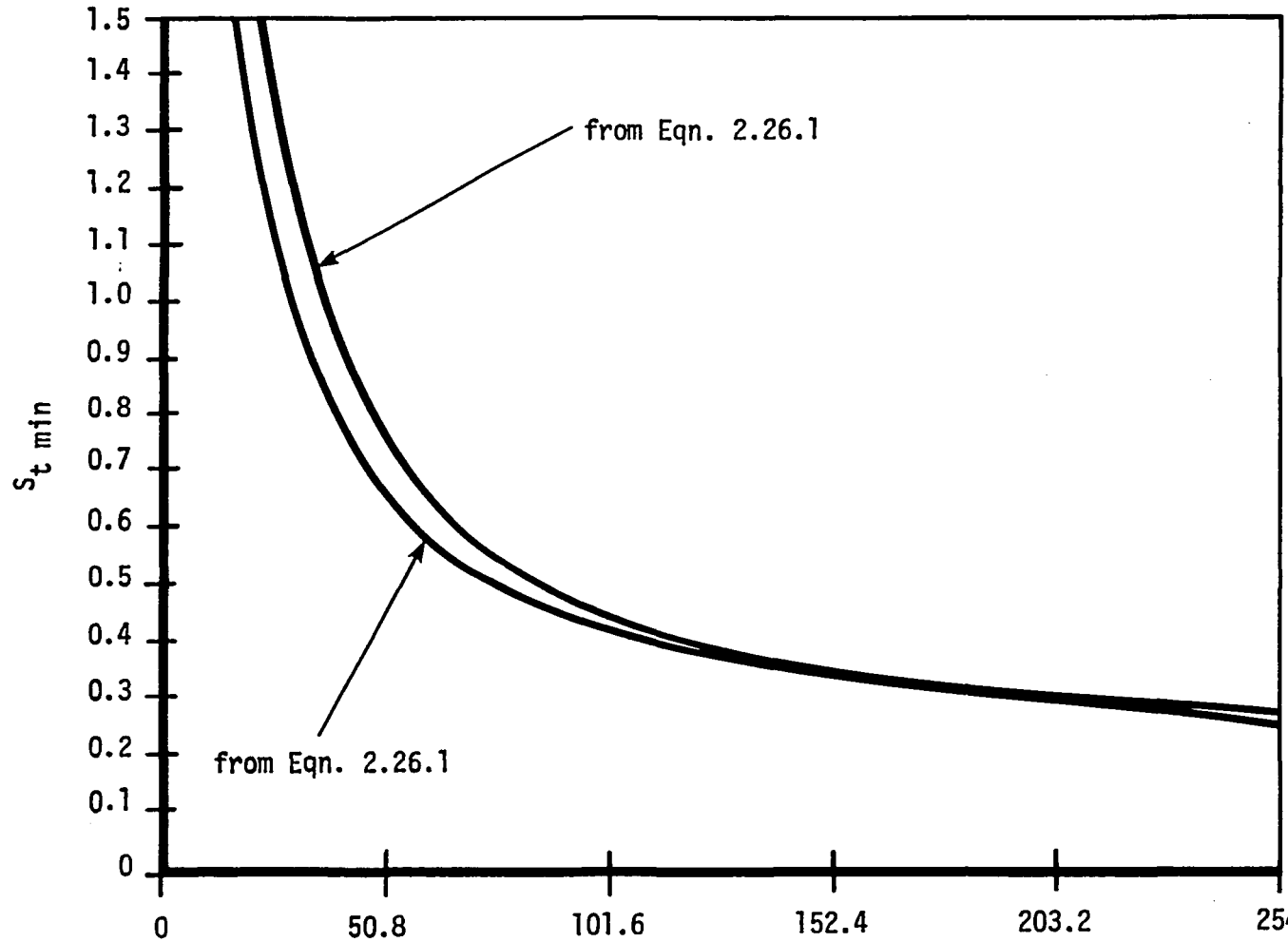

STANTON NUMBER AT ZERO INTERFACIAL VELOCITY

FIGURE 24.

The larger of the two H values is used in the analysis, since it corresponds to the .254 mm diameter nozzle, which was used for the final design.

Determination of the value of the vapor mole fraction at the jet interface, Y_{Vi}, will be discussed next. For this determination, the assumption is made that the noncondensable gas is not soluble in the liquid, which simulates a higher concentration (worst condition).

At any axial location in the vapor funnel, the bulk gas (vapor plus noncondensable gas) has a local bulk mole fraction of $Y_{NG\infty}$. The noncondensable gas is carried along with the vapor molecules in the bulk flow toward the liquid jet surface[24] at a bulk flow velocity of V_B. This situation is illustrated in Figure 25. Assuming the liquid interface does not absorb noncondensable gas molecules, the noncondensable gas sets up a concentration gradient which results in a diffusion flux away from the interface which exactly balances the bulk flow flux of noncondensable gases toward the interface. The bulk flow flux of noncondensable gas is the local product of bulk velocity and the noncondensable mole fraction while the diffusional flux is the product of the gradient of the mole fraction and the diffusion coefficient.

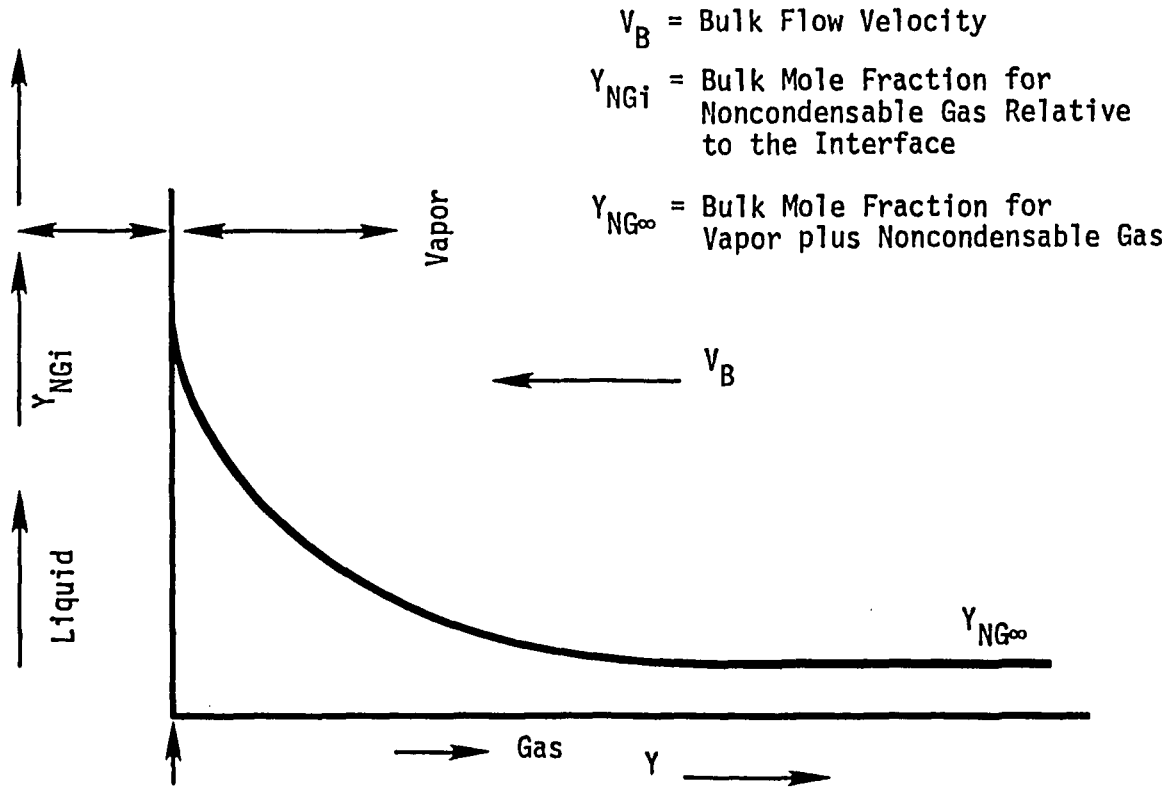

NONCONDENSABLE GAS INTERACTION WITH VAPOR AND LIQUID

FIGURE 25.

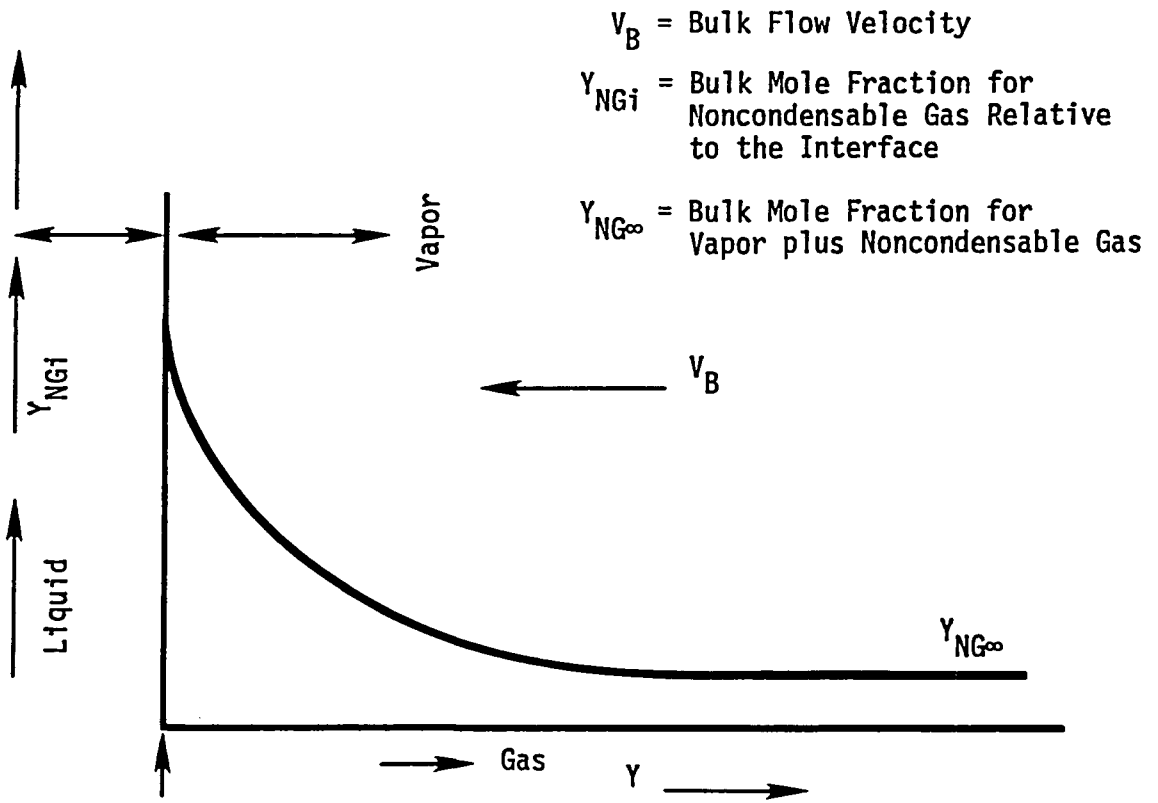

NONCONDENSABLE GAS INTERACTION WITH VAPOR AND LIQUID

FIGURE 25.

Thus,

$$V_B\ Y_{NG} = -D_{V-NG}\ \frac{dY_{NG}}{dy} \qquad \text{EQN 2.42}$$

holds from the bulk free stream to the liquid interface, where

D_{V-NG} = The vapor-noncondensable gas diffusion coefficient.

$\frac{dY_{NG}}{dy}$ = Gradient of noncondensable mole fraction away from the interface.

The definition of the mass transfer coefficient (similar to heat transfer coefficient) is

$$H_D = \frac{-D_{V-NG}\ \frac{dY_{NG}}{dy}}{(Y_{NGi} - Y_{NG\infty})} \qquad \text{EQN 2.43}$$

using the definition of H_D equation (2.43) in equation (2.42) results in

$$V_B\ Y_{NGi} = H_D\ (Y_{NGi} - Y_{NG\infty}) \qquad \text{EQN 2.44}$$

upon rearranging,

$$Y_{NGi} = Y_{NG\infty}\ \left(\frac{H_D}{H_D - V_B}\right) \qquad \text{EQN 2.45}$$

The problem now is how to evaluate H_D. The approach taken is to view the situation of the vapor condensing on the liquid jets and the noncondensable gas diffusing away from the liquid jets similar to the situation of mass transfer in laminar flow over a flat plate with suction at the wall, which is similar to Bakay et al.[20] This problem is treated in the classical boundary layer-stream function approach in numerous texts such as Rosenhow.[25] The resulting differential equations, shown in Appendix B, have been solved numerically. The results are presented in Figure 26. as the ratio H_D/H_{DO} as a function of the suction parameter,

$$V_o/V_\infty \sqrt{Rex}$$

for various Schmidt numbers, S_C.

In the boundary layer analysis, V_o, is the bulk velocity normal to the wall, and is identical to V_B, the velocity normal to the jet surface. V_∞ is the free stream axial velocity, which is identical to V_{NG}, the bulk vapor and noncondensable gas axial velocity in the funnel. The Reynolds number, Re_x is based on the bulk gas velocity and the distance, x, from the inlet.

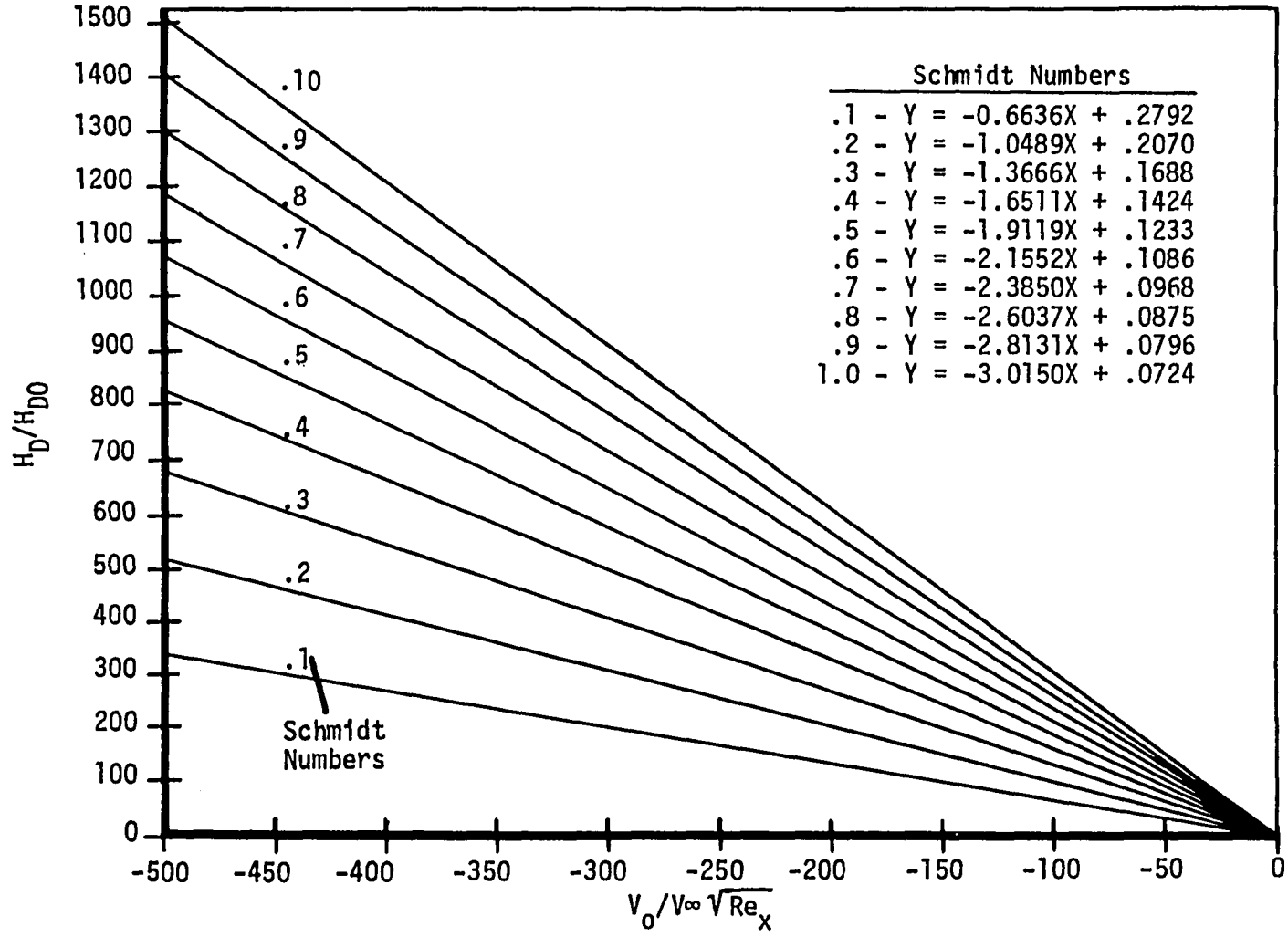

SCHMIDT NUMBERS VS. SUCTION PARAMETER

FIGURE 26.

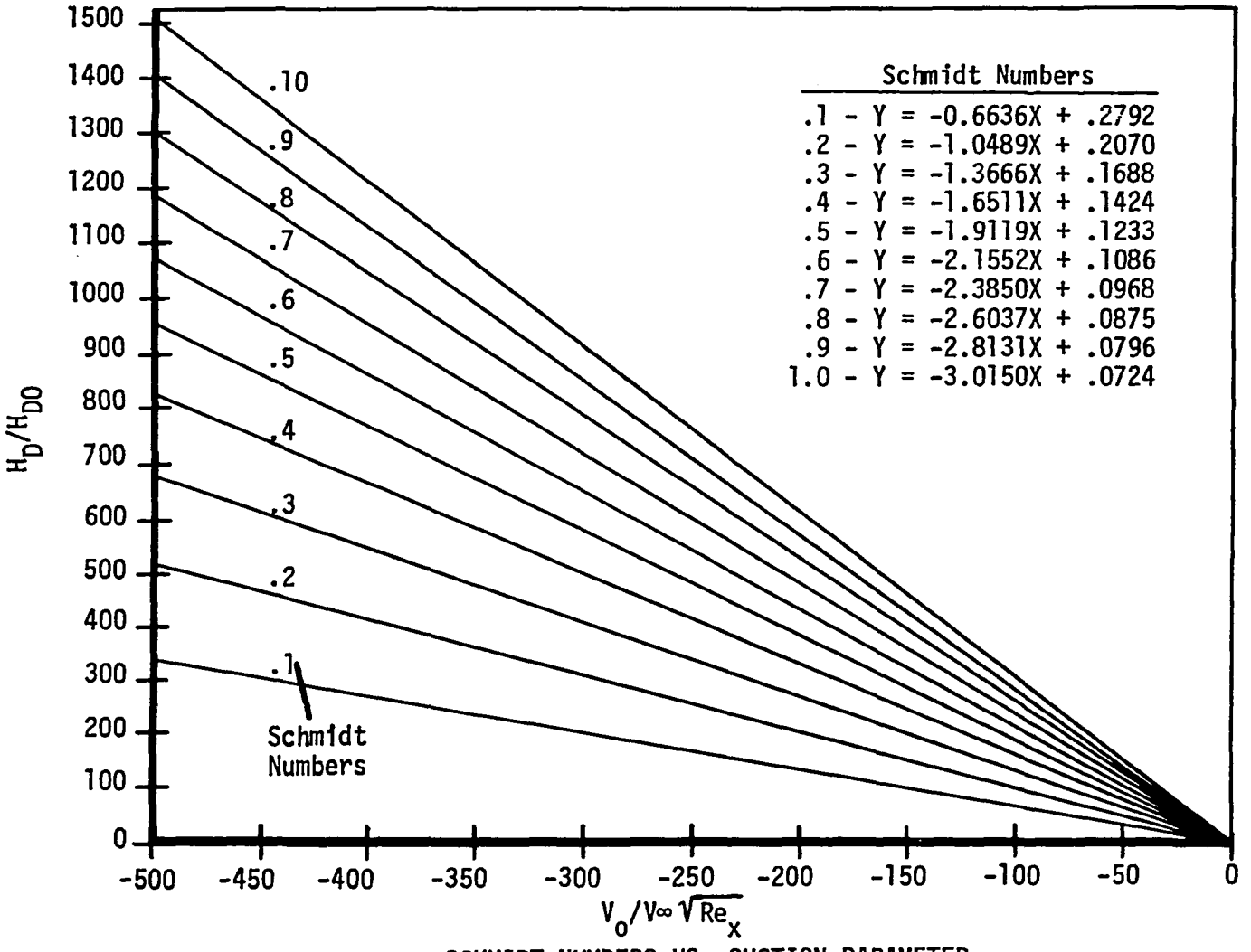

SCHMIDT NUMBERS VS. SUCTION PARAMETER

FIGURE 26.

H_{DO} is calculated from

$$H_{DO} = .332 \frac{D}{x} S_C .343 \sqrt{Re_x} \qquad \text{EQN 2.46}$$

where $S_C = \frac{\mu}{\rho D}$ EQN 2.47

and μ is the gaseous phase viscosity

ρ is the density.

D is the diffusion coefficient.

Knowing Y_{NGi} allows Y_{Vi} to be calculated from

$$Y_{Vi} = 1 - Y_{NGi} \qquad \text{EQN 2.48}$$

At this point in the analysis it can be seen that if the value of vapor velocity, V_{NG}, pressure, P, liquid velocity, V_L, free stream noncondensable gas mole fraction, $Y_{NG\infty}$, vapor temperature, T_V, bulk liquid temperature, T_{BL}, are known at any axial location, x, then the values of the interfacial velocity, V_i, liquid surface temperature, T_{SL}, and the condensing mass flux, W/A cond., can be found which satisfy equations (2.30) through (2.48). Determining these values is an iterative task and can be done on a digital computer.

Once W/A cond. is known, an energy balance on the liquid stream results in the bulk liquid differential equation,

$$\frac{dT_{BL}}{dX} = \frac{W \text{ cond.}}{A \dot{m}_L C_{PL}} (h_V - h_{LSL}) N \pi D_j \qquad \text{EQN 2.49}$$

and the mass balance equations

$$\frac{dW}{dX} = \frac{-W \text{ cond.}}{A} N \pi D_j \qquad \text{EQN 2.50}$$

$$\frac{d\dot{m}_L}{dX} = \frac{-dW}{dX} \qquad \text{EQN 2.51}$$

where

W = The gaseous phase mass flow rate.

$\dot{m}_L$ = Liquid mass flow rate.

N = Number of liquid jets.

D_j = Diameter of individual jets.

Assuming that the noncondensable molecules have the same bulk velocity and temperature, gives

$$Y_{NG\infty} = \frac{\frac{\dot{m}_{NG}}{M_{NG}}}{\frac{\dot{m}_V}{M_V} + \frac{\dot{m}_{NG}}{M_{NG}}} \qquad \text{EQN 2.52}$$

from which

$$\frac{dY_{NG\infty}}{d_x} = \frac{\frac{-\dot{m}_{NG}}{M_{NG}}}{\frac{\dot{m}_V}{M_V} + \frac{\dot{m}_{NG}^2}{M_{NG}}} \frac{dW}{d_x M_V} \qquad \text{EQN 2.53}$$

where

$\dot{m}_{NG}$ = Mass flow rate of noncondensable.

M_{NG} = Molecular insight of noncondensable.

M_V = Molecular weight of vapor.

$\dot{m}_V$ = Vapor mass flow rate.

The molecular weight of the gaseous phase is

$$M = Y_{NG\infty} M_{NG} + (1 - Y_{NG\infty}) M_V \qquad \text{EQN 2.54}$$

At this point, we can simplify the momentum equation (2.28) by utilizing V_{NG} to denote the gaseous phase velocity. Rewriting equation (2.28) yields

$$\frac{dP}{dx} = -\left\{\frac{\rho}{2g}\frac{dV_{NG}^2}{dx} + \frac{\rho V_{NG}^2}{2g}\left[\left(\frac{4f_w}{D_w} + \frac{1}{\frac{PV_{NG}^2 A}{2g}}\right)\frac{dX}{dx} + \frac{2}{w}\left(1 + \frac{V1}{V_{NG}}\right)\frac{dw}{dx}\right]\right\} \qquad \text{EQN 2.55}$$

In this equation dw/dx is given by equation (2.50), and dX/dx can be calculated from the gaseous phase relative to velocity V_{NGi} and the interfacial friction coefficient[5] $(fi)_{NG}$ as

$$\frac{dX}{dx} = \pm (fi)_{NG} \frac{\rho V_{NGi}^2}{2g} \cdot N \pi D_j \qquad \text{EQN 2.56}$$

where the sign is positive (+) when the $V_{NG} > V_L$, and negative (-) when $V_{NG} < V_L$.

The wall friction coefficient, f_w, is calculated based on the velocity, V_{NG}, and the wall diameter, D_w, from Shapiro[23] for a Reynolds number for incompressible fully developed flow, as,

$$f_w = .046 \left(\frac{\rho V_{NG} D_w}{\mu}\right)^{-.2} \qquad \text{EQN 2.57}$$

The quantity V_{NG}^2 is calculated from the mass flow rate, pressure, temperature, molecular weight and flow area from Fox et al.[26], as,

$$V_{NG}^2 = \left[\frac{W R T_V}{P M A}\right]^2 \qquad \text{EQN 2.58}$$

Assuming that the vapor temperature, T_V, is constant throughout the funnel since the vapor velocities are relatively low, the absolute temperature level is 391.7°K. The vapor is slightly superheated (~2.8°K) so that little error is involved by assuming it constant. Assuming T_V constant allows equation (2.58) to be easily differentiated to show that

$$d\left(V_{NG}^2\right) = 2\,V_{NG}^2\left(\frac{dW}{W} - \frac{dP}{P} - \frac{dM}{M} - \frac{dA}{A}\right) \qquad \text{EQN 2.59}$$

Substituting equations (2.58) and (2.59) into equation (2.55) and rearranging results in

$$\frac{dP}{dx} = \frac{\frac{\rho V_{NG}^2}{g}\left[\frac{1}{A}\frac{dA}{dx} + \frac{1}{M}\frac{dM}{dx} - \frac{1}{W}\frac{dW}{dx}\left(2 - \frac{V_i}{V_{NG}}\right) - \frac{2f_W}{D_W}\right] - \frac{1}{A}\frac{dX}{dx}}{1 - \frac{M\,V_{NG}^2}{g\,RT_V}} \qquad \text{EQN 2.60}$$

where $$\rho = \frac{M\,P}{R\,T_V} \qquad \text{EQN 2.61}$$

Specifying a funnel geometry establishes the value of A and dA/dX. The value of dM/dX is derived by differentiating (equation 2.54)

$$\frac{dM}{dX} = \left(M_{NG} - M_V\right)\frac{dY_{NG\infty}}{dX} \qquad \text{EQN 2.62}$$

Having defined differential equations for dT_{BL}/dx (equation 2.49), dW/dx (equation 2.50), $\dot{m}_L/dx$ (equation 2.51), $dY_{NG\infty}/dx$ (equation 2.53), dP/dx (equation 2.60), dA/dx from the funnel geometry, and dM/dx (equation 2.62), these differential equations can be integrated by a suitable numerical method. From Mochalova et al.[9], it will be assumed that the liquid jet with an initial temperature T_o discharges through a circular orifice at $x = 0$. It has a radius R_o for a given velocity distribution over its cross section into a space that contains saturated vapor of the liquid at temperature T_{SL}. The radial temperature gradient in the jet is larger than the axial one.

The initial and boundary conditions for the numerical method are:

$$\text{at } x = 0 \quad u = U_o, \; T = T_o;$$

$$\text{at } y = 0 \quad \frac{\partial u}{\partial y} = v = 0, \; \frac{\partial T}{\partial y} = 0,$$

$$\text{at } y = H(x) \quad \frac{\partial u}{\partial y} = 0, \; T = T_{SL},$$

A Runge-Kutta routine[9] was incorporated into a digital computer program which performed the iterative process to determine the values of T_{SL}, W/A cond., and V_i to allow the differentials to be evaluated. The numerical solution yielded the shape of the jet as well as its longitudinal velocity and temperature profiles. The difficulty in the analysis is integrating from the jet liquid injection plane where the mass flows and temperatures are specified. The integration is carried out for various gaseous phase inlet pressures until that value which allows the full vapor flow to be condensed within the jet condenser vapor funnel is determined.

The jet condenser analytical model with 45-.3683 mm diameter jets was a tool used in an attempt to match the measured performance of the actual development jet condenser. It was found necessary to increase the jet heat transfer coefficients (equations 2.40 and 2.41) by a factor of ~5 in order to match the measured jet condenser data. Only those data where the presence of noncondensable gas was very low (<5 ppm) were used when the model assumed zero noncondensables.

Predictions obtained using the jet condenser analytical model applied to the development jet condenser are illustrated in Figure 27. Vapor mass flow, vapor velocity, vapor pressure bulk liquid and jet surface temperatures, and vapor funnel geometry are all shown as a function of distance from the injector. Most of the predicted values are within expected ranges; i.e., Vapor Velocity is > 92 m/sec, $T_{SL} \leq 372.2°K$. Vapor pressure at the inlet was above design at .759 kPa.

A comparison of the analytically predicted jet condenser inlet vapor pressure as a function of liquid inlet temperature with experimentally measured values for the development jet condenser with liquid mass flow rates of ~.127 kg/sec and vapor flow rates of ~.0145 kg/sec is shown in Figure 28. The agreement of this prediction and actual test data is within 10%, (see Figure 28).

Predictions obtained using the analytical model as applied to the 90-nozzle .254 mm diameter jet condenser are shown in Figure 29. Again actual values obtained deviate less than 5% from predicted values. The predicted jet condenser inlet pressure as a function of liquid inlet temperature for the 90-nozzle system is shown in Figure 30. Actual results of .690 kPa, at 348.9°K, were better than predicted values of .7935 kPa at 349°K by 15.2% (percent).

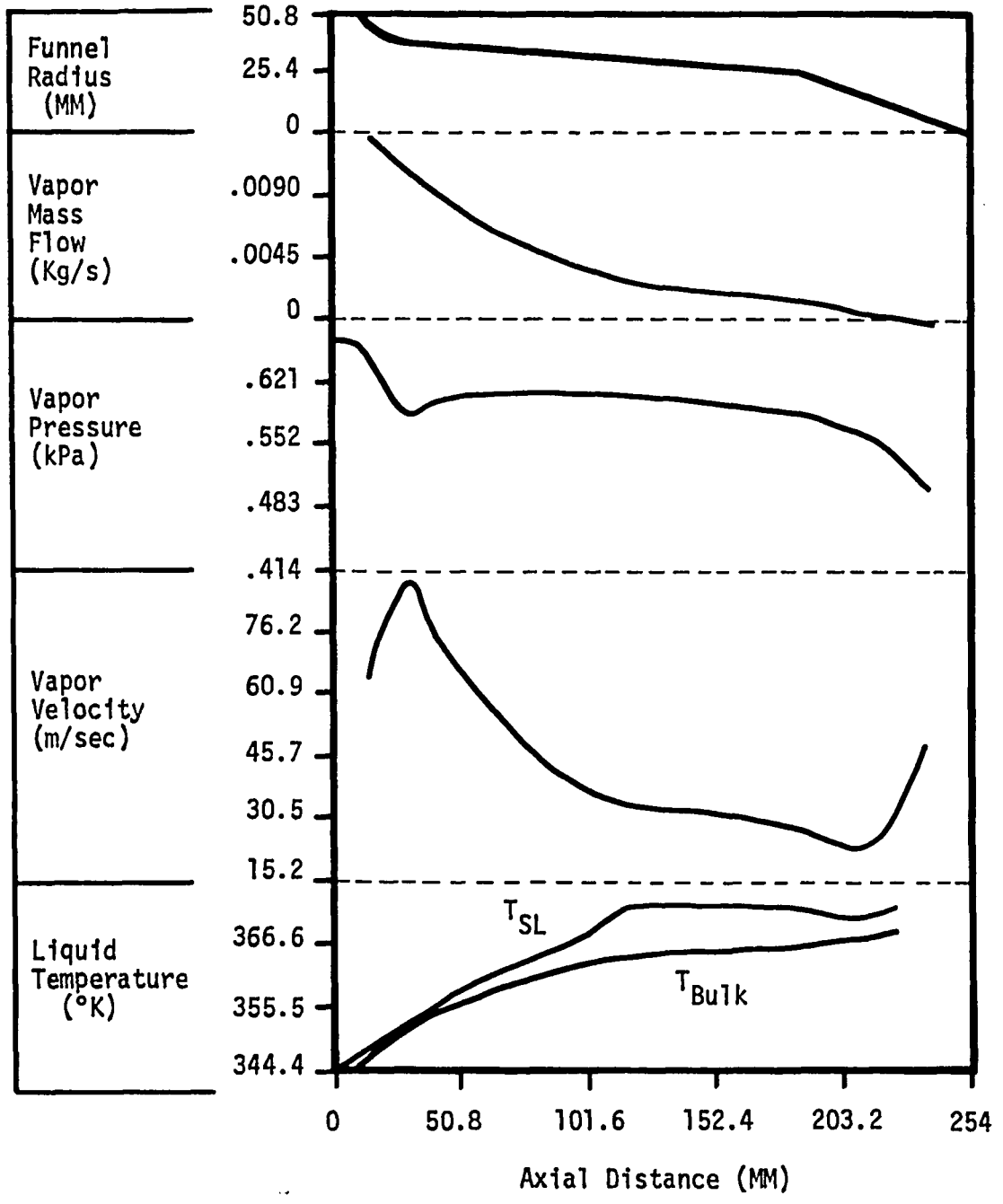

DETAILED RESULTS - 45 NOZZLE SYSTEM

FIGURE 27.

The effect of noncondensable gas on jet condenser operation was not investigated with the jet condenser analytical model, although the model allowed for such investigation. By the time the noncondensable analysis was included in the analytical model, actual test data were available which showed the sensitivity of the development jet condenser to noncondensable gas. These test data indicated the need to maintain noncondensable gas concentrations (air) to low levels <10 ppm. The model predicted levels had to be maintained at < 20 ppm.

As mentioned above, actual results showed the 90-nozzle jet condenser successfully lowered the inlet pressure by 15.2% (percent) and thus reduced the backpressure of the turbine in the Organic Power System. This allowed the turbine efficiency to rise by 1.68% percent which improved the overall system efficiency.

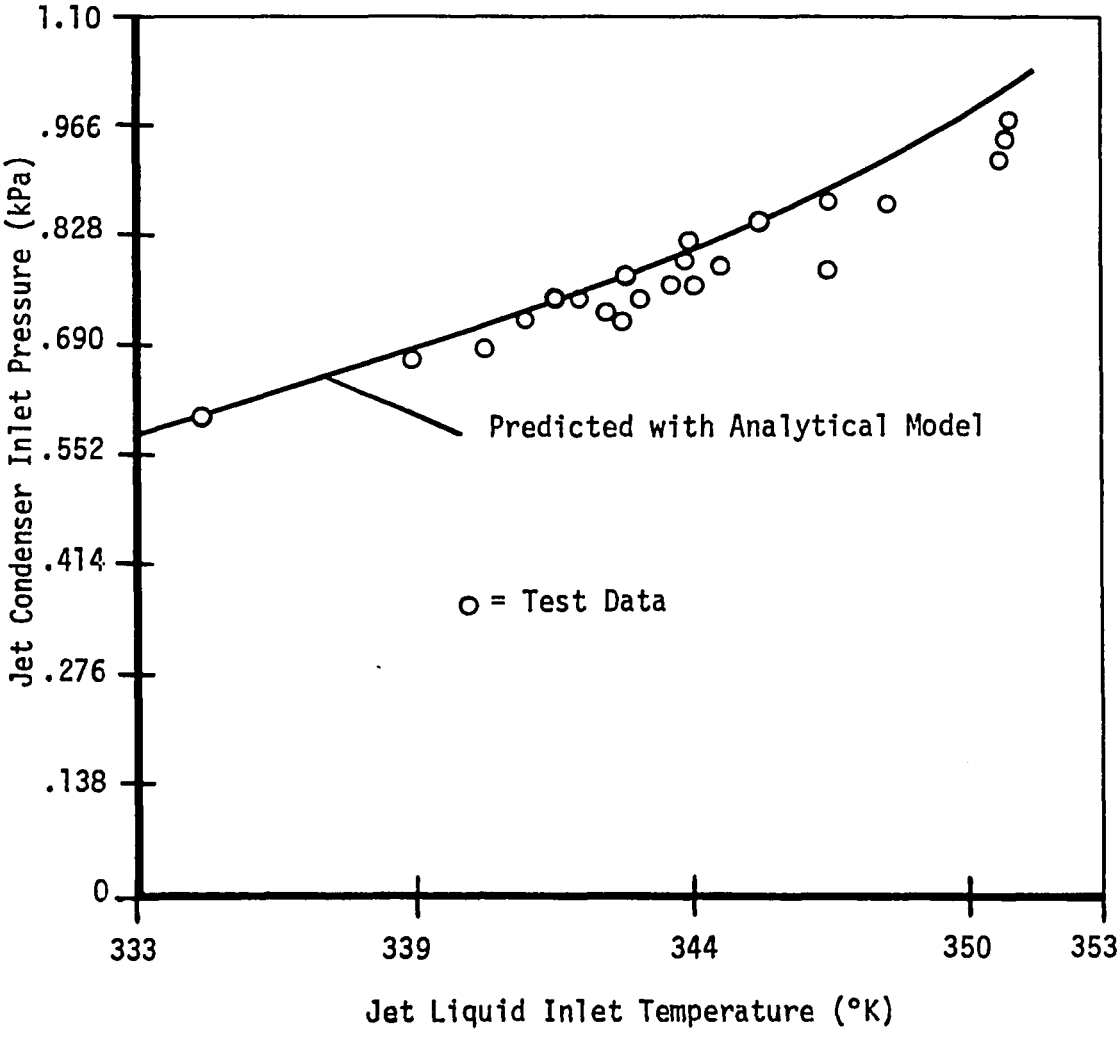

COMPARISON OF MEASURED AND PREDICTED VALUES
45 - .3683 MM DIAMETER NOZZLES

FIGURE 28.

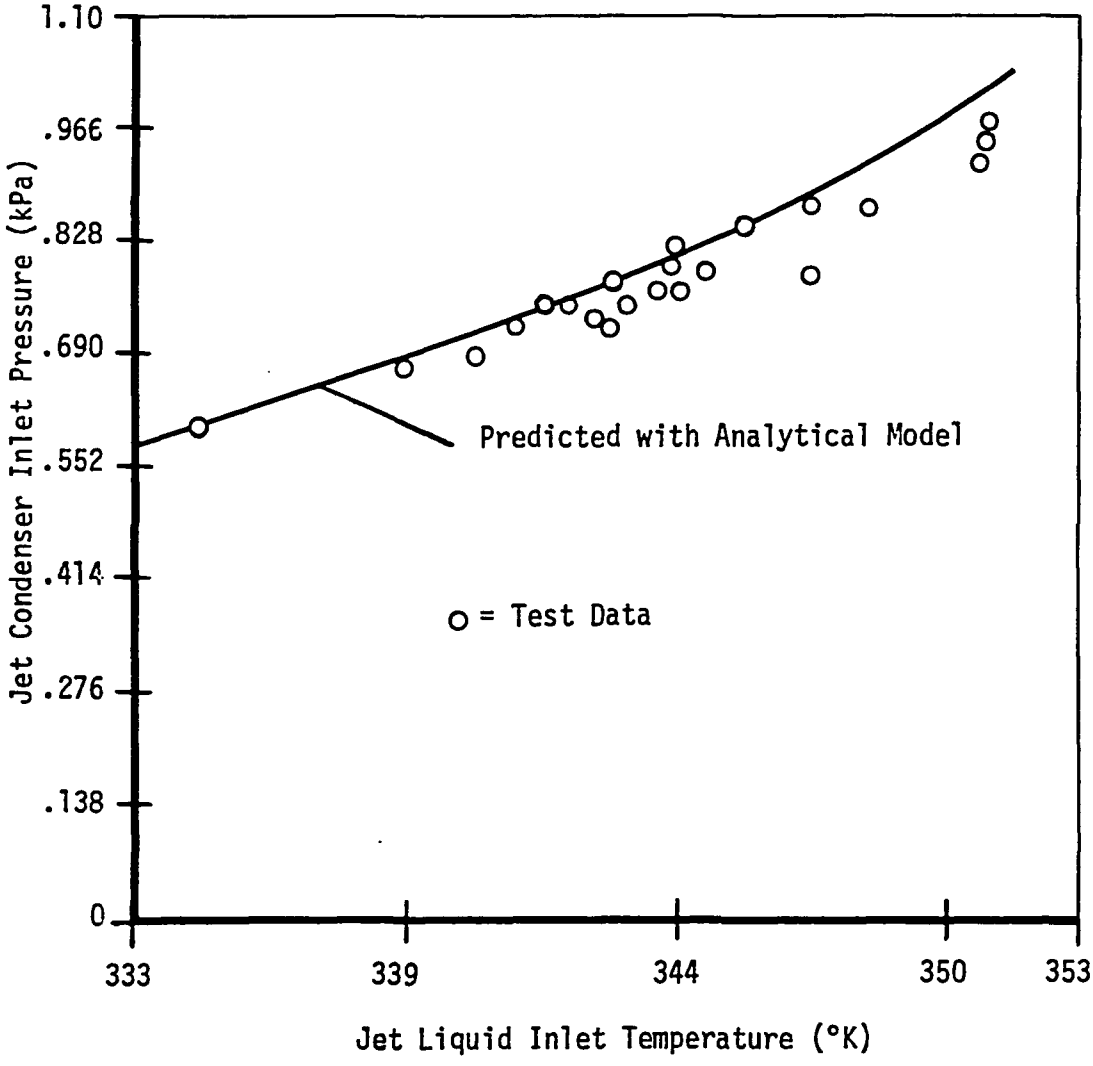

COMPARISON OF MEASURED AND PREDICTED VALUES
45 - .3683 MM DIAMETER NOZZLES

FIGURE 28.

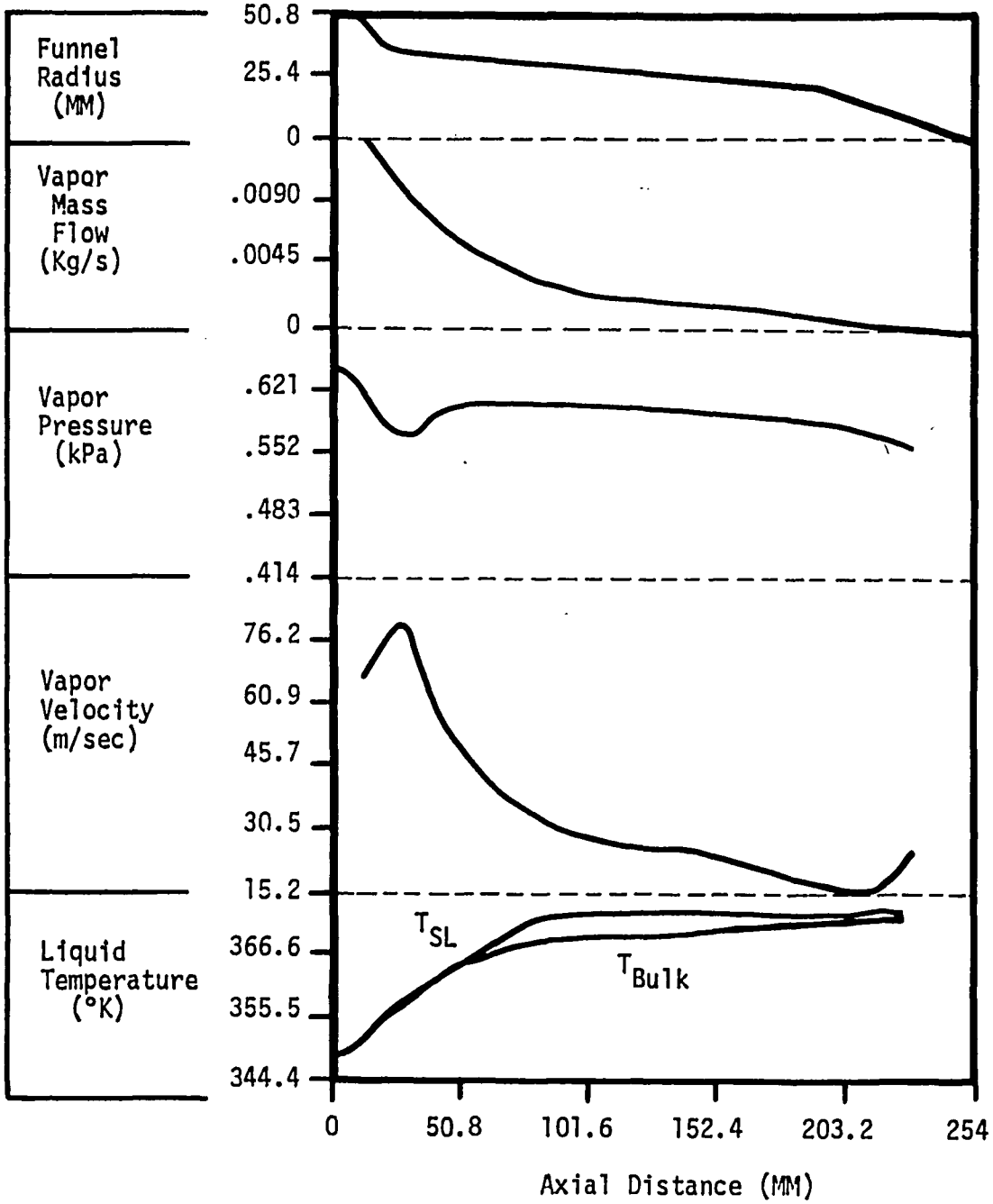

DETAILED RESULTS - 90 NOZZLE SYSTEM

FIGURE 29.

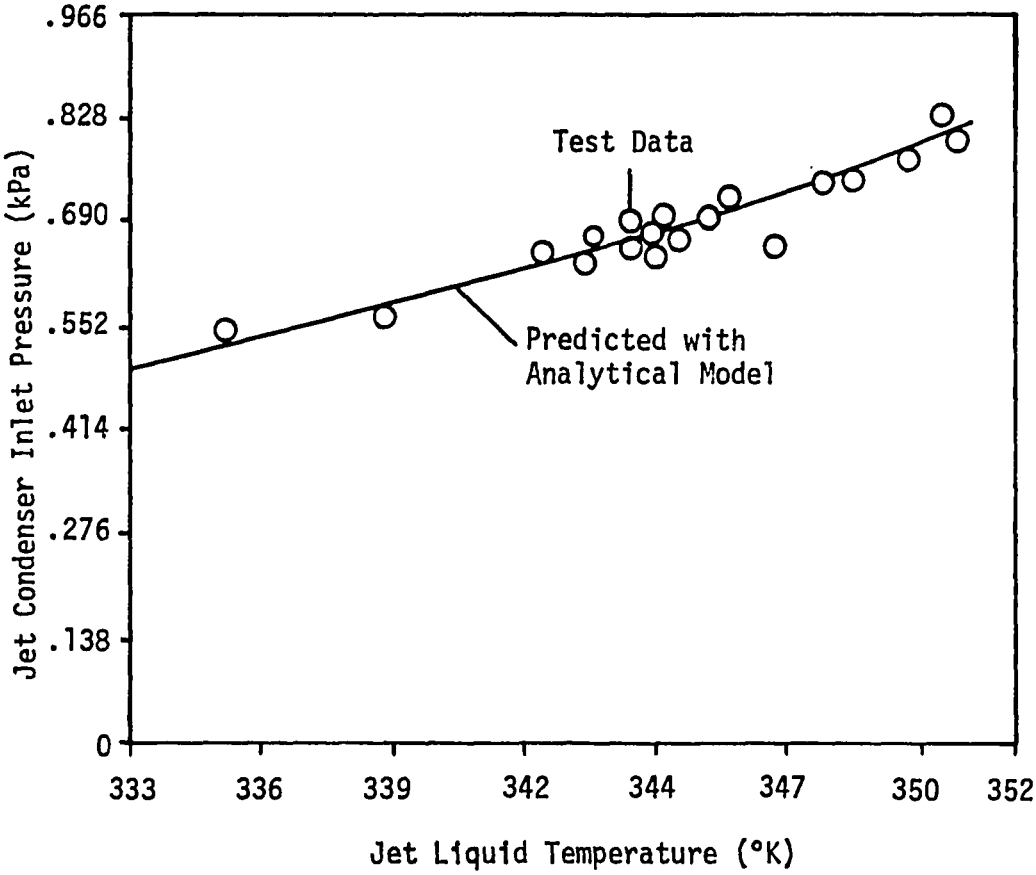

COMPARISON OF MEASURED AND PREDICTED VALUES

90 - .254 MM DIAMETER NOZZLES

FIGURE 30.

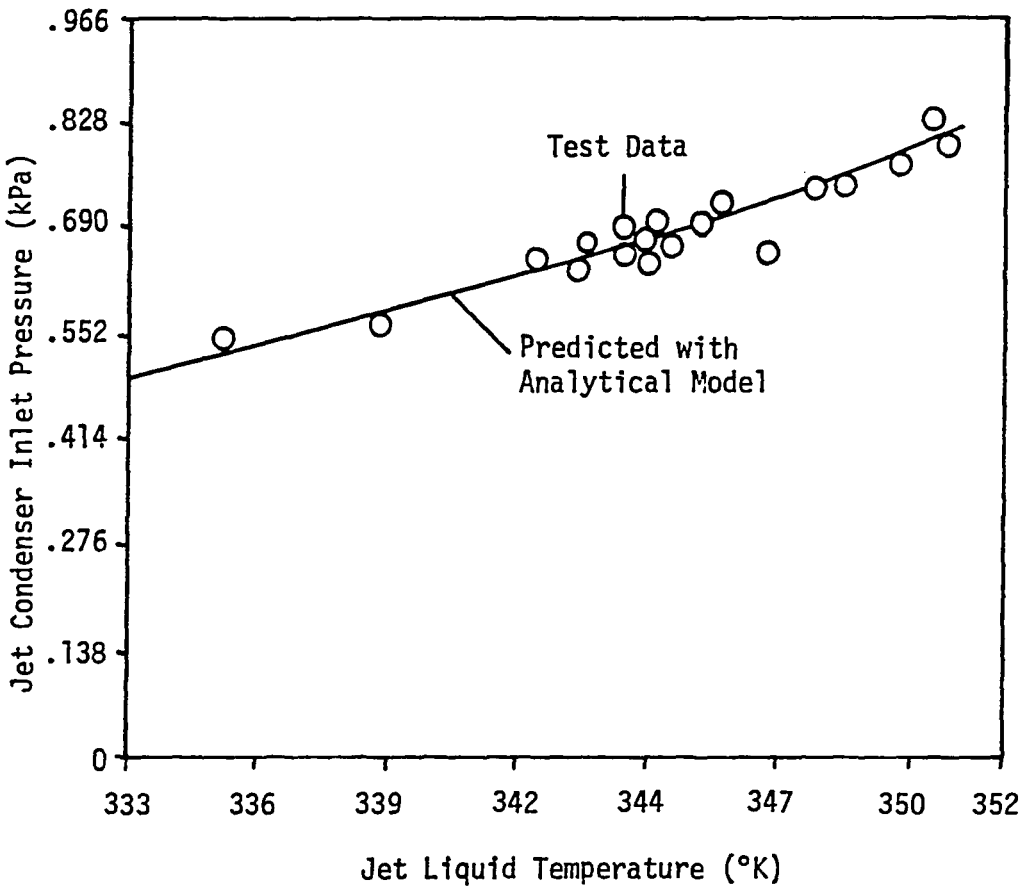

COMPARISON OF MEASURED AND PREDICTED VALUES

90 - .254 MM DIAMETER NOZZLES

FIGURE 30.

2.4 Stanton Number Multiplier caused by Noncondensable Gas Accumulation

At the end of Section 2.2, it was stated that a multiplier (factor of 5) for the Stanton Number was used in order to match the correlated test data on the development jet condenser. It is theorized that the steam/water test data may have been influenced from the effects of noncondensable gas accumulation. Within the Jet Condenser operation, the noncondensable gas accumulates in the vapor funnel as follows: Vapor continuously condenses on the liquid jets, and after a period of time, degradation of the liquid in the form of noncondensable gas diffuses away from the liquid stream and collects at a slow rate.

With the use of actual test data, an attempt is made to determine a representative gas concentration level, and verify the existence of the noncondensable gas. To model this particular case, an approach in classical Boundary Layer Theory is employed. This is simulated by mass transfer in a laminar flow over a flat plate with suction at the wall, as mentioned in Section 2.3. To establish parameters for the model, representative test data for the 50.8 mm jet lengths are shown in Figure 31, for the .254 and .3683 mm diameter jets. As is evident from the data, the Stanton Number increases as the heat

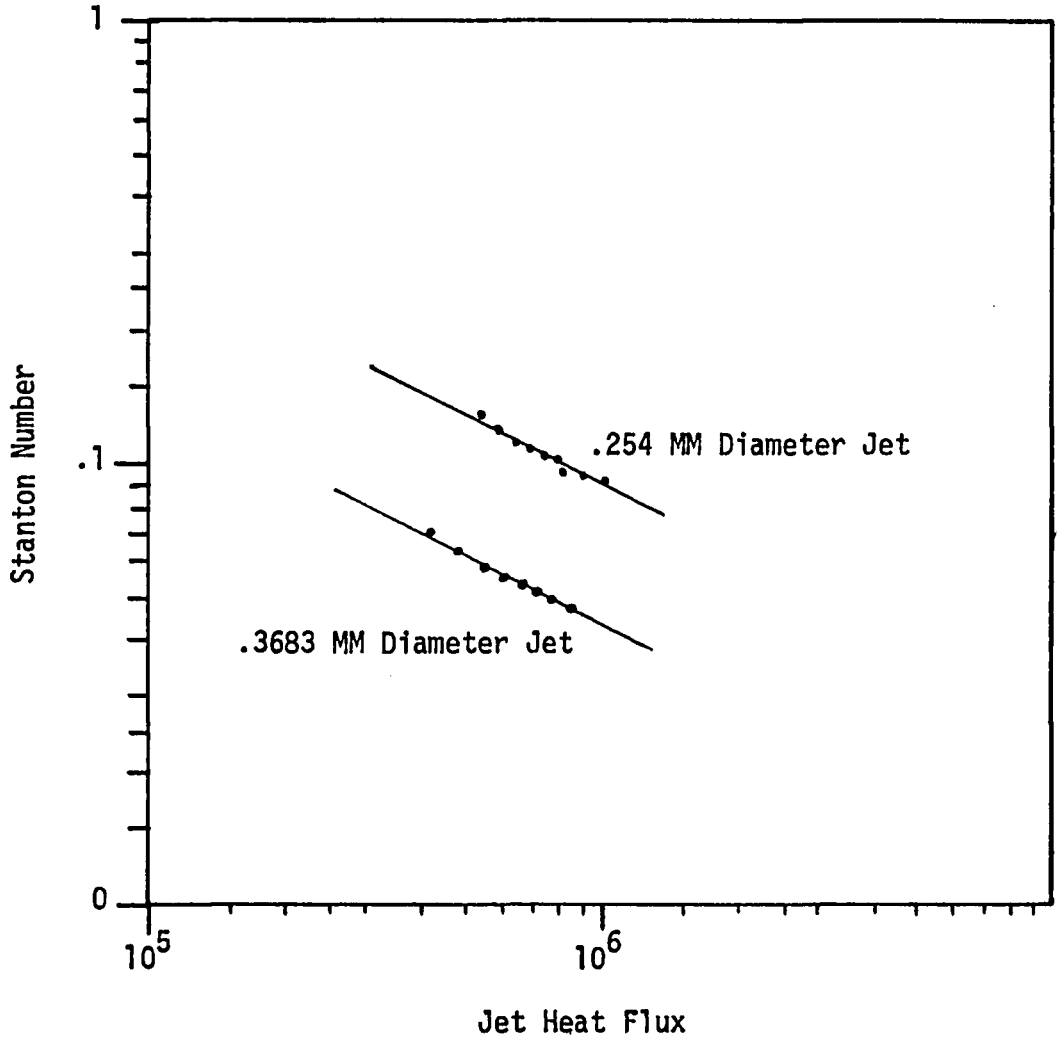

50.8 MM JET LENGTH DATA FOR .3683 AND .254 MM DIAMETER NOZZLES

FIGURE 31.

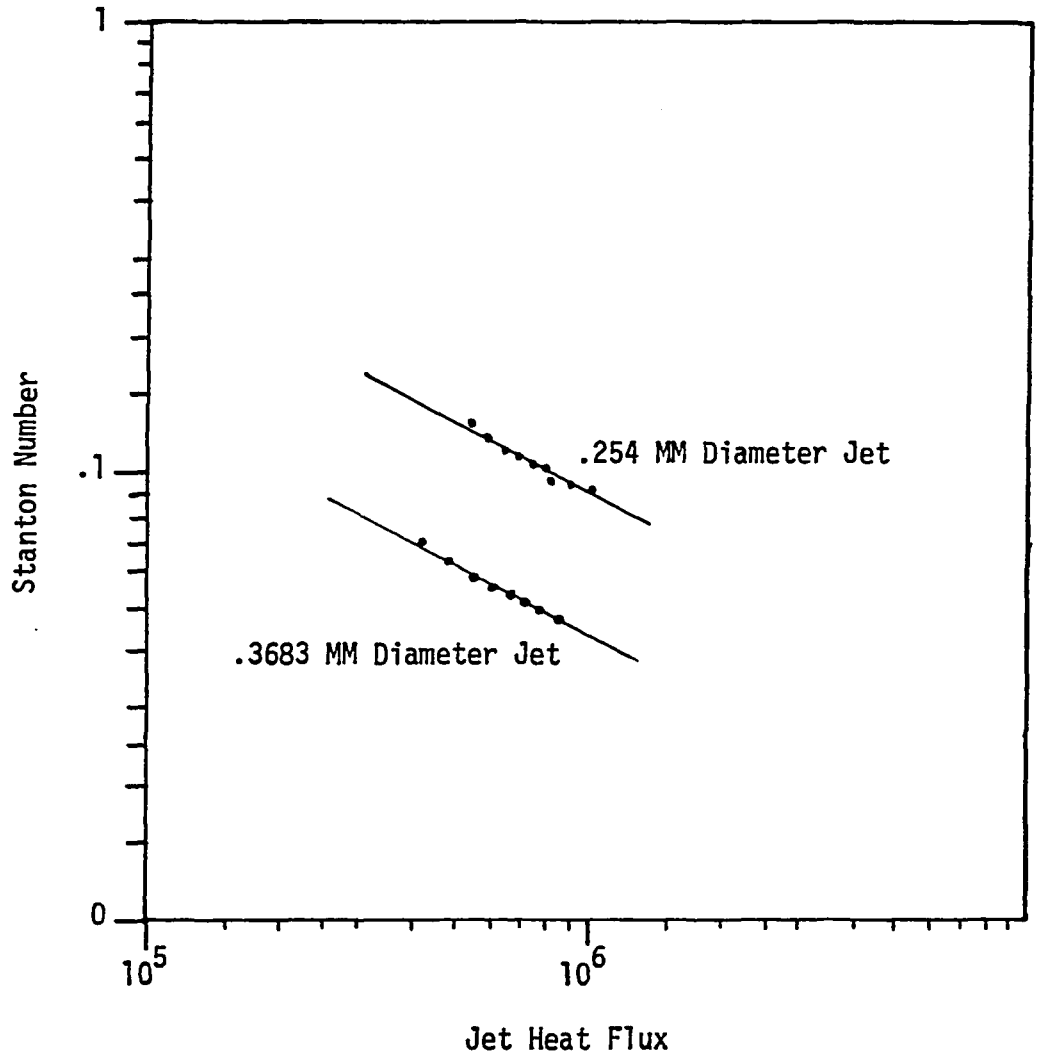

50.8 MM JET LENGTH DATA FOR .3683 AND .254 MM DIAMETER NOZZLES

FIGURE 31.

flux is decreased, and lower heat fluxes occur at lower steam pressures. The value of the diffusion coefficient, D, as predicted from equation (2.47), increases as the pressure is decreased, so it is possible that increasing the diffusion coefficient decreases the amount of noncondensable gas in the vapor funnel. Decreasing the amount of noncondensable gas is desirable because in addition to the underperformance, (low Stanton Number), it causes the vapor pressure to rise above design conditions of .69 kPa.

For the simulation, two data points for the .254 mm diameter jet were used to analyze the noncondensable jet equations presented in Section 2.3. The jets were treated as one increment[10,27] to represent the laminar flow over the flat plate. Data points over an incremental jet length were chosen to represent state points for the flow.

One data point was at 3.45 kPa, 299.4°K, and the second at 4.83 kPa, 306.11°K. Using 25.4 mm as the characteristic flow length, the suction parameter at the wall is given as

$$\left[\frac{V_o}{V_\infty}\left(\sqrt{Re_x}\right)\right]$$

with

V_o = Bulk velocity normal to the wall.

V_∞ = Free stream axial velocity.

Re_x = Reynolds number based on the bulk gas velocity, and distance x from the vapor inlet.

The suction parameter was calculated and found to be 48.9 for the higher pressure, and 36.2 for the lower pressure data point. It was also assumed that the Stanton Number without the noncondensable gas was 0.55 which is ~ five times the average for the 50.8 mm jet. With the above assumption, it was possible to calculate the average liquid surface temperature in order to determine the noncondensable gas concentration from equations (2.34) and (2.48) in Section 2.3. First, interfacial gas mole fractions of 0.33 and 0.39 for the 3.45 and 4.83 kPa pressures were found so values of the diffusion coefficient could be determined. The value of the diffusion coefficient for steam/air is 2.58×10^{-2} km^2/hr, and 1.85×10^{-2} km^2/hr at the 3.45 and 4.83 kPa pressure levels.

Utilizing (equation 2.46) with a S_C = .226 for the simulated model, values for H_{DO} of 2.34 km/hr and 2.0 km/hr also correspond to the 3.45 and 4.83 kPa data points. The data from Figure 26 are rearranged to show the mass transfer coefficient ratio minus the Bulk velocity

$$\left(\frac{H_{DO} - V_O}{H_{DO}}\right)$$

as a function of the suction parameter as shown in Figure 32. From this figure it is estimated that the mass transfer ratios are equal to .242 and .261 for the 3.45 and 4.83 kPa pressure points, respectively. The suction velocities are 95.6 and 108 km/hr, respectively, for the 3.45 and 4.83 kPa points. Thus, from equation 2.45 the free stream to interface concentration ratios are calculated to be 170 and 207 for the 3.45 and 4.83 kPa data points.

The resulting estimate for Free Stream Noncondensable Gas Concentration for air in the steam is .001904 and .00195 for those two pressure data points. The fact that they are approximately equal indicates that an abundance of noncondensable gas does exist and its effects are responsible for the steam/water test results being low. Actual numbers for noncondensables were not available because vapor samples were not taken from the steam/water test rig. The reason samples were not taken was that the underperformance was established after testing was completed.

Full noncondensable tests were set up to be taken on Dowtherm, but were not completed in the first series of tests because of the presence of air in the test rig. A gas sample

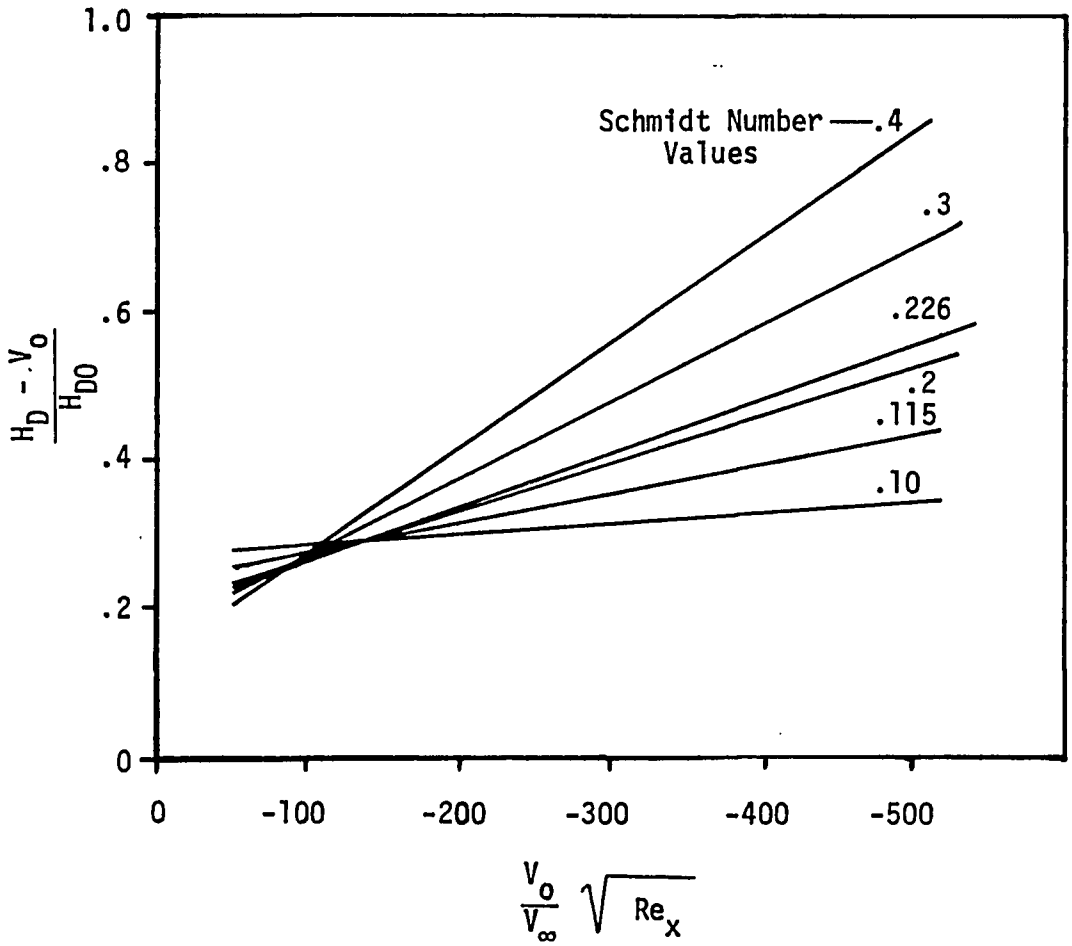

Note: Data from Figure 26. was used to compute above.

RATIO OF MASS TRANSFER COEFFICIENT NORMAL TO THE WALL VS. SUCTION PARAMETER

FIGURE 32.

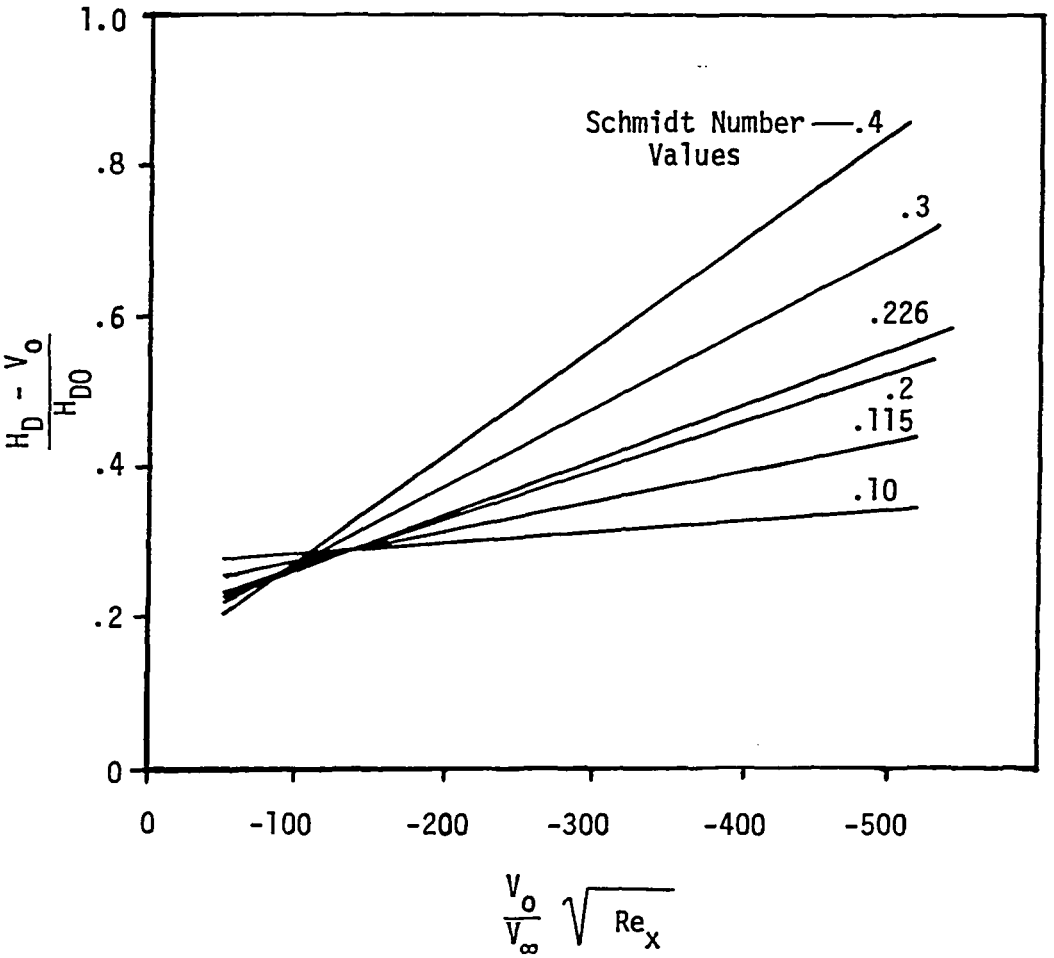

Note: Data from Figure 26. was used to compute above.

RATIO OF MASS TRANSFER COEFFICIENT NORMAL TO THE WALL VS. SUCTION PARAMETER

FIGURE 32.

was later taken on the system and the concentration of air was determined to be 0.03, which is of the proper magnitude, per the analysis technique used herein to assess the noncondensable gas effects, to cause the initial poor jet performance.

CHAPTER 3. JET CONDENSER MECHANICAL COMPONENTS

3.1 General

The jet condenser consists of three basic components:

1) The Vapor Funnel or Mixing Chamber,
2) The Liquid Injector with Nozzles,
3) The Diffuser.

The assembly is represented in Figure 33, along with the design parameters for the liquid, vapor, and condensate. The turbine is part of the power conversion system of the Organic Rankine System, and it delivers its exhaust gases at a temperature and pressure of 392.2°K and .69 kPa, as saturated vapor to the jet condenser. The system pump delivers subcooled Dowtherm "A" at a temperature and pressure of 348.7°K and 552 kPa. The low pressure vapor is ducted into a funnel coaxially, where it will mix with the liquid jets that are subcooled from the injector head. The liquid jets are injected into the vapor at 117.4 km/hr. and are aimed at the throat of the vapor funnel as shown in Figure 2. The objective of the condenser is to enable the vapor to condense on the subcooled liquid jets and have the combined liquid jet or condensate pass through a throat and into the diffuser, where it will undergo a sudden

SUBCOOLED LIQUID		
	Design	Test
Flowrate	.125 Kg/s	.125 Kg/s
Pressure	552 kPa	552 kPa
Temperature	349.4 °K	348.9 °K

Jet Condenser

CONDENSATE		
	Design	Test
Flowrate	.158 Kg/s	.158 Kg/s
Pressure	331.2 kPa	310.5 kPa
Temperature	373.3 °K	370 °K

HOT VAPOR		
	Design	Test
Flowrate	.139 Kg/s	.139 Kg/s
Pressure	.69 kPa	.79 kPa
Temperature	390°K	391.7°K

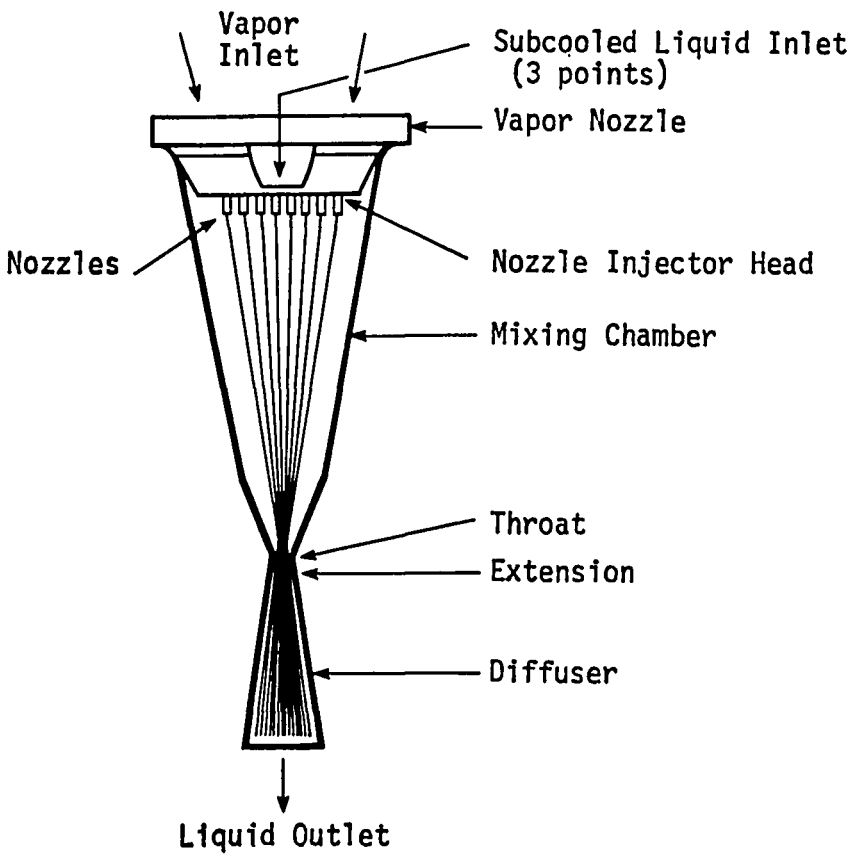

JET CONDENSER DESIGN SPECIFICATIONS AND COMPONENTS

FIGURE 33.

expansion to fill the entire cross-section of the diffuser. When this sudden expansion occurs, there is a loss of total pressure, but a gain in static pressure of the liquid stream.[28] The behavior of the liquid in the diffuser is identical to that which occurs in the diffuser of a cavitating venturi. The downstream condensate exits the diffuser and enters the expansion compensator or accumulator. The liquid exits the accumulator at a constant pressure of 262.2 kPa irrespective of the pressure recovery fluctuations. (Section 4. will show that a 50% recovery pressure was achievable during various tests.) With the liquid exiting the accumulator, it is delivered back to the system pump where it is split into two loops, one for the jet condenser to complete the cycle herein, and the other to the regenerator where the liquid temperature is raised to 505.5°K before entering the heat source. Since the process is based on liquid momentum for its operation[28], there is no requirement for a specific vapor pressure drop to insure proper condensate flow directions in a negative "g" field. This is the case for surface condensers, as discussed in Section 1.1. Thus, an achievement of a very low backpressure is used to improve turbine isentropic head and volumetric flow,[28] and to increase turbine and overall system efficiencies by as much as 1.8%, as discussed in Section 5.

Overall system parameters that were maintained at specific statepoints are discussed in Section 1.2, and shown in Table 2. The following sections describe the components of the jet condenser individually. The Liquid and Vapor are discussed within each area, along with their effects to each downstream component. The geometrical design of Sections 3.2 to 3.6 are based on the results achieved from the theoretical model that is described in Sections 2.1 and 2.2.

3.2 Vapor Nozzle

The saturated vapor is emitted from the turbine as exhaust gases at a Mach number ≥ 1, so the throat of the vapor nozzle had to be properly sized to allow for this parameter while at a pressure of .69 to .79 kPa, and a temperature of 392.2°K. The curved V-shape of the vapor nozzle is shown in Figure 34. The vapor enters the circular V-shape pattern as a result of the shape of the regenerator, which is mounted just above the jet condenser assembly. The high vapor velocity can result in a momentum interchange between the vapor stream at 392.2°K, M = 1, and the subcooled liquid stream at a temperature and speed of 348.9°K and 117.4 km/hr, thus yielding a greater pressure recovery at the diffuser outlet. This allows for a higher turbine efficiency at lower backpressures, as discussed in Section 3.1. The smooth-curved converging shape of the sonic

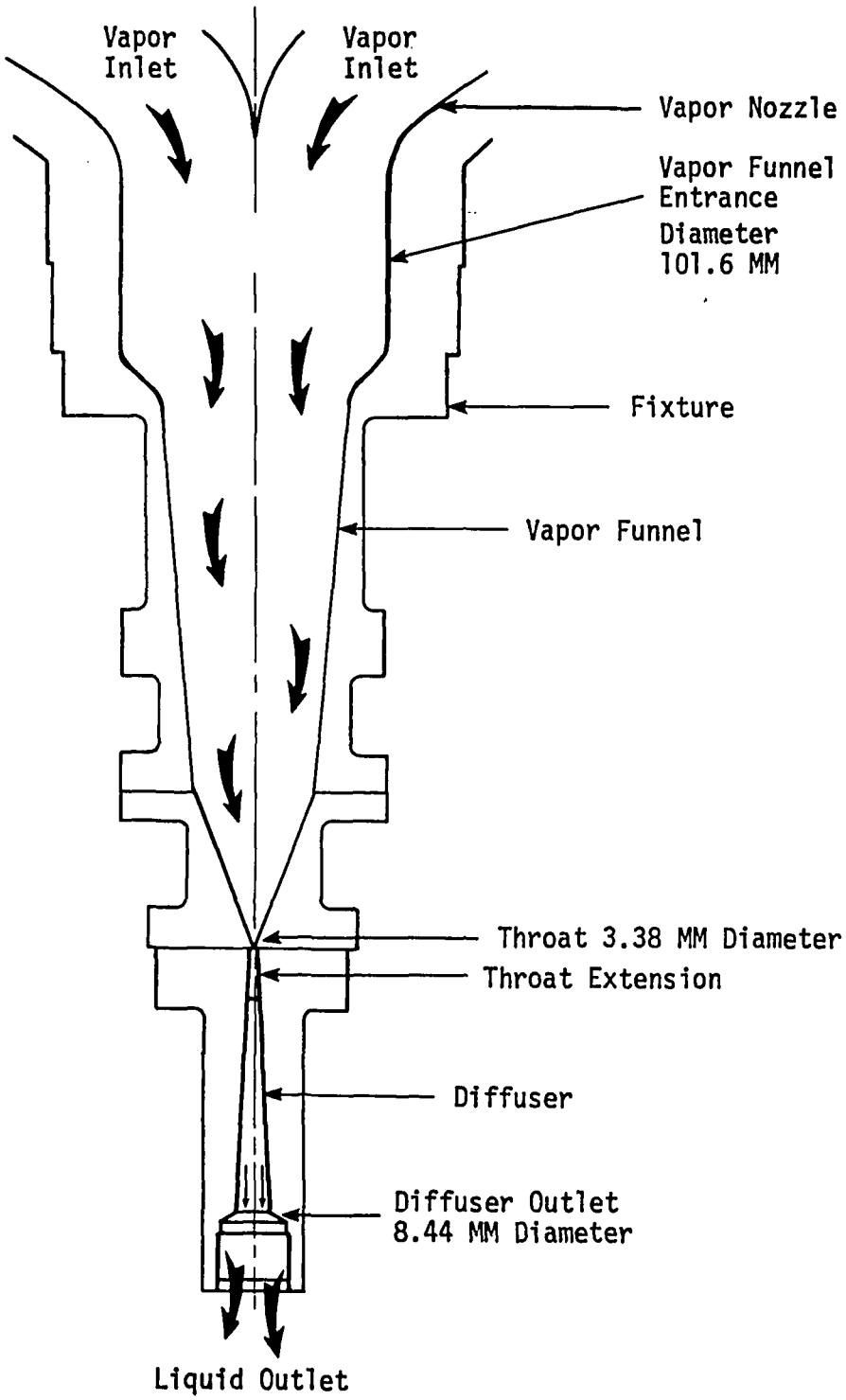

JET CONDENSER DETAILED MECHANICAL COMPONENTS

FIGURE 34.

nozzle head, as shown in Figure 34, also removes the adverse effect of any mixing chamber pressure fluctuations from the turbine, according to Chapman et al.[29]

The desired principle has been established. The significant point is that for a subsonic outflow, the exit plane pressure must equal the imposed backpressure, and thus the backpressure has an effect on the flow state upstream in the passage. However, if the outflow becomes supersonic the exit plane pressure need not equal the backpressure, and the upstream flow is not directly affected by the backpressure because an external adjustment is possible, as per Fox et al.[26]

3.3 Injector Head and Liquid Nozzles

After introduction of the saturated vapor to the entrance of the vapor funnel, the 348.9°K subcooled liquid steams are introduced through a certain number of nozzles that are mounted in an injector head. The injector head is appropriately sized to accommodate a series of nozzles which reduce the stream of liquid to an array of liquid jets, providing maximum surface area for vapor condensation. From the design criteria in Section 2.2, the number of nozzles was originally determined to be 45. When this particular unit underperformed, as discussed

in Sections 4.3 and 4.4, Sections 2.3 and 2.4 took additional parameters into account (noncondensable gas).

With the analytical analysis complete on Section 2.3, an injector head with 90 nozzles was designated as the proper size to deliver the liquid streams at .254 mm in diameter to the vapor funnel throat, and achieve a desired thermal performance of $\geq$ 19.5°K. The performance is the measured difference between the inlet vapor temperature in the mixing chamber, 391.7°K and the final condensate temperature in the diffuser prior to expansion $\leq$ 372.2°K (see Table 2). The necessary 19.5°K was determined to be the minimum amount required since the pump inlet temperature was designed to operate at $\leq$ 372.2°K, and the vapor temperature (from the turbine exhaust) was constant at 391.7°K. A pump temperature > 372.2°K would cause downstream component problems to the alternator and auxiliary cooler, such as premature bearing wear, and below normal efficiency.

Several nozzle configurations were evaluated on steam/water and Dowtherm, to determine which nozzle design would yield the highest thermal and hydraulic performance without producing significant amounts of noncondensable gas as discussed in Sections 2.4 and 5.3. Initial testing showed acceptable results with a stainless steel nozzle which has an

orifice length of 1.016 mm, and diameter of .254 mm, or an L/D = 4 (length to diameter ratio). The nozzle configuration is shown in Figure 35. Each nozzle was tested individually as described in Sections 4.1 and 4.2, with results discussed in Section 5.3. Upon successful thermal and hydraulic performance, the nozzles were incorporated into the multiple injector head, as described in Sections 4.3 and 4.4, for further performance testing. Results of the multiple nozzle testing are discussed in Section 5.4.

As described in the first paragraph of this section, initial performance for the 45-nozzle system was somewhat lower than anticipated even though Section 2.3 theoretically predicted it to be sufficient, and a 90-nozzle injector was redetermined to yield sufficient flow area for the vapor. Sections 4.4 and 5.4 describe the steps of how the stainless steel nozzles were initially used in the 90-nozzle system but could not meet the hydraulic requirements of Section 4.3 (focusing). Section 5.3 will discuss the design effort that was conducted to determine the proper material and orifice shape that finally yielded an acceptable liquid stream. The critical factor for the nozzle is the length to diameter ratio, (L/D), of the orifice. Various configurations with different L/D ratios are tested in Sections 4.1 and 4.2 to determine

which would give the best results (Chapter 5). From Chapman, et al.[29], the critical L/D ratio for a nozzle is that at which the jet does not reattach to the orifice walls from the vena contracta and represents an unstable condition. With an injection pressure of 552 kPa, and flow of 117.4 km/hr, the maximum critical L/D was found to be 3.5 from an empirical relationship in Fox et al.[26] As discussed in Chapter 5, a final L/D of 4 yielded a stable flow (Section 5.1) for the necessary jet condensation length, (Section 5.2).

Chapters 4 and 5 will also introduce the synthetic sapphire jewel nozzle. It is the nozzle that gives the best columnated jet due to its obtainable shape and finish after polishing. The design is shown in Figure 36, and was used in the 90-nozzle injector head for the final testing that was conducted. Results of the jewel nozzle are tabulated for comparison with other nozzles in Table 5.

3.4 Mixing Chamber

The mixing chamber is smoothly contoured to accept the vapor from the turbine exhaust after it has gone through the regenerator (see Figure 34). The profile of the vapor funnel or mixing chamber was designed in Section 2.3, and is based on the rate of condensation of the Dowtherm "A" working fluid.

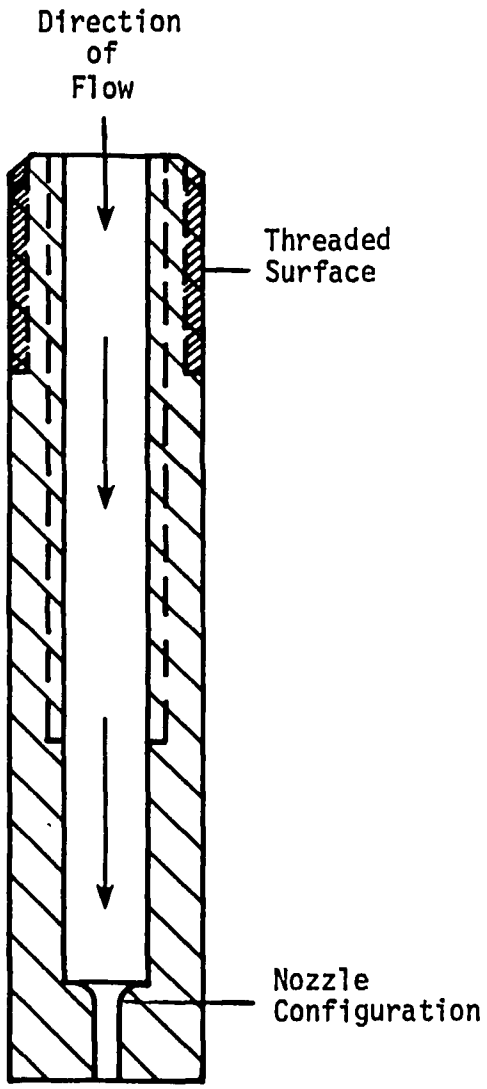

CHARACTERISTICS

ORIFICE DIAMETER	0.254 MM
ORIFICE LENGTH	1.016 MM
SURFACE FINISH	16
EXIT CORNER BREAK	0.0254 MM

STAINLESS STEEL JET CONDENSER NOZZLE

FIGURE 35.

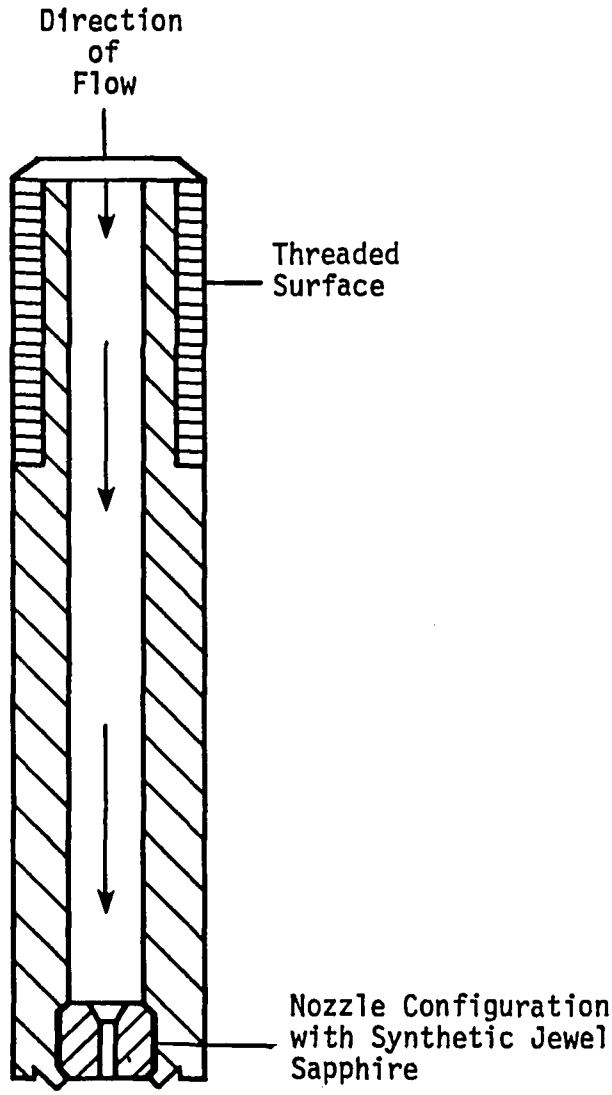

CHARACTERISTICS

ORIFICE DIAMETER	0.254 MM
ORIFICE LENGTH	1.016 MM
EXIT CORNER BREAK	0.0254 MM

JEWELL SAPPHIRE JET CONDENSER NOZZLE

FIGURE 36.

Figures 27 and 29 showed the actual chamber profile, and how it compared with the obtained results for optimum performance. The actual size of the chamber is based on the required area needed for the vapor (which is at a given velocity in relation to the liquid stream) to condense on the subcooled liquid. The size of the funnel and the number of nozzles are also based on the rate of condensation determined from the calculations in Section 2.3. The diameters of the funnel were given in Table 1. The shape of the mixing chamber provides sonic flow for both the vapor and liquid nozzles.[28] The narrow outlet end of the mixing chamber is contoured to allow a smooth flow of the condensate (combined liquid and condensed vapor) to the mixing chamber throat (Figure 34).

3.5 Throat

Assuming that all of the vapor is condensed (condensate) by the time the fluid passes through the throat region, a total flowrate is determined, and the throat design can be determined as follows: An approximate throat cross-sectional area and diameter are computed from continuity equations 2.1 to 2.3 in Chapman et al.[29] This is based on the assumption that the area just upstream and downstream of the throat can be assumed to be a sonic convergent-divergent nozzle in order to check for $\dot{m}_C$, the mass flowrate. As in the general case in Chapman et

al.[29], the supply stagnation states, Po_1 and T_o are known to be constant for ideal conditions. With the backpressure known, the throat, A_t, corresponds to the greatest mass flow density. When the mass flow density has reached its maximum value, we have the following at ideal conditions:

$$\frac{\dot{m}_c}{A_t} = \frac{Po_1}{\sqrt{T_o}} \sqrt{K/R} \left(\frac{2}{K+1}\right)^{(K+1)/2(K-1)} \qquad \text{EQN 3.63}$$

To determine whether the mass flowrate is great enough to produce choking at the throat, the operating pressure ratio P_b/Po_1 is reduced from unity, and flow passes through the throat. At this point, if the mass flow rate, $\dot{m}$, is compared to the choked mass flowrate, $\dot{m}_c$, and is found to be $\dot{m}/\dot{m}_c < 1$, the Mach number at the throat is subsonic. As a result, the flow in the diffuser is subsonic, and verifies that there is a pressure rise. With P_b/Po_1 determined, the first critical pressure ratio, r_{p1}, is found in the isentropic tables based on an exit to throat ratio. With all quantities now known, A_t was calculated and found to be .3378 mm. The throat diameter was verified with a flow test simulating the funnel conditions, (combined multiple liquid streams) and results showed that a combination of the proper diffuser and throat (.3378 mm diameter) gave good results to achieve a 50% pressure recovery for the jet condenser assembly.

3.6 Diffuser

As mentioned in the previous section, once the liquid condensate passes the throat, it enters the diffuser region as shown in Figure 34. The term diffuser denotes a flow passage which decelerates flow, thereby producing a fluid pressure rise. In this region, it is desired to convert the velocity head of the liquid condensate to a static pressure rise. The greater the pressure recovery (rise in pressure) of the jet condenser assembly, the lower the pumping power requirements, which results in a higher system operating efficiency. As discussed in Section 3.1, the liquid exits the diffuser, passes to the accumulator to reduce pressure fluctuations and is sent to the pump. A higher pressure sent to the pump reduces the effective work (in the form of outlet pressure) done in the cycle.

The diffuser used in this assembly is defined by Chapman et al.[29] as a duct diffuser, since it receives its liquid supply from a closed duct (vapor funnel assembly). Reviewing Figure 34. shows that the diffuser inlet diameter corresponds to the throat diameter (.3378 mm), per Section 3.5, while the diffuser outlet diameter is designed to assure that all of the liquid stream (condensate) velocity head is converted to static

pressure. According to Chapman et al.[29] for sonic situations the geometry of the diffuser need only be a constant divergence without any curvature present in the direction of the flow area.

The performance of the diffuser is described by a certain parameter. This parameter, the energy efficiency[29,30] is defined as the ratio of the actual kinetic energy that has been converted into a pressure rise to that which would have been converted into the same pressure rise had the diffusion been isentropic. For ideal conditions, the energy efficiency is

$$n_e = 1 - \frac{(\frac{Po_1}{Po_2})^{(K-1)/K} - 1}{\frac{K-1}{2} M_1^2}$$

with

Po_1 = Stagnation pressure at the throat

Po_2 = Stagnation pressure at the diffuser exit

K = Gas constant

M_1 = Mach number at the throat

As mentioned in the beginning of this Section, the velocity head of the liquid entering the diffuser is converted to a static pressure rise. To insure that this is accomplished, the outlet diameter, 8.45 mm, was designed to be 2.5 times the

inlet diameter, 3.38 mm, and the diffuser angle is at 6.5° which is in accordance with diffuser designs by Chapman et al.[29] The area ratio for the diffuser $(Do/Di)^2$, was 6.25.

Finally, the equation used to define the pressure recovery (rise in pressure) of the diffuser is in agreement with Garcia[4], and is given as

$$\psi = \frac{\text{Diffuser Outlet Pressure Rise}}{\text{Throat Inlet Pressure Rise}}$$

Even though specific individual pressure readings were obtained for the diffuser, they are considered as a pressure rise in relation to the pressure readings of the liquid stream from the injector nozzles. The actual pressure recovery (rise) is tested in Section 4.3 to determine the highest possible recovery. Table 3 within Section 4.3 is a typical data sheet that is used to record the various parameters of the test.

CHAPTER 4. TEST LOOP APPARATUS AND PROCEDURES

4.1 Steam and Water Test Apparatus

In order to obtain a data base to develop the jet heat transfer correlations, a test stand utilizing steam and water was developed. The stand is shown schematically in Figure 37. It was designed so that the temperature rise of a single liquid jet through steam could be reasonably measured.

Cold water is injected through the injector nozzle and passes a steam space and then through a focus/target plate into a dewar flask containing a thermocouple. By measuring the liquid inlet temperature at the nozzle and the liquid temperature in the dewar flask (see Figure 38. for dewar thermocouple installation), the jet temperature rise was measured. The steam condition was measured using a thermocouple and a manometer. The steam was introduced by boiling deaerated water in a hotwell tank mounted directly beneath the jet/dewar assembly. The hotwell was heated with an electrical blanket heater. Jet length is varied by repositioning the baffle plate which holds the dewar flask. Another component in the stand is a cold trap, plumbed to provide a steam flow past the liquid jet in an attempt to sweep away any noncondensable gas which might accumulate around the

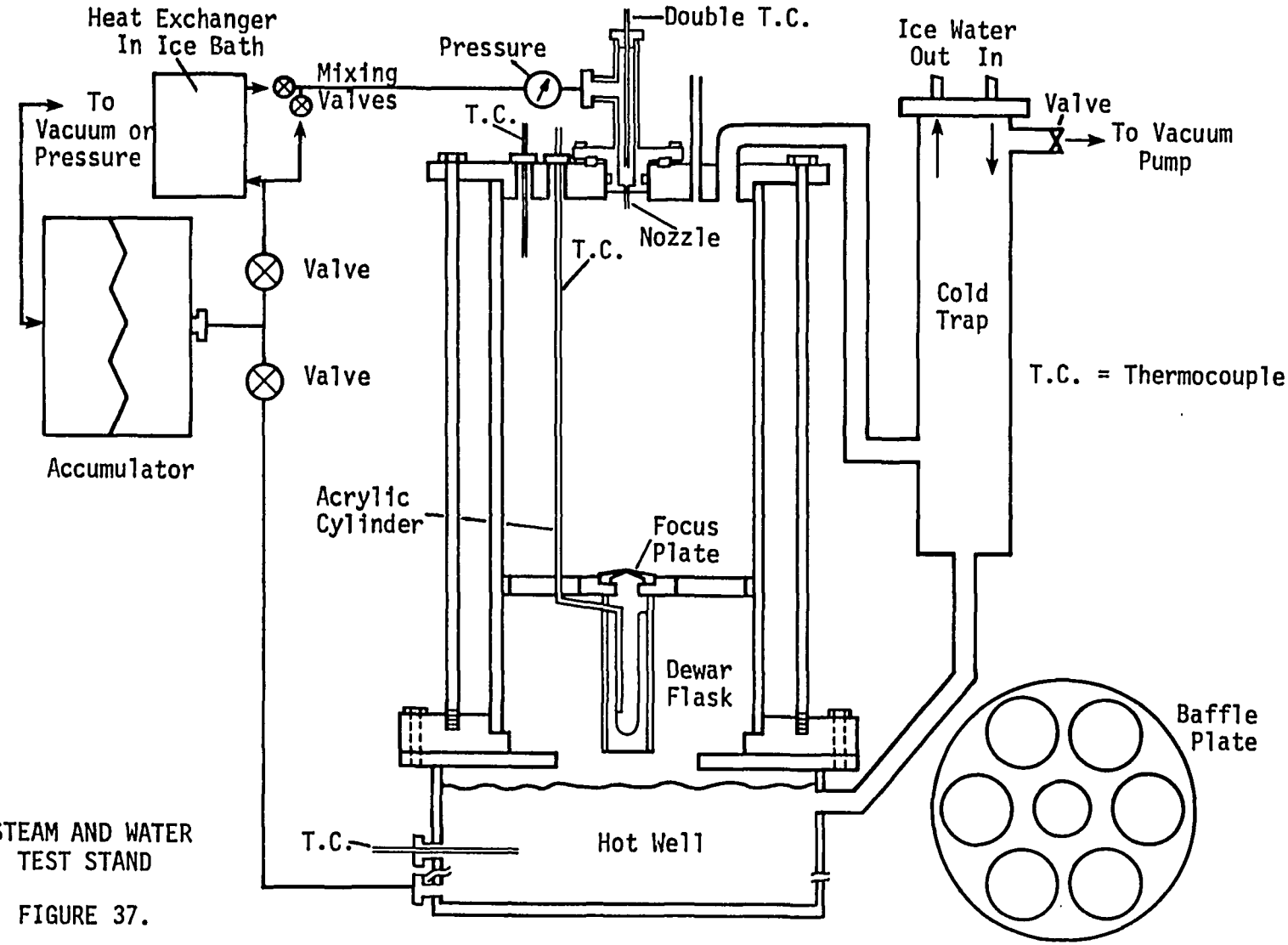

STEAM AND WATER
TEST STAND

FIGURE 37.

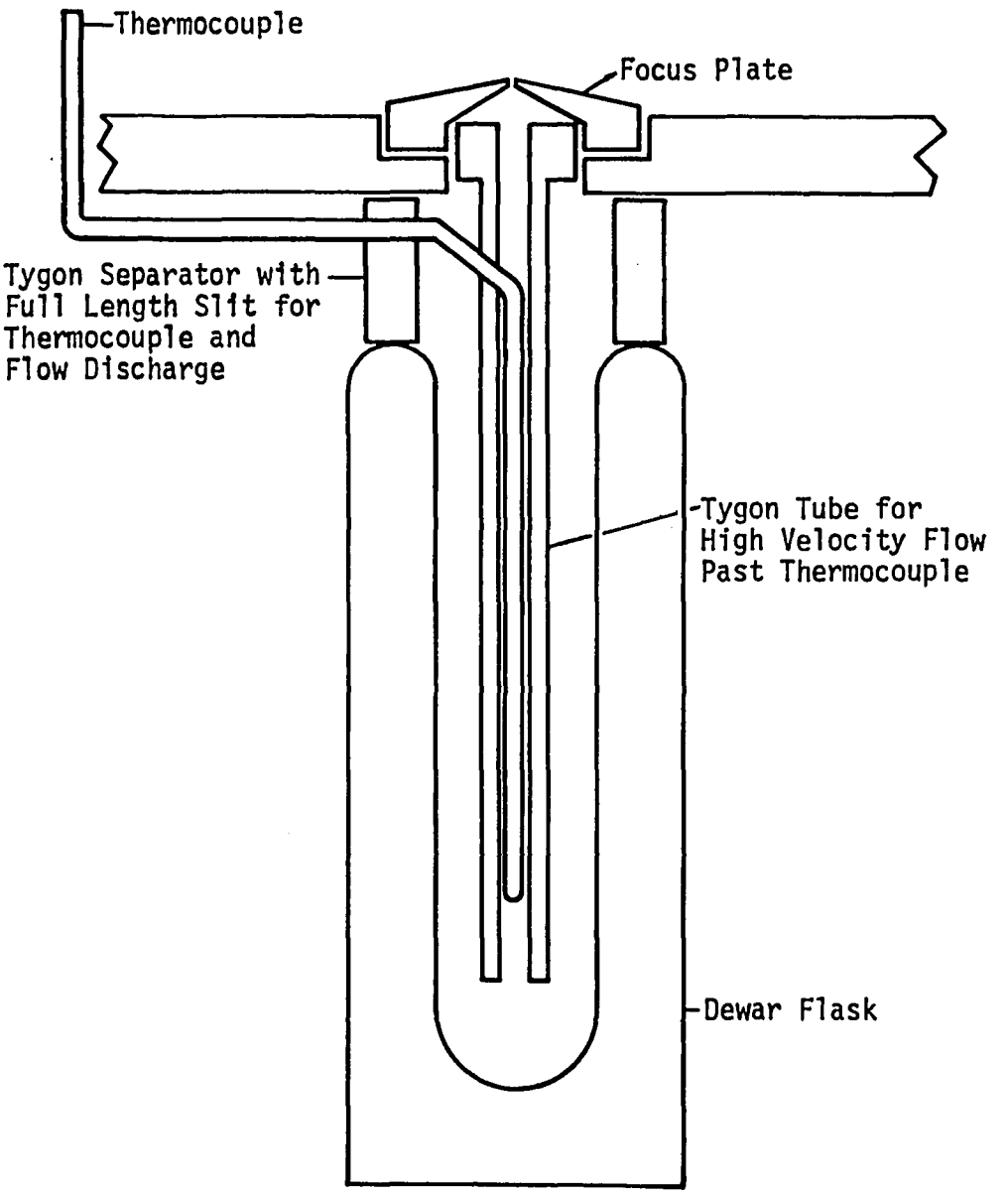

INJECTOR JET END TEMPERATURE MEASUREMENT

FIGURE 38.

liquid jet. The gases were pumped out of the cold trap using a vacuum pump. The pump also created a vacuum for the stand to simulate space conditions. Since the nonhermetic test stand had an air leakage rate of ~ 0.006 scc/sec, the simulated flow of the condenser was not considered ideal. The liquid was supplied to the injector nozzle from a bladder-type accumulator with deaerated water on one side and nitrogen gas on the other side. The liquid supplied to the nozzle was cooled to the desired inlet temperature via an ice-cooled heat exchanger and a bypass mixing valve.

The heater was insufficient in maintaining a constant heat input for the steam which varied the pressure slightly, so data were taken over a range of high to low steam pressures. A typical run took about 15 minutes during which 9 data points were taken. Several tests were repeated and the heat transfer results (Stanton Numbers) for nearly identical test conditions were found to vary by less than 5% (percent), when compared to Section 2.2.

4.2 Liquid Dowtherm Test Rig (Single Nozzle)

4.2.1 Scope. The test procedure used is part one of three parts. It provides a description for one of the verification methods used in the overall development of the jet condenser.

The test verifies adequate thermal and hydraulic performance for each nozzle individually.

4.2.2 Objectives. To verify on dowtherm the results of the steam/water testing for nozzle selection, targeting capability, and the tendency toward unstable flow. It is also desired to characterize the condensing rate performance at varying lengths, velocities, and states for possible orifice configurations. Finally, to determine the sensitivity of the jet condenser to noncondensable gases.

4.2.3 General. The test equipment that is used was manufactured to quality control specifications and general cleanliness conditions per specification CP14.57-01.[31] The instrumentation for the test rig has been previously specified[31], and at the time of the test could have been substituted for instruments of equivalent characteristics and tolerances. The following parameters were monitored and data recorded:

Description	Units	Designation
Injector Flow	cm^3/sec	QL
Injector Pressure	kPa	PL
Injector Temperature	°K	TL
Vapor Temperature	°K	TV
Outlet Temperature	°K	TO
Pump Outlet Pressure	kPa	PPO
Pump Inlet Temperature	°K	TCO
Hotwell Temperature	°K	TB
System Pressure	Microns of Hg	P2
Hotwell Pressure	Microns of Hg	P3

The testing was conducted at existing laboratory ambient conditions.[31] The test fluid used is Dowtherm "A", and is specified as reagent grade Biphenyl-Biphenyl Eutectic Ether. The nozzle examination consists of visual inspection, with a twenty-five (25) power microscope, for damage or corrosion prior to and after all tests.

4.2.4 Test Plan. The thermal performance test consists of establishing representative liquid flows and temperatures, vapor temperatures, and measuring the liquid jet temperature rise due to condensation. At design conditions, the liquid inlet pressure and temperature are 448.5 kPa, and 348.89°K, while the vapor temperature is 391.67°K, and the liquid delta temperature must be $\geq$19.4°K.

In order to completely characterize each tested configuration, and to verify the thermal model in Section 2.3, tests are performed at jet lengths of 50.8, 127, and 254 mm, with liquid injection temperatures of 344.45 - 350°K, and liquid injection pressures of 448.5 - 586.5 kPa. In addition, noncondensable concentrations are determined during certain tests by opening the cleaned and pumped-down noncondensable concentration instrumentation (valved bottle on the test rig), as shown in Figure 39. The "bottle" at ambient temperature provides a surface for condensation, while a thermal pumping

(diffusion pump principle) action is established. By properly sloping the test section, the condensate drains by gravity into the bottle, with the noncondensables collecting in a cloud above the liquid. This stage is characterized by the bottle and feed tubes becoming hot due to the condensation on the inner wall. The noncondensable cloud in turn effectively blocks off a portion of the condenser (bottle) surface. This action continues until the cloud is of sufficient size to cover the available condensation surface. This is characterized by the bottle and tubes returning to ambient temperature and marks the end of a test. The concentration is obtained by measuring the collected liquid in the bottle, knowing both total volume of the tested section, and the recorded pressure (microns) during the test. Equations in Appendix A have the following units

$$\text{Concentration } C \ \frac{\text{parts}}{\text{million}} = \frac{\text{moles noncondensable X } 10^6}{\text{moles Dowtherm}}$$

As an example, with the bottle full after a given test ~307 ml (see Figure 39), the calculated concentration of noncondensables is ~20 ppm. Floodout occurs at ~90 ppm, thus showing the sensitivity of the test. This data allows both incorporation of the effect on noncondensables into the thermal model (Section 2.3), and experimental verification of the results from (Section 2.4). Further details and effects of the noncondensables are given in Appendix A.

The first configuration tested was the one utilizing the stainless steel nozzle (Section 3.3), Figure 35. The second configuration tested, employed the synthetic sapphire jewel insert (Section 3.3), Figure 36 with an L/D (length to diameter ratio of the orifice base) of four (4). As previously mentioned, different L/D ratios other than four gave poorer flow characteristics.

The attempt here is to determine the design margin, to establish reasonable production tolerances on length, and establish a new baseline while verifying the thermal model. The baseline nozzles from the steam testing in (Section 4.1) will be retested on the Dowtherm test rig. These include the nozzles initially installed in the injector head, [.3683 mm diameter, with an L/D = 4].

4.2.5 Dowtherm Test Schematic (Single Nozzle). A schematic diagram of the Single Nozzle test rig is shown in Figure 39. The main components for the rig are:

1. Vacuum Pump - evacuates entire test stand to simulate space conditions, and creates the low pressure for the saturated vapor.

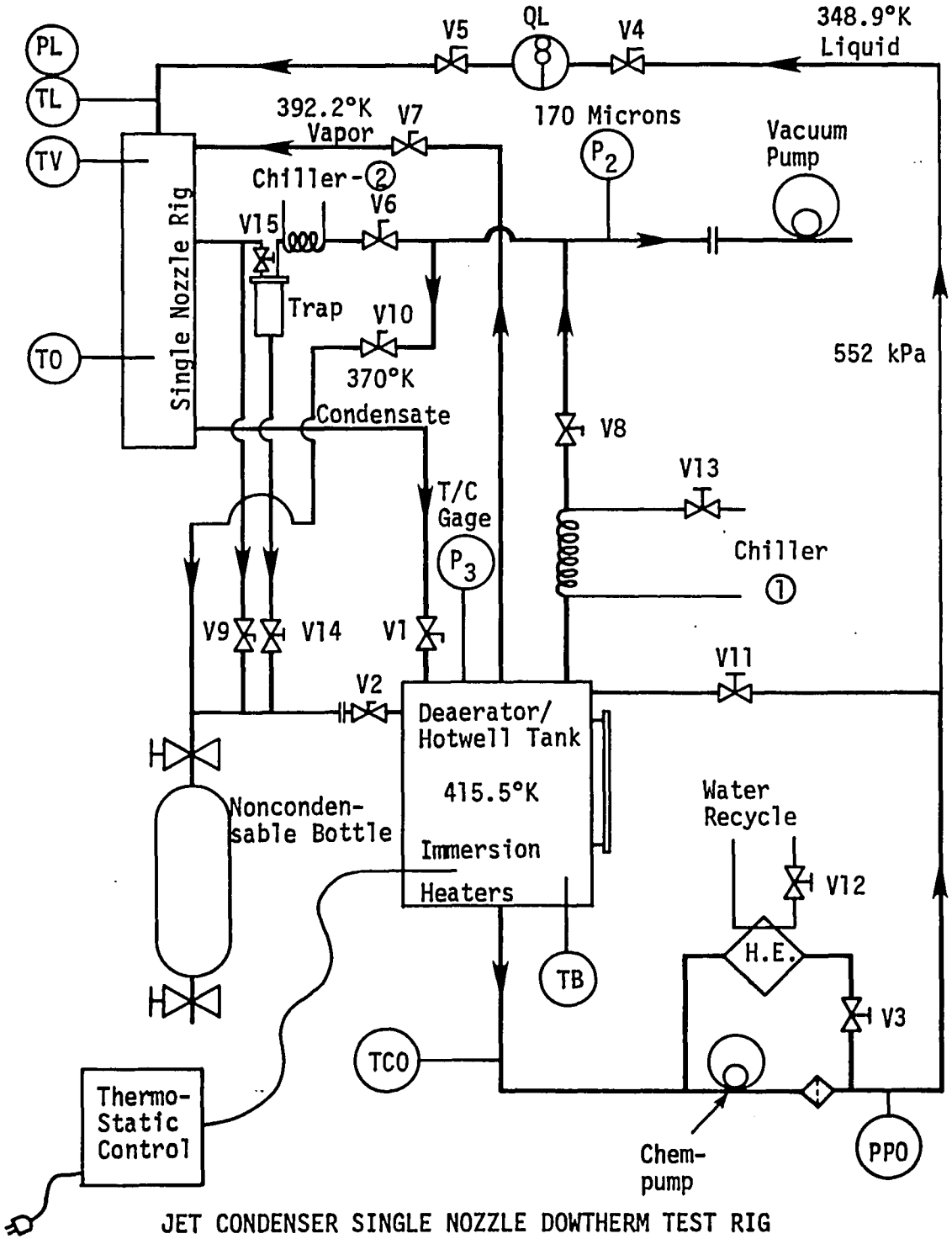

JET CONDENSER SINGLE NOZZLE DOWTHERM TEST RIG

FIGURE 39.

2. Hotwell Deaerator - this component is a collection tank and is used to create the saturated vapor at 391.7°K from the turbine exhaust, and provide liquid for the nozzles.
3. Heat Exchanger and Pump - these components receive hot Dowtherm from the hotwell tank and cool the liquid to the nozzle inlet temperature, 348.9°K, while delivering it at a pressure of 448.5 kPa.
4. Nozzle Housing - the stainless steel fixture where the nozzle is mounted and its liquid stream is viewed and measured for performance. The housing is easily converted to adjust for the different jet lengths to be tested.
5. Noncondensable Bottle - as mentioned in 4.2.4, this component collects the noncondensables to determine their concentration.
6. Thermo-Static Control - temperature control for the immersion heaters within the hotwell tank to heat the liquid.
7. Cold Trap - collects liquid in lieu of the noncondensable bottle when there is no testing. The trap also allows the vacuum pump to continuously draw a vacuum without removing liquid from the stand.

4.2.6 Test Procedures. There are two modes that the stand is normally in: 1) Standby Operation (short-term shutdown), and 2) General Running. Mode 1 allows the stand to remain

deaerated at 170-200 microns prior to a test while the liquid is heated and circulating between the heat exchanger and hot tank. Mode 2 is for actual testing and has the following conditions:

- Pump Outlet Pressure 793.5 kPa
- Hot Tank Controller 413.9°K
- Stand Vacuum $\leq$ 200 microns of Hg
- Hot Tank Vacuum $\leq$ 850 microns of Hg

4.2.7 Acceptance Testing. Table 2 is a typical data sheet that is used when testing a nozzle. As previously mentioned, the liquid inlet/outlet temperature difference must be at least 19.4°K to achieve thermal performance. The stability of the jet stream is discussed in (Section 5.1). Representative numbers that correspond to a test with typical synthetic sapphire jet nozzles are shown in Table 2. Results of various tests run on the test rig for various nozzles are presented in (Section 5.3).

4.3 Jet Condenser Focusing Test Rig (Multiple Nozzle)

4.3.1 Scope. The test procedure described herein provides a detailed description of the jet condenser focusing method. This is the second of three parts used in the development of the jet condenser for the Organic Rankine Power System.

TABLE 2.

SINGLE NOZZLE TEST DATA SHEET

ITEM	P/N	REV.	DIAMETER	CHECK (X) IF ACCEPTABLE PRE-CLEAN	CHECK (X) IF ACCEPTABLE DAMAGE
Orifice Nozzle	7285	E	.254 mm	X	

HYDRAULIC PRE-SCREENING ACCEPT: X REJECT: _____

PARAMETER	ACRONYM	ACTUAL
Injector Pressure	PL	488.5 kPa
Injector Temperature	TL	348.9°K
Vapor Temperature	TV	391.7°K
Outlet Temperature	TO	370.0°K
Pump Inlet Temperature	TCO	414.4°K
Injector Flow	QL	1.01 cm^3/s
Hotwell Temperature	TB	415°K
Hotwell Pressure	P_3	690 μ
Tank Pressure	P_2	187 μ
Pump Outlet Pressure	PPO	793.5 kPa
Jet Test Length	XL	254 mm

Liquid Temperature Difference (TO-TL) must be 19.4°K Minimum. 21.1°K
(May be different at other than design inlet conditions)

Accept X

Reject _____

Noncondensable Concentration (if applicable) 3 Parts Per Million

Performed by: Marco F. Bucchi

Test Surveillance: Sam Gall Date: 7/16/79

4.3.2 Objectives. To focus the individual nozzles of the jet condenser together, thereby verifying the total flow passes through the throat and achieves hydraulic performance or flow stability.

4.3.3 General. The instrumentation used for the focus test has been previously specified[32], but may have been substituted for equipment with equivalent characteristics in the event of a malfunction. This does not invalidate testing accomplished prior to such repair or replacement.[32] The following parameters are monitored and data recorded at the appropriate intervals to establish unit performance.

Parameter	Units	Designation
Injector Flow	°K	QL
Injector Pressure	kPa	PL
Injector Temperature	°K	TL
Outlet Pressure	kPa	PO

The test fluid is deaerated distilled water and is filtered per specification NAS1638, Class 4 or better.[32]

4.3.4 Detailed Test. The performance is executed in two parts:

1) Focus test verification,

2) Recovery test verification.

The focus test has the injector head with the nozzles mounted in the jet condenser housing, as shown in Figure 40. The deaerated water must be maintained at 300°K $\pm$ 5.5°K. With verification that all equipment is in operation, the supply line is attached to the injector head. The single orifice focus plate is initially installed to allow proper alignment of each nozzle individually. This is accomplished by capping all but one nozzle, turning the system on at the rated pressure, and with a suitable tool adjust the flowing nozzle until the effluent passes through the fixture target orifice. When completed, the focused nozzle is capped with a specified color and the procedure is repeated until all nozzles have been properly aligned. The caps are rated for 552 kPa operation, while the supply is maintained at 345 kPa throughout the focus test. The orifice on the focus plate is 3.175 mm. This is 6% smaller than the actual throat diameter of the vapor funnel (3.38 mm), to allow for a margin of safety.

After acceptance of the focus test, the vapor funnel assembly is attached to the injector head for alignment prior to the recovery test. With the vapor funnel in place, the injector flow is once again engaged with the release of the supply valve. The "jacking screws" are adjusted for proper alignment of the main flow stream in relation to the throat. After verification that the merged jet stream does indeed pass

through the throat, the test is repeated a number of times to ensure the stream consistently passes through it. With final adjustments completed, the supply pressure is varied to verify alignment for 276 - 552 kPa.

The recovery test has the nozzle injector head and vapor funnel assembly mounted as in the case of the focus test. The addition to this portion of the testing is the diffuser with a pressure gauge to measure the outlet pressure. With the supply pressure at 448.5 kPa, the supply valve is opened and the minimum pressure recovery (rise) is recorded. The valve downstream of the diffuser (Figure 40.) is closed slightly to raise the pressure outlet PO, by 34.5 kPa. If "floodout" does not occur, the pressure outlet reading is recorded as the maximum recovery. The step is repeated in 13.8 kPa increments to verify all obtained results. This is done until a "floodout" does occur.

4.3.5 Acceptance Testing. Tables 3. and 4. are typical data sheets used for the focus and recovery tests. Representative numbers are shown for each that were obtained for actual conducted tests that were acceptable.

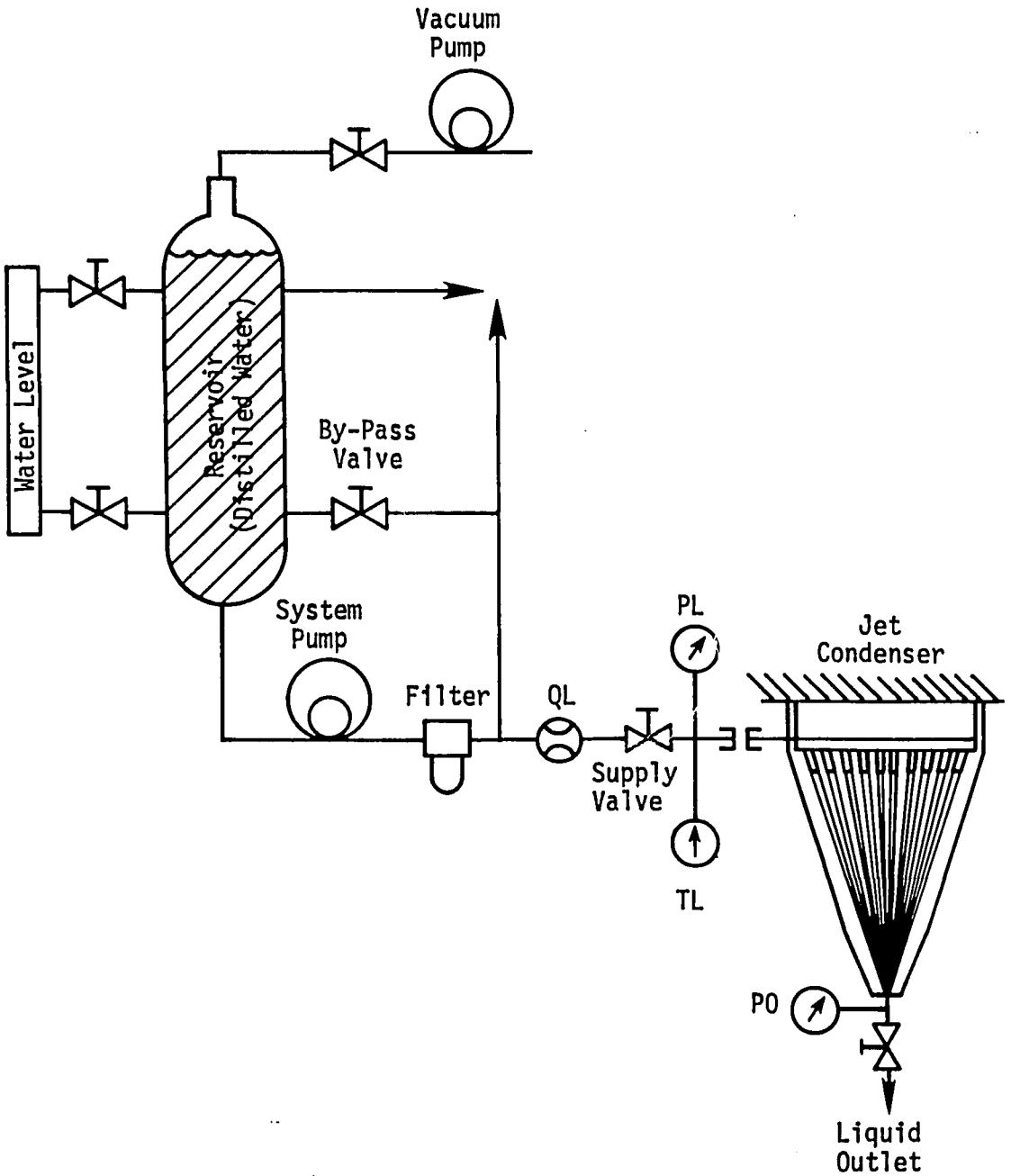

JET CONDENSER FOCUSING TEST RIG

FIGURE 40.

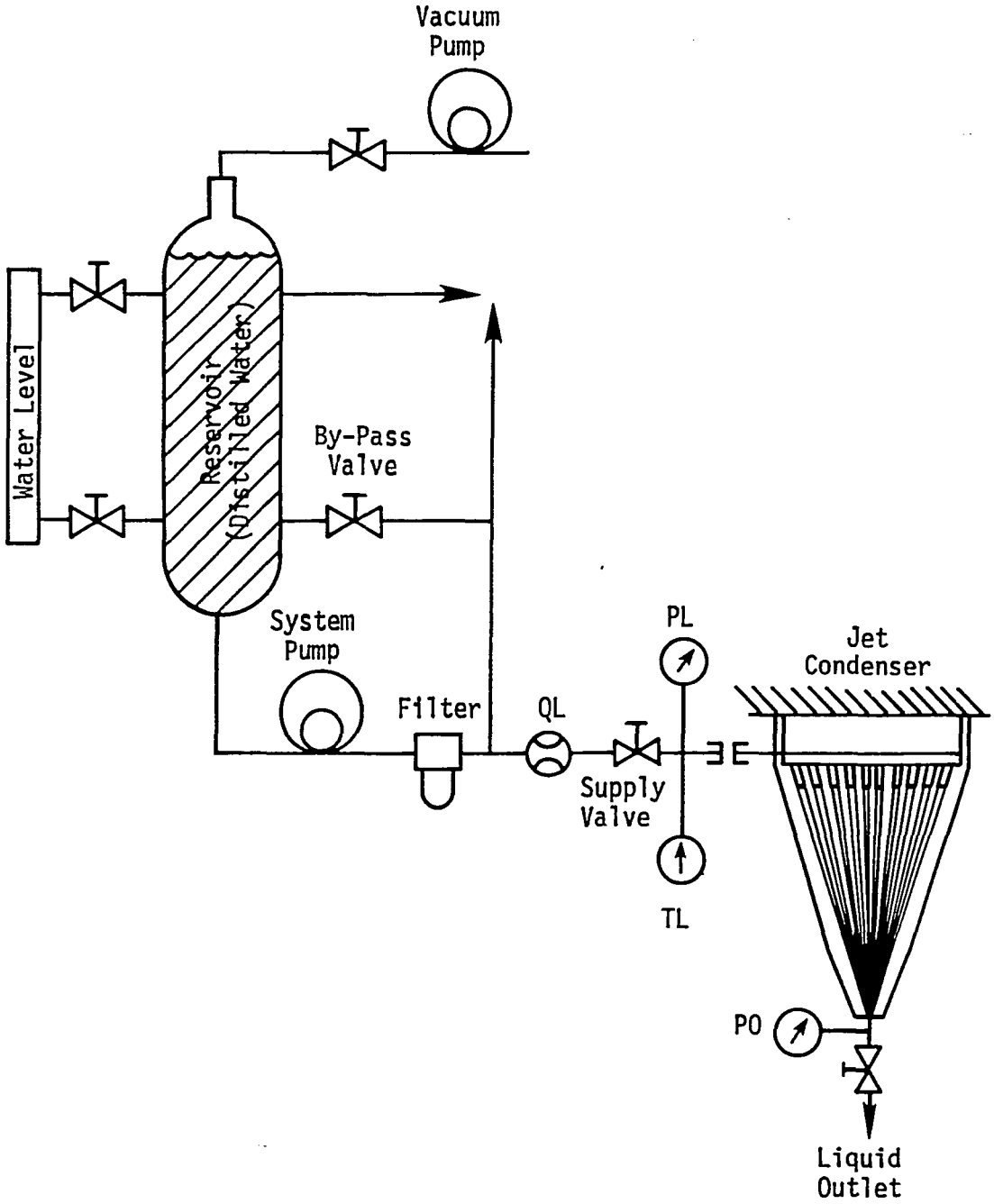

JET CONDENSER FOCUSING TEST RIG

FIGURE 40.

TABLE 3.

TYPICAL FOCUS TEST DATA SHEET

Pump, Flowmeter, Gauge Operating	(X) if acceptable	X
Each Orifice Targeted Through Plate	(X) if acceptable	X
Epoxylite Applied to Each Orifice	(X) if completed	
Epoxylite Cured	Cure Temperature	588.9°K
	Total Cure Time	36 hrs
Merged Jet Passes Through Throat	(X) if acceptable	X

INJECTOR	REQUIRED	ACTUAL
Pressure	414 ± 20.7 kPa	427.8 kPa
Flow	90.0 cm³/sec	90.3 cm³/s
Temperature	300°K	298.9°K
Pressure	345 ± 20.7 kPa	345 kPa
Flow	76.5 cm³/sec	73.2 cm³/s
Temperature	300°K	300°K
Pressure	276 ± 20.7 kPa	282.9 kPa
Flow	61.2 cm³/sec	59.93 cm³/s
Temperature	300°K	299.4°K

Performed By: Marco F. Bucchi

Test Surveillance: Sam Gall Date: 9/17/79

TABLE 4.

TYPICAL RECOVERY TEST DATA SHEET

$$\% \text{ Recovery} = \frac{PO + 14.4}{PL + 14.4} \times 100$$

	PL	PO	RECOVERY
Minimum Recovery	448.5 kPa	227.7 kPa	50.7%
Maximum Recovery	441.6 kPa	248.4 kPa	56.2%
Maximum Recovery	448.5 kPa	255.3 kPa	57.0%

Performed by: Marco F. Bucchi

Test Surveillance: Sam Gall Date: 9/18/79

CP14.57-01, Paragraph 4.1.2.2 Inspect, (X) if completed X

Assembly Cleaned, Packaged and Stored, (X) if completed X

Performed by: Marco F. Bucchi

Test Surveillance: Sam Gall Date: 9/18/79

PARAMETER	UNITS	DESIGNATION
Jet Condenser Liquid Temperature Inlet	°K	JCLTI
Jet Condenser Liquid Pressure Inlet	kPa	JCLPI
Jet Condenser Liquid Temperature Outlet	°K	JCLTO
Jet Condenser Liquid Pressure Outlet	kPa	JCLPO
Jet Condenser Vapor Pressure Inlet	kPa	JCVPI
Regenerator Temperature Vapor Inlet	°K	TRVI
Regenerator Pressure Vapor Inlet	kPa	PRVI
Regenerator Temperature Vapor Outlet	°K	TRVO
Regenerator Pressure Vapor Outlet	kPa	PRVO
Regenerator Temperature Liquid Outlet	°K	RTLO
Regenerator Pressure Liquid Outlet	kPa	RPLO
Accumulator Supply Pressure	kPa	ASP
Accumulator Pressure Outlet	kPa	APO
Turbine Bearing Supply Temperature	°K	TTBS
Turbine Bearing Supply Pressure	kPa	PTBS

With this test loop, (see Figure 41.), it was possible to accurately set all state points surrounding the jet condenser.

4.4.4 Detailed Tests. The total performance of the jet condenser is a combination all of the component testing previously completed (Sections 4.1 - 4.3), i.e., single nozzle thermal and hydraulic performance for steam/water vs. Dowtherm, and multiple nozzle-focusing and recovery pressure. This was considered the final verification prior to the actual installation within the power system.

The noncondensable concentration is determined by the same method as mentioned in (Section 4.2.4) for the regenerator as well as the jet condenser. Although not shown, the valving and

PARAMETER	UNITS	DESIGNATION
Jet Condenser Liquid Temperature Inlet	°K	JCLTI
Jet Condenser Liquid Pressure Inlet	kPa	JCLPI
Jet Condenser Liquid Temperature Outlet	°K	JCLTO
Jet Condenser Liquid Pressure Outlet	kPa	JCLPO
Jet Condenser Vapor Pressure Inlet	kPa	JCVPI
Regenerator Temperature Vapor Inlet	°K	TRVI
Regenerator Pressure Vapor Inlet	kPa	PRVI
Regenerator Temperature Vapor Outlet	°K	TRVO
Regenerator Pressure Vapor Outlet	kPa	PRVO
Regenerator Temperature Liquid Outlet	°K	RTLO
Regenerator Pressure Liquid Outlet	kPa	RPLO
Accumulator Supply Pressure	kPa	ASP
Accumulator Pressure Outlet	kPa	APO
Turbine Bearing Supply Temperature	°K	TTBS
Turbine Bearing Supply Pressure	kPa	PTBS

With this test loop, (see Figure 41.), it was possible to accurately set all state points surrounding the jet condenser.

4.4.4 Detailed Tests. The total performance of the jet condenser is a combination all of the component testing previously completed (Sections 4.1 - 4.3), i.e., single nozzle thermal and hydraulic performance for steam/water vs. Dowtherm, and multiple nozzle-focusing and recovery pressure. This was considered the final verification prior to the actual installation within the power system.

The noncondensable concentration is determined by the same method as mentioned in (Section 4.2.4) for the regenerator as well as the jet condenser. Although not shown, the valving and

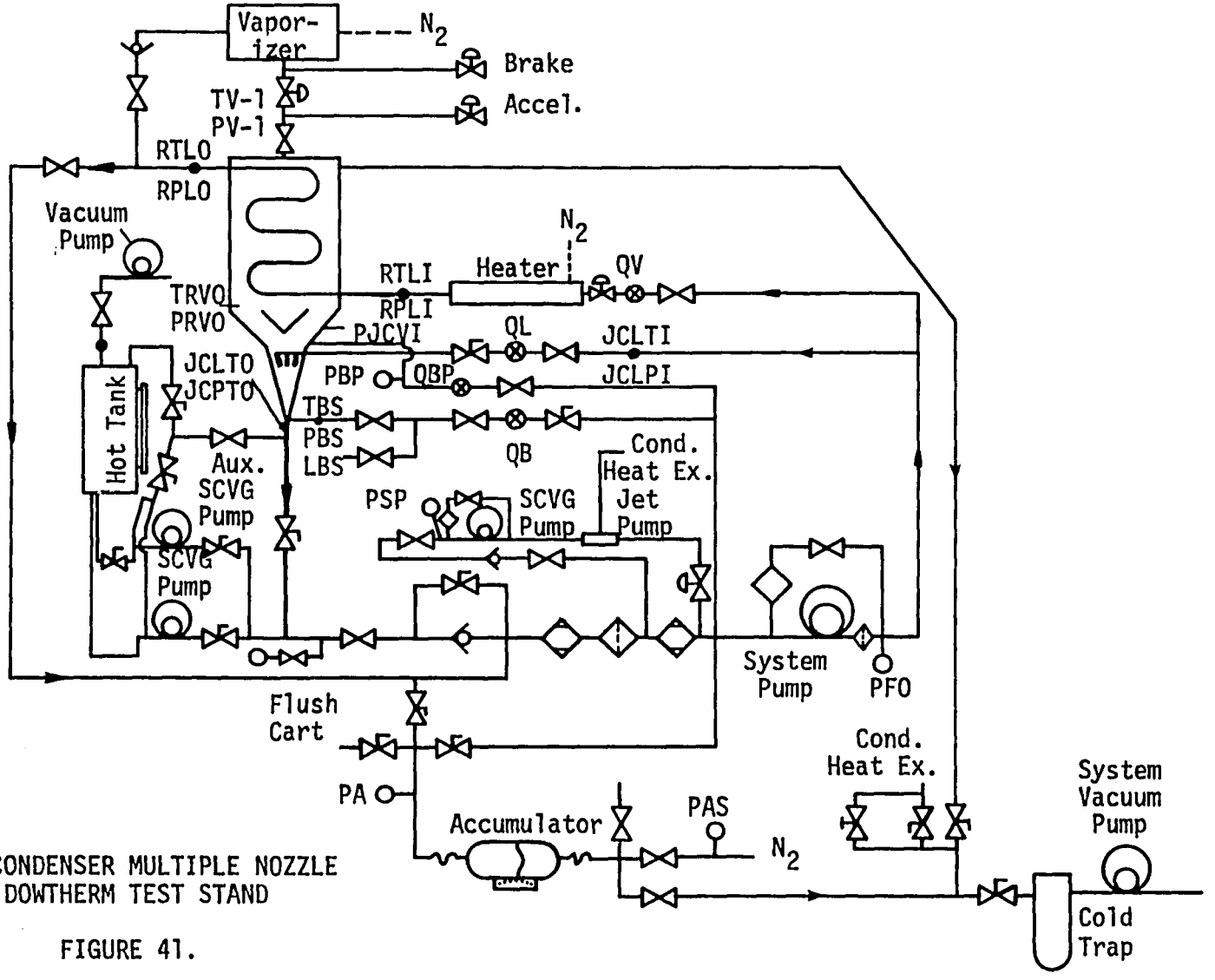

JET CONDENSER MULTIPLE NOZZLE
DOWTHERM TEST STAND

FIGURE 41.

apparatus are similar to that used on the Single Nozzle Test Stand (Figure 39). Tests were performed at the 254 mm jet length only, and the following were not varied as in previous tests:

- Jet Condenser Liquid Inlet Temperature 348.9°K
- Jet Condenser Vapor Inlet Temperature 391.7°K

The chronological order of testing that emerged over a period of time during development is as follows:

1-a) Various nozzle configurations on the Steam/ Water test rig.

2-a) Single Stainless Steel Nozzle tests on Dowtherm. (.3683 mm diameter.)

3-a) Multiple Stainless Steel Nozzle focus and recovery test.

4-a) Multiple Nozzle total performance test.

1-b to 4-b) Repeat of 1-a to 4-a with the Synthetic Sapphire Nozzles.

The second series of tests were performed because the results of 3-a and 4-a indicated an underperformance for the jet condenser which is discussed in (Sections 5.3 and 5.4).

4.4.5 Acceptance Testing. Representative data sheets for the total performance tests collected similar information as the Single Nozzle testing, with the addition of Vapor Pressure (see Table 2.). Additional parameters for system simulation were also set and monitored (see Section 4.4.3). It should be noted that tests 1-a to 4-a were conducted without critical consideration towards the noncondensable gas accumulation. Once the underperformance was discovered, a fluid degradation rate vs. time was established in relation to the amount of noncondensables in parts per million.

4.5 Instrumentation

Temperatures and pressures for the liquid nozzles and vapor were measured at key locations. They were measured with thermocouples, static or total pressure tubes, and pressure gauges. The final Organic Rankine Power System would not need the amount of instrumentation used for the tests in (Section 4.4).

The instrumentation was primarily mounted with connections that secured a tight seal. The key locations are as follows: The vapor funnel inlet was instrumented with four total pressure tubes equally spaced around the annulus, all at the same axial location. The tubes were connected to a manifold in order to provide a measurement of average Dowtherm total pressure.[32] The vapor funnel length was instrumented with thermocouples and pressure tubes so they just pierced the inside surface wall. The instrumentation was mounted every 50.8 mm over the 254 mm length. The diffuser was instrumented with a thermocouple and a total-pressure tube. The total-pressure tube was located at the center of the diffuser cross section.

Thermocouple outputs were recorded directly as temperatures by multiple-point self-balancing potentiometers. The pressure tubes were connected to pressure transducers whose electrical outputs were recorded by other multiple-point self-balancing potentiometers. Flow of the liquid entering the condenser was measured by a turbine flowmeter located in the line leading to the injector head. Initially, two sizes of flowmeters were used to cover a range of flow. The output of the flowmeter consisted of electrical pulses, which were measured by a frequency meter.

4.6. Augmented Pressure

A direct condenser combines the functions of a condenser and radiator, as mentioned in (Section 1.0). When used with a Rankine system, a pressure drop will occur in the flow through the condenser, and the feed pump will experience cavitation as per Garcia.[4] With the jet condenser used in the analysis herein, it is possible by means of the pumped liquid flow to increase the pressure of the condensate to more than offset the loss to be expected in the radiator and other piping. The measured pressure augmentation is the ratio of the static-pressure rise to the dynamic pressure of the entering vapor. The static-pressure rise can be several times the vapor dynamic pressure, but as the condensation length increases, the pressure rise decreases because of the greater flow losses. As previously mentioned, a 60% recovery was the maximum tested.

Pressure recovery data was plotted vs. condensation length for various tests. The pressure decreased slightly (less than 5%), for the 254 mm (10 inch) length vs. the shorter lengths tested. The pressure rise increases with liquid velocity from the jets, and exceeds the vapor dynamic pressure at the point where the liquid velocity achieves its highest value. This zone is in the throat, and the size of the liquid nozzle has little effect on the degree of the pressure rise experienced by

the condensate. This was evidenced when similar performance data with the .3683 mm and .254 mm nozzles were compared. It is theorized that a higher pressure rise is possible because of the power used in pumping the flow to the injector head.

The feed pump is used to deliver the liquid to the jet condenser. The pumping power required to overcome the flow losses in the condenser is the product of the liquid nozzle volume flow and the total-pressure loss measured from the inlet of the liquid nozzle to the diffuser downstream of the test section[3]. The power required becomes dimensionless when divided by the power equivalent of the heat of condensation of the liquid. After a period of running time the liquid tends to increase in temperature which causes the condensation region to increase in length. This results in greater flow losses, and requires more power to effectively pump the liquid. The vapor velocity was increased since it reduces the power-required ratio (Power required/Power liquid) in Watts because the energy of the liquid aids the vapor flow. Pressure recovery data were compared to corresponding values of power-required ratios. Tests were in agreement with Platt[3] that for a given power ratio and condensation length, the highest pressure rise is obtained with the largest nozzle surface area. For the present case a higher recovery pressure was verified by the 90-nozzle condenser producing 15% higher recovery (rise), than the

45-nozzle condenser. A larger ratio of vapor nozzle area to liquid nozzle area is therefore more efficient in that pressure augmentation is accomplished with less pumping power per unit of vapor flow.

CHAPTER 5. RESULTS OF CONDUCTED TESTS

5.1 Stability of Flow

Evaluation of hydraulic performance or flow stability was conducted on various designs of nozzles individually, with both steam/water, and liquid Dowtherm. Test procedures were discussed in Sections (4.1 and 4.2); the results appear in Section 5.3. Multiple nozzle performance tests were also conducted and are discussed in Sections (4.3 and 4.4), with results presented in Section 5.4. The multiple nozzle tests screened the ability of nozzles to separate the flow into several individual liquid streams and concentrate these streams in the throat of the jet condenser vapor funnel. Each one of the individual tests allowed the operator to observe the flow for acceptability characteristics. There are three modes that indicate failure and are checked during each test. A nozzle was rejected if one or more of the following were measured.

1. Hydraulic Flip - characterized by multi-stable positions during operation in which the jet jumps from one stable position to another. Allowable nozzle movement is a function of the quantity of nozzles, fluid stream diameters, jet length, and throat diameter. The nozzle is rejected if the jet moves once, or more, a distance of

$\pm$ .762mm from centerline or greater, when measured 254mm from the nozzle exit plane during a ten-minute period. Using 90 nozzles with a combined fluid stream of 3.05 mm, at a 254 mm jet length, a 10% (percent) safety factor was used in establishing an allowable nozzle movement of $\pm$ .762 mm for the 3.38 mm diameter throat.

2. Instability - characterized by the jet flow wandering about without finding a stable position. The nozzle is rejected if the jet wanders more than $\pm$ .762mm from centerline, when measured 254mm from the nozzle exit plane during a ten-minute period.

3. Brooming - characterized by the jet flow spreading uniformly and continuously from the nozzle exit plane. A nozzle is rejected if its jet spreads to a diameter greater than 1.524 mm when measured 254 mm from the nozzle exit plane for a ten-minute period. A stable combined fluid stream of 3.05 mm could be obtained with no more than a 1.524 mm diameter/nozzle of brooming. This is due to the fact that the focus angle of the individual nozzles allowed the fluid streams to intersect just upstream of the throat and form an overall diameter of $\leq$ 3.18 mm. This was verified in Section 4.3. The tests were

considered valid for noncondensable concentration levels of $\leq$ 20 parts per million (ppm). Results of Sections 4.2 and 4.4 showed typical concentration levels of 3-12 ppm. Tests were also run for different periods of time, varying from 10 minutes to as long as 84 hours, to test for endurance.

The ability of the nozzles to concentrate the individual liquid streams at the jet condenser throat is a strong function of the fabrication of a particular design. Extremely critical to the fabrication on all of the nozzles is the exit corner break, or radius at the orifice outlet. An absolute maximum radius of .0254 mm was allowed. All screened sample nozzles tested with a radius larger than allowed resulted in failure modes 1, 2, or 3 as discussed in this Section. Considerable differences in nozzle performance are noted in Section 5.3. Some of the more recent designs of various nozzles are shown in Figures 3, 7, 35, and 36 of this text.

5.2 Condensation Length

One of the critical design features for the jet condenser's proper operation as part of a space power system is the proper condensation length. Initial tests were run with a condensation length of 25.4, 50.8, 127, 152.4, 203.2, and

254 mm, to determine the optimum length. From Section (4.1), it was found that the condensation length was affected by numerous parameters such as water temperature and velocity, steam static pressure and velocity, and vapor funnel size. In order to determine the condensation length that is needed for the condenser, an analysis was developed in Section (2.2) to correlate the net condensation rate with the Stanton Number, which is based on the liquid interfacial velocity. Numerous factors played key roles in determining an allowable condensation length for both the liquid nozzle stream and the saturated vapor. This is in agreement within the majority of sources cited within this text.[1,2,5-11,14-18,20,24,33]

Data correlation between the tests that were run at jet lengths of 50.8, 127, and 254 mm, with .254 and .3683 mm nozzles, and condensation properties of Section (2.2), were within 10% (percent). Detailed figures that provide the results for the correlation of the parameters mentioned in the previous paragraph are Figures 8, 12, 16-21, 28, and 30. When the condenser was tested at the 254 mm length, it achieved its highest thermal efficiency, but became very sensitive to any change in test conditions. Testing had also determined that in order to maintain liquid flow stability, the nozzles had to be maintained at the same mass flow rate, within .01 Kg/sec. The established design parameters for the 254 mm condensation

length were correlated with Section 2.2 via the Stanton Number based on velocity differences and are shown in Figures 8, 23, and 24. The results correlated well with the predicted results within ±6.5% and with the work from Young and Yang[17].

5.3 Single Nozzle Design

Single nozzle tests were utilized to determine the best orifice configuration. The tests were run with deaerated steam/water, and Dowtherm at typical system states as discussed in Sections (4.1 and 4.2). Checks were made (as previously mentioned in Section 5.1), for hydraulic stability and condensing capabilities.

5.3.1 Steam/Water. In preliminary testing, difficulty was experienced with air in the system. This leakage caused poor initial results thermally, and contributed to flow instability. It is believed that the air was leaking in at various pipe seals (poor "u.c." rings) as well as specific component leakages. Repairs were made at all points. The test stand vacuum was enhanced with the addition of a cold trap as shown in Figure 37. As previously mentioned in Sections 4.1 and 4.2, the trap enables the stand to operate at $\leq$ 170 microns of Hg. during periods of temporary shutdown (overnight), and $\leq$ 200 microns during actual nozzle testing.

Results and observations on the steam/water test rig (converted in Table 5.) indicated considerable differences in performance for each nozzle configuration shown in Figure 7. The liquid streams all failed the hydraulic test per Section 5.1, items 2 and 3. Nozzle patterns were visually observed on water from each nozzle to the focus plate by a clear acrylic cylinder (see Figure 37.). Liquid streams from poorly machined nozzles resulted in the inability to pass through the focus plate. When this occurs, a simulated jet condenser floodout takes place and the mixing chamber (Acrylic Cylinder) fills with water. A predicted success/failure analysis was made for each nozzle, and is in agreement with the following from Garcia.[4]

> "For a given throat dimension, it is possible to quantitatively determine the success or failure of a given orifice plate to concentrate individual streams of fluid. This is simply done by varying the flow rate through the orifice, and observing the flow rate at which the assembly floods. Even with a "perfect" orifice, the throat diameter is small in relation to that required to pass the design flow rate. The throat diameter is, of course, calculated to pass the design flow rate, but a 2.0% (percent) safety margin is required with streams."

The steam/water test apparatus demonstrated nozzle feasibility for the jet condenser design by the Stanton Number results that were obtained in Section 2.1, and allowed the next phase of testing to take place with liquid Dowtherm (Hot-gas tests).

TABLE 5.
RESULTS ON INDIVIDUAL NOZZLE COMPARISONS TESTED ON LIQUID DOWTHERM*

	Nozzle Diameter Designation	Temperature Liquid Inlet (°K)	Temperature Vapor (°K)	Temperature Condensate (°K)	Flow (cm^3/s)	Injection Pressure (kPa)
	Figure 3.	348.9	391.7	373.9	1.38	448.5
	.254 Short Sharp Edge	349.4	392.2	375.5	1.38	448.5
	Figure 7.	348.9	392.2	375.5	1.45	448.5
	A - .254 - Aluminum	349.4	392.2	376.7	1.45	448.5
	Figure 7.	349.4	392.2	375.5	1.51	448.5
	B - .254 - St. Stl.	350	392.7	376.7	1.51	448.5
	Figure 7.	348.9	392.2	380	1.38	441.6
	C - .3683 - St. Stl.	350	392.2	380.5	1.38	448.5
	Figure 7.	348.9	392.7	379.4	1.45	441.6
X	D - .3683 - Aluminum	350	393.3	382.8	1.45	434.7
	Figure 35.	348.9	390.0	373.9	1.00	448.5
	1 - .216 - Aluminum	350	391.1	375.5	1.00	448.5
	Figure 35.	348.9	391.1	372.7	1.57	448.5
	2 - .254 - St. Stl.	349.4	391.7	373.9	1.57	448.5
		348.9	391.1	372.2	1.00	441.6
	.3683 Gatti - Jewel	349.4	391.7	373.9	1.00	448.5
		348.9	391.7	372.2	1.17	448.5
	.254 Swiss - Jewel	349.4	391.7	373.3	1.17	448.5
		348.9	391.1	371.6	1.00	441.6
	.3683 Bird - Jewel	349.4	391.7	372.2	1.00	448.5
		348.9	391.7	372.2	1.00	448.5
	.216 Bird - Jewel	350	392.2	372.7	1.00	441.6
		348.9	391.7	370.5	1.42	448.5
✓	.254 Bird - Jewel	349.4	392.2	371.6	1.42	448.5
		348.9	392.2	370	1.41	448.5
✓	.254 Bird - Jewel	350	392.7	370.5	1.42	448.5

X = Worst performance
✓ = Best performance

* = Jet test length was 254 mm for all results.

5.3.2 Dowtherm. The Liquid Dowtherm Tests were also deaerated, and actual parameters were used for individual nozzles, as described in Section 4.2. The desired goals for this phase of testing are consistent with the first paragraph of Section 5.3, and in addition, to achieve simulated operation of the design inlet vapor pressure at .69 kPa at the design flow rate. As in the case of Garcia[4], many of the initial tests required loop shakedowns to correct stand problems involving various components, the majority being not able to maintain proper vacuum when running hot. As is the case with steam/water, a cold trap was added to the test rig for better deaeration, and various "u.c." rings and seals were periodically replaced to overcome the leaking problem.

The first test results were run with the nozzle configuration shown in Figure 3 (the short sharp-edge orifice jet). The results (see Table 5) indicated a significant underperformance in condensation rate, except at a very high liquid injection pressure (~ 2.5 x design value). It was theorized that at the high injection pressures, the laminar jets issuing from the sharp edge orifices were becoming more turbulent and breaking up, thus causing more surface area for liquid vapor contact. Nozzles shown in Figure 7 were also retested with Dowtherm with performance results given in Table 5. These conventional orifices had a rounded inlet and

an orifice length to diameter ratio of ~ 3 to 5 with turbulence promoting screw threads in the upstream feed tubes. The injection pressure was varied from 621 - 1,345 kPa on the short sharp-edge nozzle, as well as the nozzles in Figure 7. It is apparent that the jets are nonturbulent at 621 kPa and that the stream is breaking up at 1,345 kPa. The nozzle that yielded the best overall performance that was used in the 45-nozzle injector head is the Stainless Steel Nozzle with an L/D = 4 as shown in Figure 35. (See Table 5 for actual performance results.)

Subsequent single nozzle testing had to be completed after the initial Dowtherm multiple nozzle test was performed (Section 5.4) on the 45-nozzle injector head. The reason the subsequent testing was necessary is twofold: 1) the 45-nozzle system did not meet the performance criteria of Section 2.3 as described in Section 4.4, and 2) in an attempt to increase the condenser performance, the Stainless Steel nozzles of Figure 35 were mounted in a 90-nozzle injector head to obtain more effective surface area for the saturated vapor to condense on, but the nozzles would not properly focus as described in Section 4.3.

The nozzle that eventually replaced the stainless steel design (Figure 35) in the 90-nozzle system was a synthetic sapphire jewel nozzle as shown in Figure 36. Results of the

different brands of synthetic sapphire nozzles are presented in Table 5, with the Bird style (.254 mm dia.) exhibiting the best overall thermal and hydraulic performance combination, while also allowing the least amount of noncondensable gas accumulation in the vapor funnel. (Recall that an abundance of noncondensable gas raises the vapor pressure to > .69 kPa, which is undesirable, because it in turn raises the backpressure of the turbine, which lowers system efficiency.) The nozzles were first tested individually per the procedure outlined in Section 4.2, and after successful results (Table 5), the Bird synthetic sapphire nozzle was selected for the 90-nozzle injector and tested as per Sections (4.3 and 4.4). Results achieved on both 45- and 90-nozzle systems per Sections 4.3 and 4.4 are presented in detail in the next Section, 5.4.

5.4 Multiple Nozzle Design

The multiple nozzle tests in Sections (4.3 and 4.4) established the performance of the 90-nozzle injector head by: 1) demonstrating the best focusing techniques, 2) determining the maximum hydraulic recovery available, and 3) measuring the total performance of the jet condenser assembly.

5.4.1 Initial focus testing was completed on the 45-nozzle injector with stainless steel nozzles (Figure 34). The

deaerated water was kept at 300° ± 5.5°K, and is injected into the nozzles at a pressure of 345 kPa. The focus was successful because the combined nozzle flow maintained hydraulic stability as it passed the focus plate without any deviation. For further details, refer back to Section 4.3. The recovery pressure was also measured and found to be 220.8 kPa. As mentioned in Section 5.3.2, the 45-nozzle injector was underperforming during hot gas testing, so after reviewing the analytical analysis in Section 2.3, a 90-nozzle injector was designed in order to yield more surface area for the saturated vapor, thus increasing the rate of condensation while effectively lowering the vapor pressure to ≤ .69 kPa.

The 90-nozzle injector was then subjected to the focus test per Section 4.3, with jets similar to Figure 35. Although the recovery pressure had increased by 15%, the focus test was marginally successful because the liquid streams would not remain focused for a long period of time. Even though this assembly was tested for total performance per Section 4.4, and results described in the following section, it was at this point, as mentioned in Sections 3.3 and 5.3, that an effort was put forth to determine a nozzle that would yield a better hydraulic stability and thermal performance for the 90-nozzle injector.

5.4.2 Results on Hot-Gas testing of the 45-nozzle injector with stainless nozzles (See Table 6.) gave a measured thermal performance that was somewhat poorer than originally anticipated based on the analytical analysis of Section 2.3. The design in Section 2.3 called for condensing .0139 kg/sec. of Dowtherm A at a vapor pressure of .69 kPa and a temperature of 391.7°K at the inlet of the jet condenser vapor funnel. The liquid side had to supply .1247 kg/sec. of liquid Dowtherm A at 348.9°K at a pressure of 552 kPa. The development jet condenser with 45 jets condensed .0139 kg/sec. of Dowtherm A at a pressure and temperature of .8142 kPa and 391.7°K when supplied with .1247 kg/sec. of liquid Dowtherm A at 348.9°K. The liquid pressure required to provide the .1247 kg/sec. flow was 690 kPa rather than the design value of 552 kPa.

Thus this build of the jet condenser was deficient in condensing capability, as evidenced by 1) A higher vapor inlet pressure of .8142 kPa rather than the design value of .69 kPa, 2) 690 kPa rather than the design value of 552 kPa for the liquid supply pressure to provide .1247 kg/sec. The combined effect of the higher than design turbine backpressure and increased pump work resulting from the jet condenser underperformance would have resulted in a loss in system efficiency by approximately 1 percentage point. This loss in system efficiency was deemed undesirable and a higher

TABLE 6.
DOWTHERM MULTIPLE NOZZLE THERMAL PERFORMANCE RESULTS

		45 Nozzle Injector with Stainless Nozzles per Figure 35.		90 Nozzle Injector with Jewel Nozzles per Figure 36.	
		Design	Test	Design	Test
Sub Cooled Liquid					
Flowrate	(Kg/s)	.1247	.1247	.1247	.1247
Pressure	(kPa)	552	690	552	552
Temperature	(°K)	348.9	348.9	348.9	348.9
Saturated Vapor					
Flowrate	(Kg/s)	.0139	.0139	.0139	.0139
Pressure	(kPa)	.69	.8142	.69	.70
Temperature	(°K)	391.7	391.7	391.7	392.2
Combined Liquid (Condensate)					
Flowrate	(Kg/s)	.158	.132	.158	.150
Pressure	(kPa)	331.2	276	331.2	314.6
Temperature	(°K)	372.2	373.3	372.2	370
Pressure Recovery	(%)	60%	40%	60%	57%

performance jet condenser design was undertaken, as previously mentioned in Section 5.3. At this time it was clear that something better than the simple condensation flux is proportional to the vapor density scaling law, based on the jet condenser operation, was required to obtain an improved design. Specifically, more had to be known about the internal heat transfer capability of various liquid jets (from vapor/liquid interface to the bulk of the jet) as well as the sensitivity of the condensation process to the presence of noncondensable gases. In order to investigate the thermal performance of various liquid jets, the latter part of Section 2.3 involves thermal performance and its sensitivity of the condensation process to noncondensable gases. Noncondensable effects are further discussed in Section 2.4, and Appendices A and B.

With the synthetic jewel sapphire nozzle recorded as the best performing nozzle per Sections 3.3 (description), 4.2 individual testing, 4.3 multiple testing, Table 5., and 5.3 results, a repeat of Hot-Gas testing was again conducted on the 90-nozzle injector with the jewel nozzles. Results that are given (see Table 6) show that the measured thermal performance was now in agreement with the predicted performance in Section 2.3. Tested results condensed .0139 kg/sec. of Dowtherm A at a saturated vapor pressure of .70 kPa, and a temperature of

392.2°K at the inlet of the jet condenser vapor funnel. The liquid side supplied .1247 kg/sec. of liquid Dowtherm A at 348.9°K at a pressure of 552 kPa. Pressure recovery was increased to a modest 57%, (only 40% was obtainable with other builds). Thus the build of the 90-jewel nozzle jet condenser met all requirements for hydraulic and condensing capability, per Sections 2.3, 4.2, 4.3, 4.4, 5.3 and this Section 5.4. This in turn reduced the turbine backpressure, and decreased the pump work, and allowed the overall system to increase in efficiency by 1.8%. Noncondensables were not eliminated due to this achievement but were controlled during the remaining parts of the program by a gas separator that was installed in the Organic Rankine Cycle System. Effects and results of noncondensables are discussed in (Section 2.4) as they compare to the analytical analysis (Section 2.3), and in Appendices A and B as they affected the actual hardware.

It is, therefore, concluded that with accurate agreement between the actual operating data and the analytical predictions within the model, the feasibility of the jet condenser design for a power system in space has been demonstrated.

5.5 Scavenging

Within the Power Conversion System there is a common shaft between the turbine and alternator. There are bearings at each end of the shaft that require lubrication during running conditions. It is required that the bearing flow be returned to the system at a given point. To achieve minimum losses, the return or scavenging needed must be done at low pressures. The best choice within the power conversion system is therefore the jet condenser. With this addition to the design, it was found that in addition to leakage at system start-up, a minimum of condensation will occur on cooler internal housings of the power conversion system upstream of the jet condenser. In a one (1) g gravity field, this condensation will drop out to the condenser where it is scavenged without causing a perturbation to the system operation. Tests were conducted in order to determine the tolerance or limitation of the scavenge flow, and its best location within the jet condenser.

As shown in Figure 42, three different areas were tested:

1. The vapor funnel wall just upstream of the liquid injector head.
2. The vapor funnel wall at midpoint between the liquid injector head and the throat.
3. The throat itself, upstream of the diffuser.

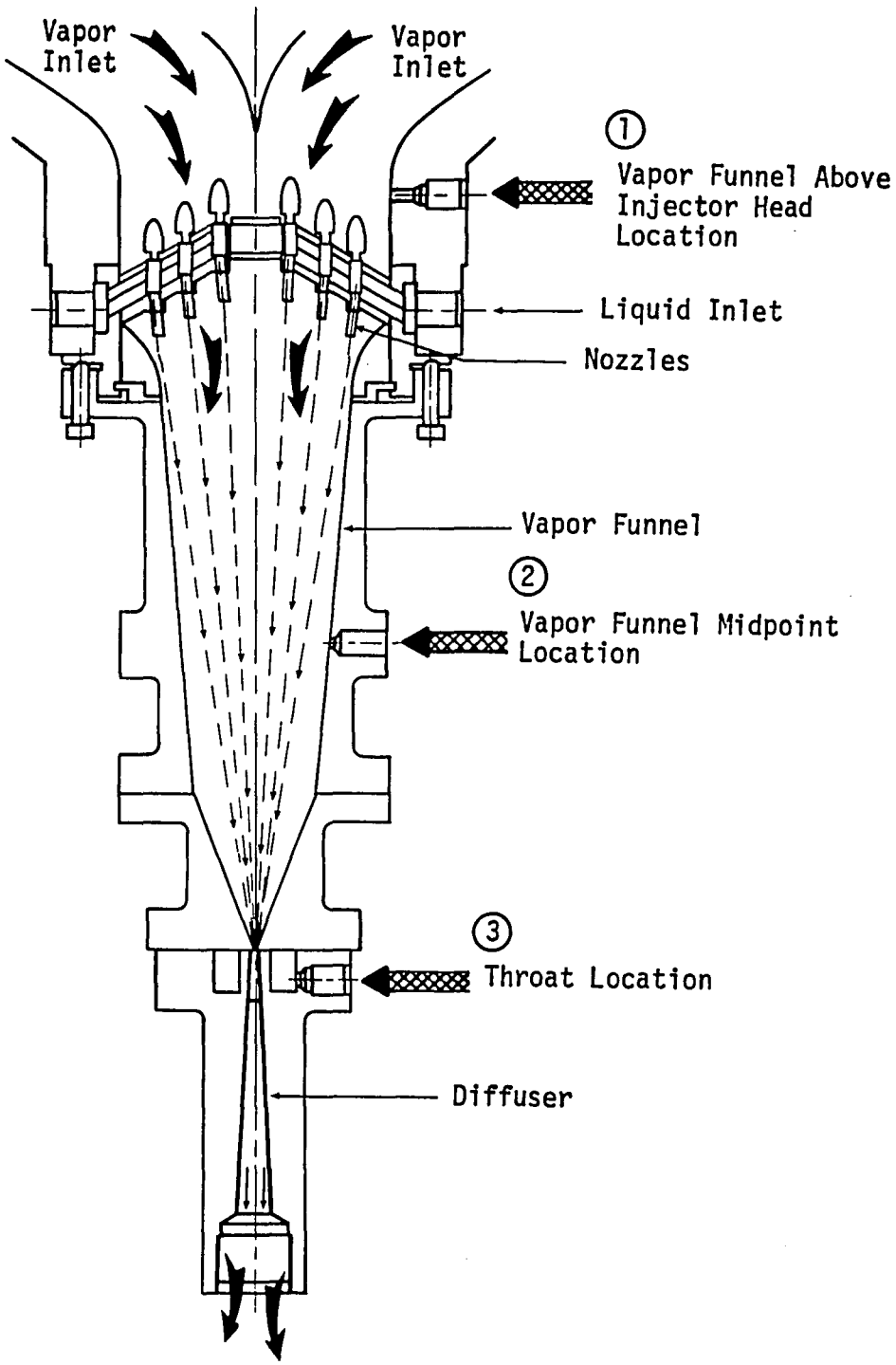

SCAVENGE FLOW AREAS

FIGURE 42.

The diameter for the duct at either of the tested locations is .254 mm. The procedure was to establish jet condenser conditions with no scavenge flow and then to introduce scavenge flow in small steps until floodout occurred. Tests were run with and without vapor flow and at varying levels of jet condenser recovery. There was no discernable change in the scavenging capability with or without vapor flowing. Even more significantly, there was no change in scavenging capability with increasing recovery pressure to within approximately two percentage points of the maximum available recovery pressure. The maximum scavenging capability was not determined due to instrumentation limitations. In all locations, scavenge flow capability exceeded 130% of the design bearing flow. One test indicated ability to scavenge up to 300% of the bearing flow. In addition, tests were made with 130% bearing flow concurrently scavenged at both the funnel wall, and at the throat.

The results indicate that the bearing flow can be successfully scavenged at any jet condenser location. Scavenge on the funnel wall or funnel center depends on vapor drag to assure proper return of the scavenge flow to the throat during operation in zero g.[32] Calculations show that the drag is marginally adequate in normal operation but in the presence of even slight accelerations opposite the flow direction, the

scavenge will be perturbed and fluid will be collected in the vapor space. This in itself is not troublesome but when the acceleration is relieved, this collected inventory tries to flush through the throat. This attempted scavenge of large amounts of fluid caused a floodout on the test rig during certain runs. Scavenging at the throat requires the bearing cavity scavenge system to generate a pressure at a design flow of at least 19.0 kPa, as shown in Figure 43. Although system power was increased slightly, the throat scavenge relies only on liquid momentum, so it will function in a zero g field as well as moderate acceleration fields generated in the direction opposite to flow. For space applications, this condition would exist primarily during a launch situation.[32] Scavenge at the throat has been selected for the system.

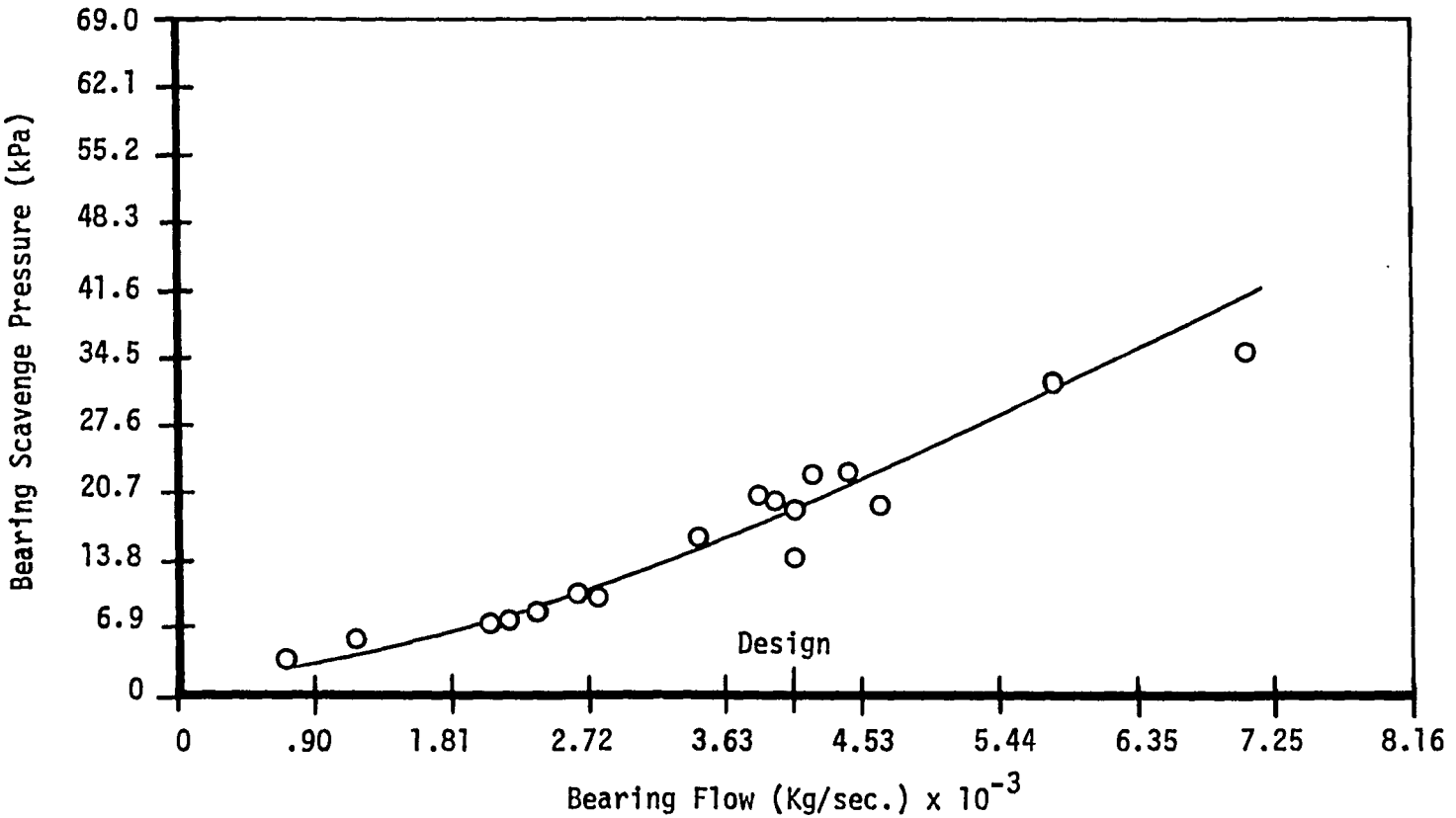

SYSTEM BEARING SCAVENGE FLOW AT THE THROAT

FIGURE 43.

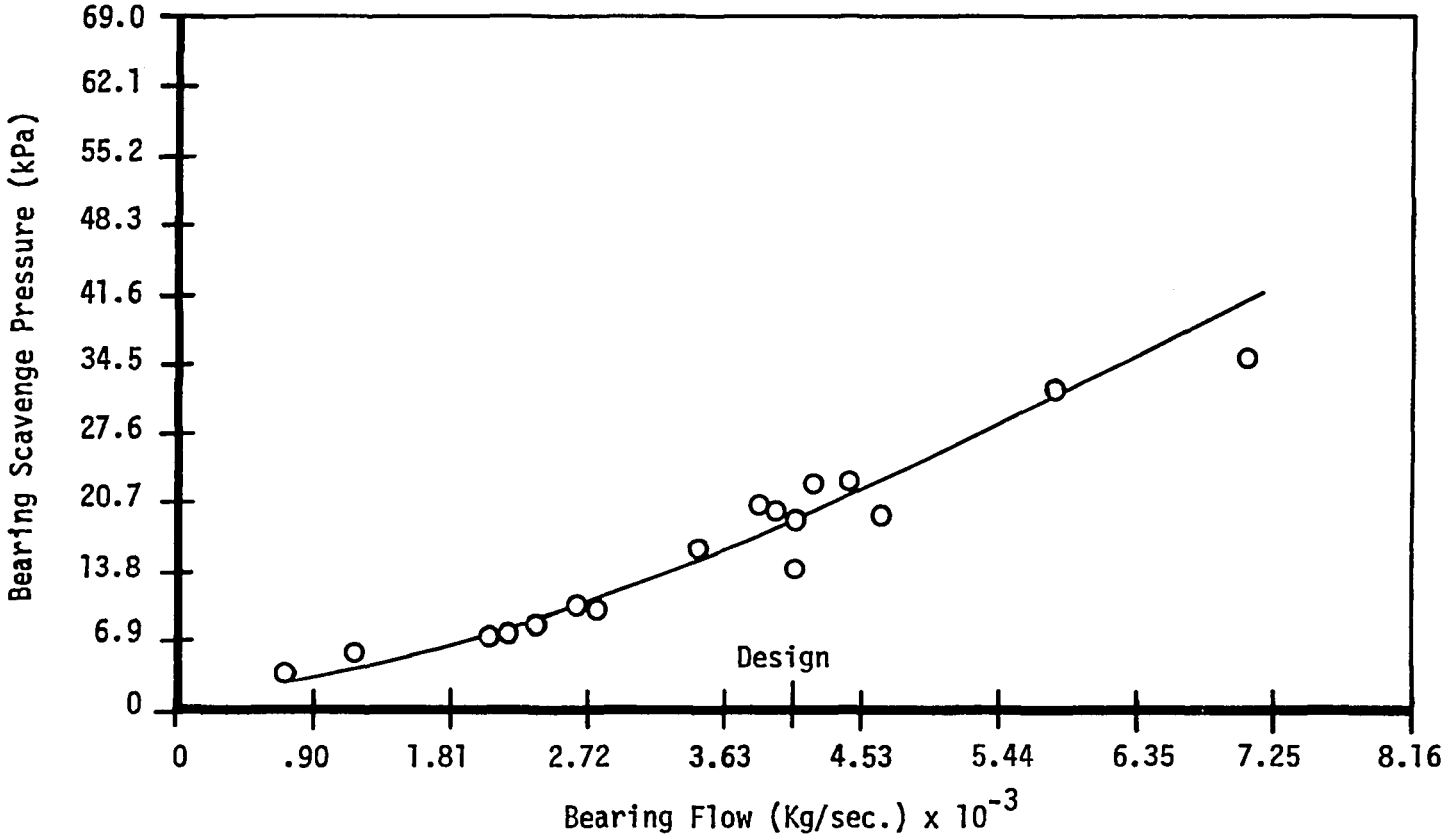

SYSTEM BEARING SCAVENGE FLOW AT THE THROAT

FIGURE 43.

CHAPTER 6. SUMMARY AND DISCUSSION

The design and performance characteristics of a jet condenser have been evaluated for suitable use in Orbiting Space Vehicles as part of an Organic Rankine Cycle Power Conversion System. The jet condenser is geared for use under zero gravity conditions since it will be used in space and is a derivative of an industrial-type jet condenser, but allows liquid and vapor contact in all attitudes.

An analytical model has been developed to predict a geometrical design that will yield a vapor inlet pressure that is required to condense a given vapor flowrate with a liquid flowrate at liquid vapor inlet temperatures. Parameters of the liquid and vapor are evaluated in a Shear Velocity Analysis to obtain a net condensation flux W/A cond., that in turn identifies the rate of condensation. The Stanton Number was determined for various jet lengths of 50.8, 127, and 254mm since it helped predict condensation rates that were based on velocity differences. This aspect was verified by running tests, which also allowed the Heat Transfer Coefficient to be determined over a jet length as a function of the jet heat flux. With a heat transfer coefficient and heat flux known, a jet condenser outlet temperature, as a function of the liquid and vapor inlet temperatures at a given jet length for a particular nozzle design, was found with a minimum error of 10%. Further testing and evaluation of the model in Section 2.3 revealed that a potential

cause of the error may have been attributed to the accumulation of noncondensable gas. (Verification was later obtained that it did effect the results of the thermal characteristics of the liquid jet and saturated vapor.)

Initial sizing calculations in Chapter 2 predicted that 45-.254mm diameter nozzles, with a 254mm jet length, would yield a desirable performance for the jet condenser. An attempt to verify this was completed during a series of tests as outlined in Chapter 4. Overall results are presented with figures 27 and 28. An underperformance was noted, and further calculations of noncondensables in Section 2.4 were discussed in Chapter 3 and verified in Chapter 4, to determine what an allowable noncondensable gas concentration level was while still maintaining the thermal and hydraulic performance of the jet condenser. This was critical since the accumulation of noncondensable gas had the tendency to raise the vapor pressure beyond its design of .69 kPa. A low vapor pressure created a low backpressure which improved turbine isentropic head and volumetric flow upstream of the jet condenser, which in turn raised the system efficiency.

As discussed in Chapter 3, optimal geometrical designs were needed in addition to proper operating parameters for the jet condenser. Once established, they were optimized in different series of tests (Chapter 4) on both steam/water initially, and the

actual system working fluid Dowtherm 'A'. These tests, presented in Chapter 5, revealed that the optimum jet length was slightly beyond 254mm, but a tradeoff had to be made since 254mm maintained flow stability, with anything beyond that length producing a flow of questionable stability. Tests also revealed that an overall misalignment of $\pm$.762mm was acceptable during launch and maneuvering jet stream conditions.

A major discovery of all nozzles tested on an individual basis revealed that the Synthetic Sapphire Jewel Nozzle gave the best overall results for hydraulic stability and thermal performance, while maintaining a minimum noncondensable gas concentration level of <20ppm. Multiple Nozzle Dowtherm Tests verified that the quantity of nozzles had to be increased to 90 to meet overall thermal performance with an established fluid degradation (noncondensable gas accumulation) over a period of time. Although the order of magnitude of the degradation was minute, it had to be considered since the life expectancy of the condenser had to be 7-10 years.

CHAPTER 7. CONCLUSIONS

An experimental investigation of a jet condenser operating under zero gravity conditions has been done. A comparative analytical model was developed and employed to establish both baseline and geometrical design parameters. Developmental tests were completed and a comparison was made between the actual operating data and the analytical predictions.

Based on the results of the study, the following conclusions are reached:

1) The optimum nozzle type is a Stainless Steel Nozzle with a Synthetic Sapphire Jewel Orifice.
2) The best nozzle configuration has a length to diameter ratio, (L/D), of four, which yields the highest overall hydraulic and thermal performance.
3) The vapor funnel design allows saturated vapor to condense on the liquid stream without creating a shock wave in the diffuser.
4) A significant recovery pressure in the diffuser will allow the upstream saturated vapor to operate at a low pressure (.69 kPa); The low pressure permits the system turbine to operate at a higher efficiency thus raising the overall power system efficiency by 1.8%.

5) System performance will degrade over a period of time if the Noncondensable Gas Concentration Level is >20 ppm.

6) During shock and vibration conditions, such as system launch, a jet condenser overspeed condition allows a jet stream misalignment to occur without affecting performance.

7) The technique of employing multiple liquid jet streams focused through the throat of the diffuser element can yield a higher performance than previous industrial-type jet condensers.

8) Demonstrated comparison of analytical predictions to within ±5% of the experimental results indicates that the analytical model can adequately predict the performance of the jet condenser when the effects of noncondensable gas are included.

9) Considering the 1.8% increase in performance obtainable with the present design, the required criteria of Tables 1 and 6 of this text are satisfied, which indicates that the present jet condenser design is feasible for use in space on an Organic Rankine Cycle Power System.

REFERENCES

1. Blume, R., "High-Vacuum Condensate Pollution Control," Monsanto Co. CEP, 1978.

2. Hays, Lance, "Investigation of Condensers Applicable to Space Power Systems," Part I - Direct Condensers, Rept. 1588-Final (Contract NAS7-11), Electro-Optical Systems, Inc., 1962, Part II - Jet Condensers, Rept. 1588-Final II (Contract NAS7-11), Electro-Optical Systems, Inc., 1962.

3. Platt, R. J., Jr., "Investigation of a Jet Condenser for Power Applications", Langler Research Center, NASA TN D-3045, pp. 1-33, National Technical Information Service, 1965.

4. Garcia, R., "Jet Condenser Development in Organic Rankine-Cycle Systems", Fourth Inter-Society Energy Conversion Conference, pp. 11-20, 1969.

5. Isachenko, V. P., Solodov, A. P., Samoilovich, Yu. Z., Kushnyrev, V. I. and Sotskov, S. A., "Investigation of Heat Transfer and Steam Condensation on Turbulent Liquid Jets," Teploenergetika, Vol. 18, pp. 8-12, 1971.

6. Miyazaki, K., Nakajima, I., Fujiie, Y. and Suita, T., "Condensing Heat Transfer in a Steam-Water Condensing Injector," Journal of Nuclear Science and Technology, pp. 411-418, 1973.

7. Kaplan, R. D. and Shendalman, L. H., "Heat Transfer to a Cylindrical Laminar Liquid Jet Ejecting into a Gas," Int. Journal of Heat Transfer, Vol. 16, pp. 1231-1244, 1973.

8. Irodov, V. F., "Problem of Describing the Flow Field in an Injection Mixing Chamber," Inzhenerno-Fizichesskii Zhurnal, Vol. 31, No. 5, pp. 1265-1269, 1976.

9. Mochalova, N. S., Kholpanov, L. P., Malyusov, V. A. and Zhavoronkvo, N. M., "Heat Transfer During Condensation of a Vapor on a Laminar Jet of Liquid with an Initial Segment," UDC 536.2, pp. 337-340, Plenum Publishing Corporation, 1981.

10. Maa, J. R., "Rates of Evaporation and Condensation Between Pure Liquids and Their Own Vapors," Industrial Engineering and Chemical Fundamentals, Vol. 9, No. 2, pp. 283-287, 1970.

11. Mills, A. F. and Seban, R. A., "The Condensation Coefficient of Water," Int. J. Heat & Mass Transfer, Vol. 10, pp. 1815-1827, Pergamon Press Ltd., 1967.

12. Hertz, H., "Uber die Verdunstung der Flussigkeiten," Inbesondere des Quecksilbers, im lufteren Raume, Ann. Phys. 17, 177, 1882.

13. Knudesen, M., "Maximum Rate of Vaporization of Mercury," Ann. Phys. 477.697, 1915.

14. Schrage, R. W., A Theoretical Study of Interphase Mass Transfer, Columbia University Press, New York, 1950.

15. Linehan, J. H., "The Interaction of Two-Dimensional, Stratified, Turbulent Air-Water and Steam-Water Flows," ANL-7444, 1968.

16. 77 "Conceptual Isotope Power System-30," from Meeting at Sundstrand Corp., pp. 1-20, 1977.

17. Young, R. J., Yang, K. T. and Novontny, J. L., "Vapor-Liquid Interaction in a High Velocity Vapor Jet Condensing in a Coaxial Water Flow," Heat Transfer Vol. III, AT ChE, 1974.

18. Gouse, S. W., Jr., Kemper, C. A. and Brown, G. A., "Heat Mass & Momentum Transfer in a Condensing Ejector Mixing Section", AIAA Paper No. 67-420.

19. Kabakov, V. I. and Alad'yev, I. T., "Survey of Mixing and Condensation in High-Speed Two-Phase Flows," Fluid Mechanics Soviet Research, Vol. 6, No. 1, pp. 59-68, 1977.

20. Bakay, A. and Jàszay, T., "High Performance Jet Condensers for Steam Turbines," Institute for Energetics, Budapest, Hungary, 1969.

21. Mills, A. F., Kim, S., Leininger, T., Ofer, S. and Pesaran, A., "Heat and Mass Transport in Turbulent Liquid Jets," Int. J. Heat Mass Transfer, Vol. 25, No. 6, pp. 889-897, 1982.

22. Dement'yeva, K. V. and Makarov, A. M., "Condensation of Vapor on Free Cold-Liquid Jets," Heat Transfer Soviet Research, Vol. 6, No. 1, pp. 116-119, 1974.

23. Shapiro, A. H., The Dynamics and Thermodynamics of Compressible Fluid Flow, Vol. 1, pp. 225, The Roland Press Co., New York, 1953.

24. Solodov, A. P., "Steam Condensation on a Laminar Plate Jet of Liquid," Teploenergetika, Vol. 18, No. 4, pp. 76-79, 1971.

25. Rohsenow, W. M. and Choi, H. Y., Heat, Mass and Momentum Transfer, Prentice-Hall, 1961.

26. Fox, R. W. and McDonald, A. T., Introduction to Fluid Mechanics, pp. 384-387, 424-432, John Wiley & Sons, Inc., 1973.

27. 77 "Ground Demonstration System Components-40," from Meeting Minutes at Sundstrand Corp., pp. 31-37, 1977.

28. 78 "Organic Power Conversion Systems-45," Sundstrand Corp., pp. 45-49, 1978.

29. Chapman, A. J. and Walker, W. F., Introductory Gas Dynamics, pp. 150-156, 171-173, Holt Rinehart and Winston, Inc., 1971.

30. Kabakov, V. I. and Teplov, S. V., "Estimate of the Efficiency and Analysis of the Performance of an Injector with Distributed Multijet Liquid Supply," Heat Transfer Soviet Research, Vol. 11, No. 4, pp. 46-54, 1979.

31. 79 "Ground Demonstration System Jet Condenser Orifice Performance-27," Sundstrand Corp., pp. 1-24, 1979.

32. 79 "Ground Demonstration System Jet Condenser Focusing-34", Sundstrand Corp., pp. 1-18, 1979.

33. Alad'ev, S. I., Krantov, F. M. and Teplov, S. V., "Outflow from a Laval Nozzle with Condensation of the Vapor Phase on a Concomitant Jet of Cold Liquid," UDC 532.522, pp. 322-334, Plenum Publishing Corporation, 1981.

APPENDIX A. NONCONDENSABLE GASES

Dowtherm undergoes a slight degradation over a period of time, due to being at its peak cycle temperature. In this degradation, several products are formed as the chemical carbon rings and chains are broken. Some of these products are noncondensable gases, mainly hydrogen and methane.[26] These gases tend to concentrate in the condenser due to natural separation of the vapor and liquid (see Figure A-44). If present in significant quantities, these gases can cause a performance degradation due to combining of the liquid streams. The performance degradation is in the form of an increased vapor pressure required to condense a given vapor flow rate. In severe cases of gas accumulation, floodout can occur due to brooming (Section 5.1). This is due to the entrained gas expanding and disrupting flow when accelerated through the liquid injectors.

The configuration for the jet condenser test was described in Section 4.4. The test consisted of establishing an equilibrium concentration of air, then measuring the concentration and thermal performance (vapor inlet pressure). The minimum concentration was achieved by forcing all the flow through the deaerator (see Figure 41). Higher concentrations were achieved by bypassing some flow around the deaerator.

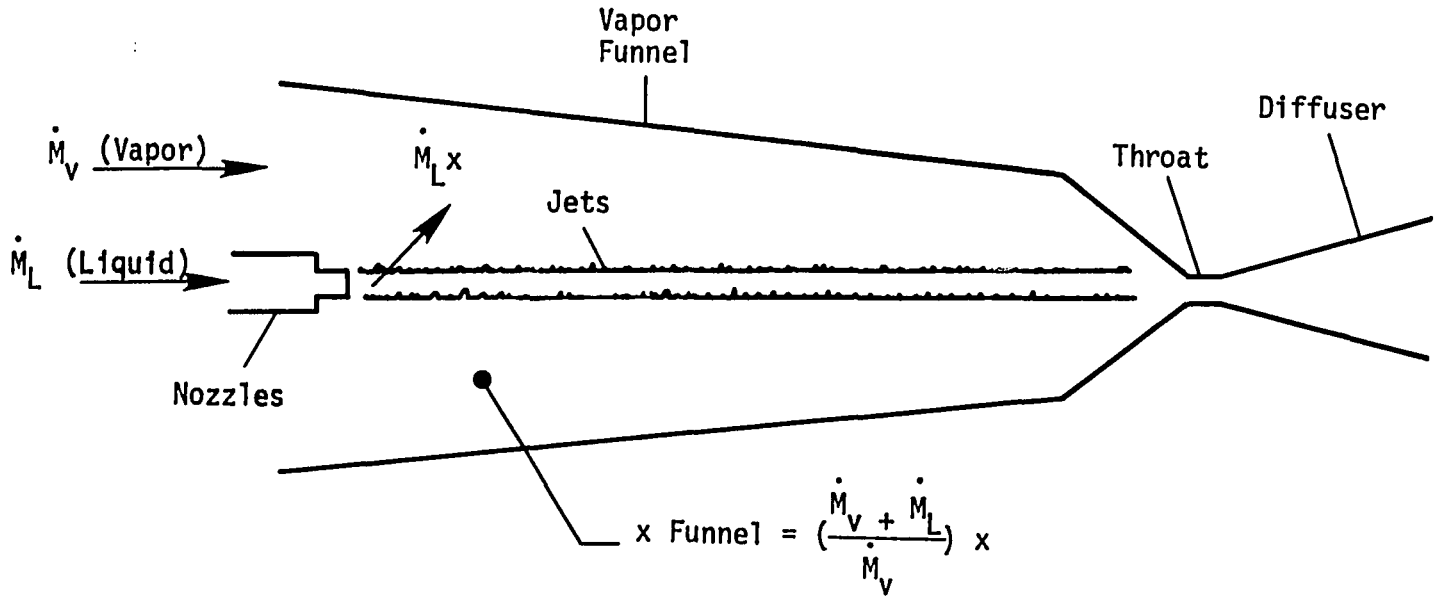

x Funnel = 10x

x = Free Stream Noncondensable Concentration

INSOLUBILITY OF NONCONDENSABLES IN LIQUID

FIGURE A-44

The concentration was measured by opening an evacuated liquid volume to the jet condenser vapor inlet. Condensation occurred on the walls of the tank until the subcooled walls were combined with the separated noncondensable gases. By measuring the volume of collected liquid and knowing the total available volume and pressure, the concentration can be calculated. This technique is illustrated below. The pressure was measured utilizing a Dowtherm liquid manometer.

Calculate Noncondensable Concentration:

$$C = \frac{\text{cc NC}}{\text{cc Dowtherm}} \text{ (PRVO) (K)}$$

where, C is in $\frac{\text{mole NC}}{\text{mole Dowtherm}}$

and, PRVO is in kPa.

ccNC = (Total Available cc) - (cc Dowtherm)

$$K = \left[\frac{1}{66} \cdot 1728 \cdot \frac{1}{.06102} \cdot \frac{166}{453.6}\right] \left[\frac{1}{22.4 \times 10^3}\right] \left[\frac{1}{14.47}\right]$$

$$K = 7.06 \times 10^{-5} \frac{\frac{\text{cc}}{\text{mole}}\Big|_{\text{Dowtherm}} \qquad \frac{\text{mole}}{\text{cc}}\Big|_{\text{NC}}}{\text{kPa}}$$

The results are presented as Figure A-45. It can be seen that at a concentration of 30 ppm, the system backpressure level is ~ 15% higher than with zero ppm. At a concentration

of approximately 90 ppm, floodout occurs. Tests that were conducted in Section (4) had typical values for noncondensables of $\leq$ 20 ppm. It was also discovered that the noncondensable concentration level would rise over a period of 2,000 - 3,000 hours of running time. A gas separator was later installed for gas removal within the Rankine power system.

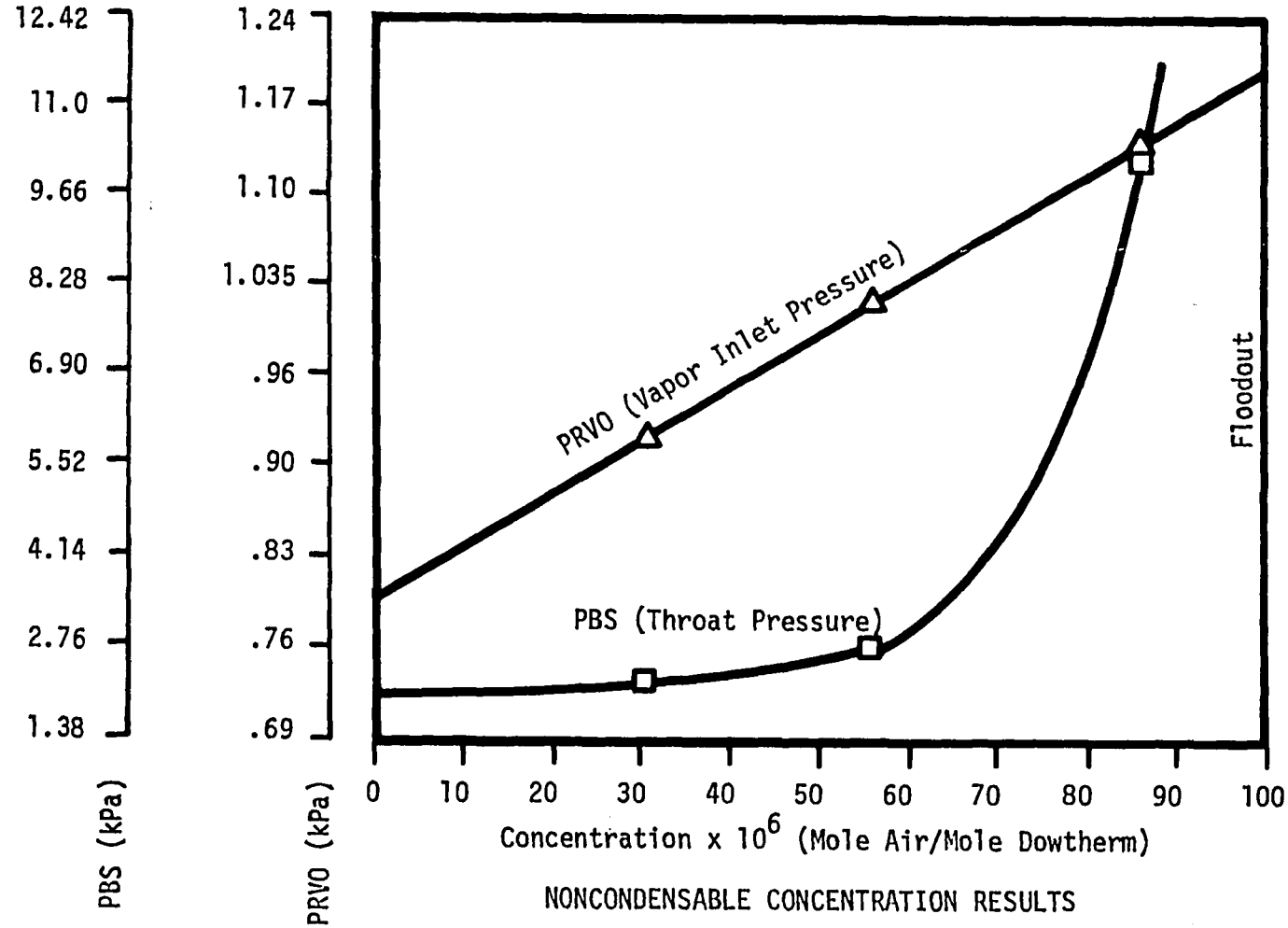

NONCONDENSABLE CONCENTRATION RESULTS

FIGURE A-45.

APPENDIX B. JET CONDENSER NONCONDENSABLE GAS BOUNDARY LAYER ANALYSIS

For the steady, two-dimensional flow of an incompressible fluid over a porous flat plate,[25,26] the simplified boundary-layer equations of momentum, energy, and mass yield a set of four nonlinear partial differential equations. Introducing the concept of the stream function and using a similarity transformation, this can be reduced to a set of three nonlinear, ordinary differential equations:[25]

$$\frac{d^3 f}{dn^3} + \frac{1}{2} \cdot f \cdot \frac{d^2 f}{dn^2} = 0$$

$$\frac{d^2 \theta}{dn^2} + \frac{1}{2} \cdot Pr \cdot f \cdot \frac{d\theta}{dn} = 0$$

$$\frac{d^2 \phi}{dn^2} + \frac{1}{2} \cdot Sc \cdot f \cdot \frac{d\phi}{dn} = 0$$

These are subject to the following boundary conditions:[10]

$$\text{at } n = 0;\ \frac{df}{dn} = \theta = \phi = 0;\ f = -\frac{2 \cdot V_o}{V_\infty} \sqrt{Re_x}$$

$$\text{at } n = \infty;\ \frac{df}{dn} = \theta = \phi = 1$$

This establishes a nonlinear two-point boundary value problem, which was solved with the use of a digital computer. The compiled program was developed at Sundstrand, and involved continuously varying the initial conditions on

$$\frac{d^2f}{dn^2}, \quad \frac{d\theta}{dn} \quad \& \quad \frac{d\phi}{dn}$$

until the final (steady state) values of

$$\frac{df}{dn}, \quad \theta \; \& \; \phi$$

equal unity.

Back transforming the above solution to find the mass transfer coefficient[25,26] results in:

$$H_D \cdot x = Re_x^{.5} \cdot \left(\frac{d\phi}{dn}\right)_o$$

For the suction parameter equal to zero, the Sherwood number is given by:

$$\frac{H_{DO}}{D} \cdot X = .332 \cdot S_C^{.343} \cdot Re_x^{.5}$$

The ratio of the mass transfer coefficients[31] is:

$$\frac{H_D}{H_{DO}} = 3.012 \cdot S_C^{-.343} \cdot \left(\frac{d\phi}{dn}\right)_o$$

The results of the digital solution were shown in Figure 26. of Section 2.3. For values of the suction parameter less than -10, an approximate linear solution exists based on the fact that f doesn't change significantly from its value at, n equals zero.[25, 26, 31]

$$\phi \doteq 1 - \exp\left(S_C \frac{V_o}{V_\infty} \cdot \sqrt{Re_x} \cdot n\right)$$

$$\left(\frac{d\phi}{dn}\right)_o = -S_C \cdot \frac{V_o}{V_\infty} \sqrt{Re_x}$$

Thus, the ratio of the mass transfer coefficients is approximately:

$$H_D \doteq -3.012 \cdot S_C^{.657} \cdot \frac{V_o}{V_\infty} \cdot \sqrt{Re_x}$$

APPENDIX C. MISALIGNMENT

When the Organic Rankine Power System is used for space applications, an induced environment is subjected to the system comprised of superimposed accelerations and vibration.[28] An example of where this occurs is during a system launch or a severe gravity change. In the jet condenser, the result of this environment is a deflection of the liquid jets relative to the throat. Acceleration causes a continuous shift proportional to the g level. Vibration causes an oscillating shift, centered about the constant acceleration shift. Deflections are illustrated in Figure C-46. These relative deflections must not cause the jet condenser to flood out.

The jet condenser was designed for conditions representative of overspeed system operation. It is preferred that launch always be taken at this higher speed in order that the benefits of stiffer bearings and condenser liquid streams be realized. It should be noted that the system's output (electrical power) can be supplied in this overspeed operation. Since the pressure available at the jet condenser liquid inlet is dependent on the electric load, several

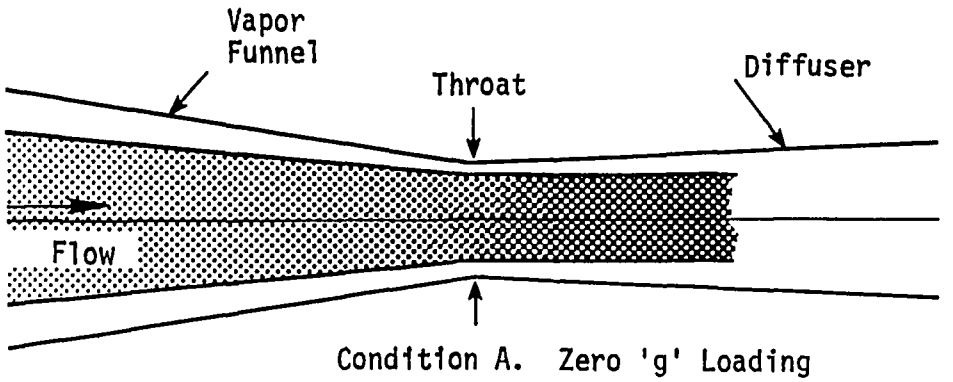

Condition A. Zero 'g' Loading

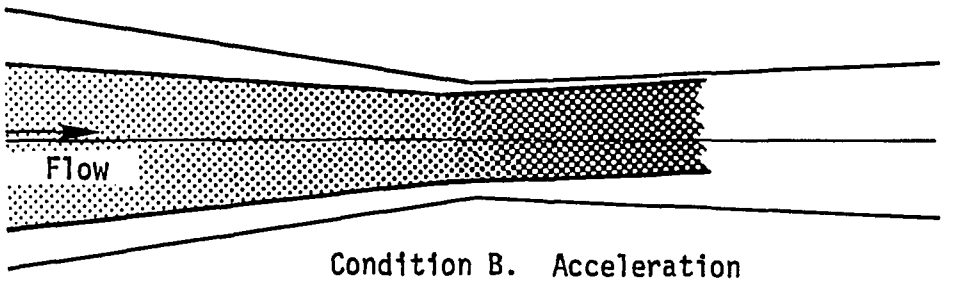

Condition B. Acceleration

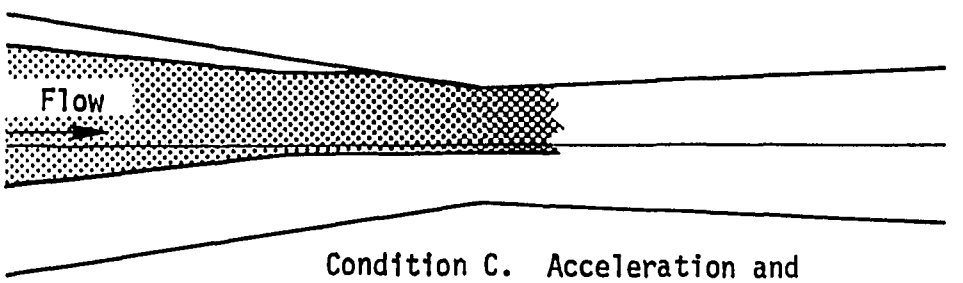

Condition C. Acceleration and
Vibration Combined

(Worst Case)

JET CONSENSER FLOW DEFLECTIONS

FIGURE C-46.

pressures bracketing the expected value were tested. Pressure recovery was set at 20% and system power loop flow was set at 115% of nominal (as in system operation at overspeed). The component downstream of the diffuser is the system accumulator. This component will maintain an essentially constant jet condenser outlet pressure, so varying the recovery pressure from 15 - 60% (percent) was accomplished without any problems. The vapor funnel was then deflected relative to the injector by moving one of the three alignment screws causing the funnel to pivot about the other two. Deflections were measured with the dial indicators. The deflection was increased in steps until floodout occurred. The funnel was then returned to its original position and the deflection repeated in the opposite direction. The test results are presented in Table C-7. As expected, the higher injection pressures achieve greater deflection capability. At the minimum elevated pressure, 1104 kPa, the capability is $\pm$ 1.524mm. As mentioned in (Section 5.5), a 130% bearing scavenge flow at the throat had no effect on the misalignment capability.

The results on the effects of deflection are shown in Figure C-47. Throat static pressure (or bearing scavenge pressure) is plotted against deflection at a given injection pressure. Deflections of $\pm$ .508 mm have essentially no effect

on system operation.[27] The constant deflection due to acceleration is predicted to be .508 mm, and the vibration defection to oscillate at is also $\pm$ .508 mm. This is a significant result in that deflections greater than .508 mm will be sinusoidal in nature, and not continuous as in the test.[27] Therefore, flows of greater amplitudes than the measured deflections in Figure C-47 may be acceptable. The throat, therefore, has been maintained at 3.378 mm based on the above results.

TABLE C-7. MISALIGNMENT RESULTS

Injection Pressure	Flowrate $\dot{M}_V$	Recovery	Bearing Flow at Throat	Maximum Deflection
(kPa)	(Kg/s)	(%)	(Kg/s)	(mm)
1380	.01565	20	.0054	+2.032
1380	.01565	20	-	+2.032
1242	.01565	20	-	+2.032
1104	.01565	20	-	+2.032
1380	.01565	20	-	-1.905
1242	.01565	20	-	-1.651
1104	.01565	20	-	-1.397

Key for Liquid Injection Pressure:

○ @ 1104 kPa

△ @ 1242 kPa

□ @ 1380 kPa

* = Floodout

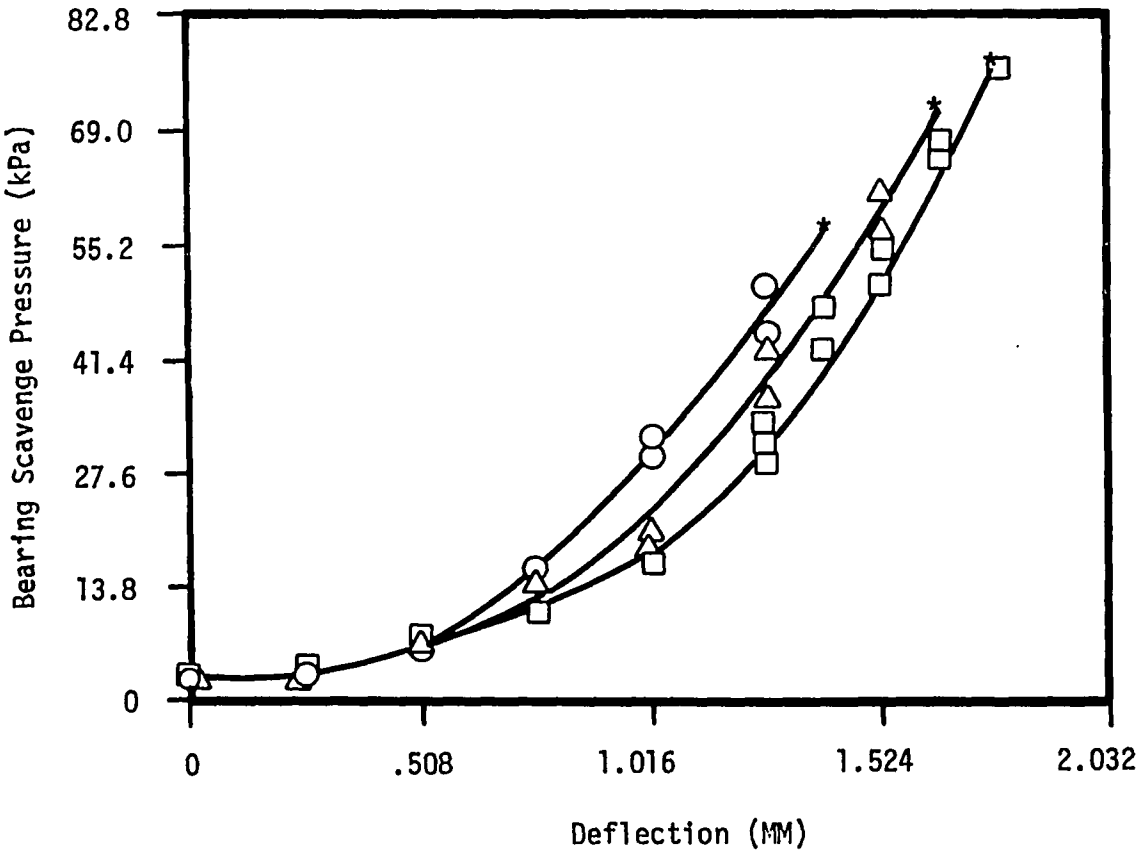

DEFLECTION EFFECTS

FIGURE C-47

APPENDIX D. PROPERTY VALUES USED IN ANALYSIS

	S.I. Units	U.S. Units
Nozzle Liquid Temperature	348.7°K	168°F
Vapor Inlet Temperature	391.7°K	245°F
Average Condensate Temperature	372.2°K	210°F
Standard Nozzle Orifice Diameter	.254 mm	.010 inches
Experimental Nozzle Orifice Diameter	.3683 mm	.0145 inches
Tested Jet Length - 1	50.8 mm	2 inches
Tested Jet Length - 2	127 mm	5 inches
Standard Jet Length - 3	254 mm	10 inches
Throat Diameter, D_t	3.38 mm	.133 inches
Diffuser Outlet Diameter	8.45 mm	.332 inches
Vapor Pressure	.69 kPa	.10 psia
Standard Recovery Pressure	220.8 kPa	32 psia
Highest Recovery Pressure	331.2 kPa	48 psia
Nozzle Liquid Injection Pressure	552 kPa	80 psid
Experimental Heat Transfer Coefficients	.271-.677 $\frac{\text{Cal.}}{\text{sec. m}^2\text{-°C}}$	200-500 $\frac{\text{Btu}}{\text{hr ft}^2\text{-°F}}$

V I T A

Marco F. Bucchi was born on November 6, 1955 in New Britain, Connecticut. He is the son of Harold and Lena Bucchi, and is married to Karin A. Miller, DMD. Marc attended New Britain High School in New Britain, Connecticut, before entering the University of Hartford in West Hartford, Connecticut. While attending the University he was Vice-Chairman of the Student Section of the American Society of Mechanical Engineers, Treasurer of the Kappa Mu Engineering Honor Society, a member of Society of Automotive Engineers, Pi Tau Sigma National Honor Fraternity, and the Engineer's Joint Council. Marc has successfully completed Part I of his Professional Engineering License and is registered in the State of Connecticut.

In June of 1977 he graduated with a Bachelor of Science in Mechanical Engineering from the University of Hartford, and became employed full-time as a Project Engineer for Sundstrand Corporation in Rockford, Illinois. In August of 1978 he began his graduate studies in Mechanical Engineering at the University of Illinois, at Urbana-Champaign.

In November 1979 he moved to the Allentown area where he is employed full-time as a Development Engineer for Air Products and Chemicals, Inc., Allentown, Pennsylvania. In Spring of 1980 he

continued his graduate studies at Lehigh University, Bethlehem, Pennsylvania, towards a Master of Science in Mechanical Engineering.

Marco is an active member of the following engineering societies in the Lehigh Valley Chapter Area: American Society of Mechanical Engineers, Pennsylvania Society of Professional Engineers, National Society of Professional Engineers, and the Society of Automotive Engineers. He has also retained alumni membership to the following: Kappa Mu Engineering Honor Society, and Pi Tau Sigma National Honorary Engineering Fraternity.